VIBROACOUSTIC COUPLING AND TRANSMISSION PATHS

Francesc Xavier Magrans Fontrodona

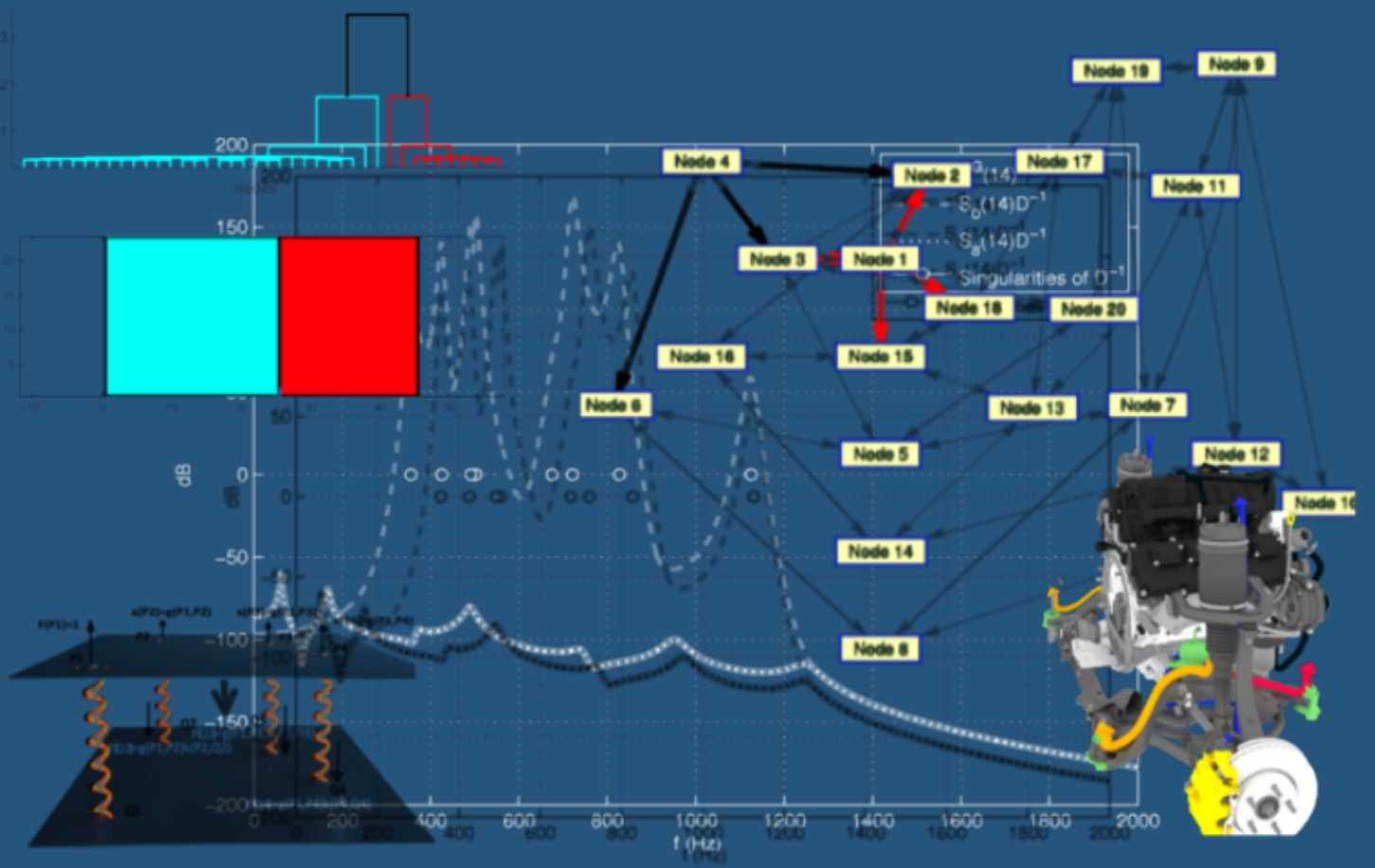

Doctoral Thesis

Barcelona November 2018

UNIVERSITAT POLITÈCNICA DE CATALUNYA BARCELONATECH

Vibroacoustic coupling and transmission paths

by

Francesc Xavier Magrans Fontrodona

VIBROACOUSTIC COUPLING AND TRANSMISSION PATHS

Francesc Xavier Magrans Fontrodona

Doctoral Thesis

Advisors: Jordi Poblet Puig & Antonio Rodríguez-Ferran

Barcelona November 2018

Departament d'Enginyeria Civil i Ambiental

Programa de Doctorat d'Enginyeria Civil

Universitat Politècnica de Catalunya
Programa de Doctorat d'Enginyeria Civil

E.T.S d'Enginyers de Camins, Canals i Ports de Barcelona

Vibroacoustic coupling and transmission paths

by

Francesc Xavier Magrans Fontrodona

Advisors: Jordi Poblet-Puig & Antonio Rodríguez-Ferran

Barcelona, September 27, 2018

Acknowledgments

My first thanks to my wife and children for being a constant support to me. Their love and help have been fundamental throughout my life. They endured without complaint my long stays away from home and on weekends dedicated to work. They have always been with me when I have needed them to give me joy, support and confidence.

Secondly, all those who have given me the opportunity to go one step further. I must mention the SEAT company that selected me as one of the twelve people to create its Technical Centre in Martorell in the distant 70s. There I was able to train in vibroacoustic in Italy, Germany or Switzerland seeing the birth of all the technologies currently used and especially the leap from analog to digital.

My partners in the first company I had, Noisetec, trusted my knowledge and embarked with me on the risky journey of making a living by successfully solving real vibroacoustic problems.

I cannot forget La Salle who put its trust in me to begin his studies in Image and Sound. It was only a year but it was motivating for me. It made me feel a little like a preacher sowing the new seed of the Vibroacoustic in a totally wasteland until then.

How can I not thank the friends who have worked with me throughout the more than 20 years of existence of my current company ICR. Many of them are now in other parts of the world, France, Australia or in other companies, but we are united by the feeling of having been a team that, back to back, made its way through very difficult circumstances.

Finally the very special team formed by Antonio Rodriguez-Ferran and Jordi Poblet welcomed me with enthusiasm the day I knocked on their door to make the road that culminates today. Four years dedicated to a Doctorate that without the experience, knowledge and, especially, patience of both would not have been possible. To them I dedicate this work, which good or bad, scarce or excessive, interesting or boring, is the academic fruit of my professional life that they have helped me to collect.

Abstract

Vibroacoustic coupling and transmission paths

Francesc Xavier Magrans Fontrodona

This dissertation deals with four topics. The first three are in the same environment, the transmission paths. The fourth refers to the synthesis of subsystems and more specifically to two subsystems linked by any number of elastic elements.

In the first topic it is proved that the solution of any linear mechanical system can be expressed as a linear combination of signal transmission paths. This is done in the framework of the Global Transfer Direct Transfer (GTDT) formulation for vibroacoustic problems. Transmission paths are expressed as powers of the transfer matrix. The key idea of the proof is to generalise the Neumann series of the transfer matrix –which is convergent only if its spectral radius is smaller than one– into a modified Neumann series that is convergent regardless of the eigenvalues of the transfer matrix. The modification consists in choosing the appropriate combination coefficients for the powers of the transfer matrix in the series. A recursive formula for the computation of these factors is derived. The theoretical results are illustrated by means of numerical examples. Finally, we show that the generalised Neumann series can be understood as an acceleration of Jacobi iterative method.

For complex geometries, the definition of the subsystems is not a straightforward task. We present as a second topic a subsystem identification method based on the direct transfer matrix, which represents the first-order paths. The key ingredient is a cluster analysis of the rows of the powers of the transfer matrix. These powers represent high-order paths in the system.

Once subsystems are identified, the proposed approach also provides a quantification of the degree of coupling between subsystems. This information is relevant to decide whether a subsystem may be analysed independently of the rest or subsystems or not. The two features (subsystem identification and quantification of the degree of coupling) are illustrated by means of numerical examples: plates coupled by means of springs and rooms connected by means of a cavity.

In the third work, Advanced Transfer Path Analysis (ATPA) is applied to a cuboid-shaped box. The simplicity of this vibroacoustic system helps to make a

detailed analysis of the ATPA method in a more controlled environment than in situ measurements in trains, wind turbines or other mechanical systems with complex geometry, big dimensions and movement. At the same time, a numerical model (based on finite elements) of the box is developed. The agreement between the experimental measurements and the numerical results is good. The numerical model is used in order to perform tests that cannot be accomplished in practise. The results are helpful in order to verify hypotheses, provide recommendations for the testing procedures and study some aspects of ATPA such as the reconstruction of operational signals by means of direct transfer functions or to quantify and understand which are the transmission mechanisms in the box.

The fourth topic introduces a method to synthesize the modal characteristics of a system from the modal characteristics of its subsystems. The interest is focused on those systems with elastic links between the parts which is the main feature of the proposed method. An algebraic proof is provided for the case of arbitrary number of connections. The solution is a system of equations with a reduced number of degrees of freedom that correspond to the number of elastic links between the subsystems. In addition the method is also interpreted from a physical point of view (equilibrium of the interaction forces). An application to plates linked by means of springs shows how the global eigenfrequencies and eigenmodes are properly computed by means of the subsystems eigenfrequencies and eigenmodes.

Contents

Acknowledgments **iii**

Abstract **v**

Contents **vii**

List of symbols **ix**
Latin ix
Greek x
Acronyms xi

1 Introduction **1**
1.1 Motivation 1
1.2 Objectives and layout of this thesis 3

2 The solution of linear mechanical systems in terms of paths **7**
2.1 Introduction 7
2.2 Definitions 10
2.3 Solution based on paths superposition: mathematical proof 16
2.4 Numerical examples 24
2.5 Conclusions 29
2.A A link with iterative solvers: the acceleration of the Jacobi method . 32

3 A subsystem identification method based on the path concept **35**
3.1 Introduction 35
3.2 State of the art 36
3.3 Methodology 37
3.4 Numerical examples and analysis 46
3.5 Conclusions 58
3.A Eigenvectors of $\mathbf{T}$ vs. vibration eigenmodes 59

4 Experimental and numerical study of ATPA **63**

4.1 Introduction 63
4.2 Results 71
4.3 Conclusions 85
4.A Calibration of the model and parameter tuning 87

5 Modal synthesis in elastically coupled subsystems 95
5.1 Introduction 95
5.2 Equivalence of the physical and algebraic problems 98
5.3 Method 100
5.4 Application of the algebraic solution to the physical problem 104
5.5 Examples 109
5.6 Conclusions 115

6 Conclusions 119
6.1 Contributions 119
6.2 Publications derived from the thesis 120
6.3 Future work 121

A Taking a walk through the paths 125
A.1 History, background and some comments 125
A.2 A glimpse of the path travelled 141

Bibliography 149

List of Symbols

Latin symbols

$\mathbf{A}$	Dynamic matrix of the mechanical system
$\mathbf{B}$	Diagonal block matrix involving matrices $\mathbf{B}_1$ and $\mathbf{B}_2$
$\mathbf{C}$	Coupling matrix, non-zero valued only at antisymmetric positions connecting $\mathbf{B}_1$ and $\mathbf{B}_2$ coefficients
$\mathbf{D}$	diagonal part of matrix $\mathbf{A}$
$\mathbf{D}_B$	Diagonal matrix of eigenvalues of $\mathbf{B}$
$\mathbf{H}$	$\mathbf{B} + \mathbf{C}$
$\mathbf{I}$	identity matrix
$\mathbf{K}$	Stiffness matrix
$\mathbf{L}$	strict lower triangular part of matrix $\mathbf{A}$
$\mathbf{M}$	Mass matrix, diagonal and positive definite
P_i	Label for the i'th connection on subsystem 1 may not correspond to degree of freedom i
Q_i	Label for the i'th connection on subsystem 2 may not correspond to degree of freedom i
$\mathbf{S}_{j,m}$	partial sum of order j (j modified parameters) and $m+1$ terms
$\mathbf{T}$	transfer matrix
$\mathbf{T}^{\mathbf{D}}$	direct transfer matrix
$\mathbf{T}^G$	global transfer matrix
$\mathbf{U}$	strict upper triangular part of matrix $\mathbf{A}$
$\mathbf{V}_B$	Matrix of eigenvectors of $\mathbf{B}$
$\mathbf{b}$	vector of forces or excitations

$c_{P_iQ_i}$	Matrix $\mathbf{C}$ coefficient linking degrees of freedom labelled as P_i and Q_i
$\mathbf{e}_{P_k}$	Base vector, unity-valued at degree of freedom labelled P_k
$\mathbf{e}_{Q_k}$	Base vector, unity-valued at degree of freedom labelled Q_k
m	Number of degrees of freedom of $\mathbf{B}$ connected by $\mathbf{C}$
m_j	jj coefficient of the mass matrix
n	problem dimension
n_ϵ	Dimension of a generic matrix ϵ
$\mathbf{u}_{P_k}$	Column vector in $\mathbf{V}_B^{-1}$ on degree of freedom labelled P_k
$\mathbf{u}_{Q_k}$	Column vector in $\mathbf{V}_B^{-1}$ on degree of freedom labelled Q_k
$\mathbf{v}_{P_k}^T$	Row vector in $\mathbf{V}_B$ on degree of freedom labelled P_k
$\mathbf{v}_{Q_k}^T$	Row vector in $\mathbf{V}_B$ on degree of freedom labelled Q_k
$\mathbf{x}$	vector of unknowns or signals

Greek symbols

$\alpha_i, \beta_{j,i}, \gamma_i$	parameters in generalised Neumann series
Γ	Function whose zeroes are eigenvalues of $\mathbf{H}$
λ	eigenvalues (typically of matrix $\mathbf{T}$)
λ_A	Any eigenvalue of matrix $\mathbf{A}$
$\lambda_{B_1,k}$	k'th eigenvalue of matrix $\mathbf{B}_1$
$\lambda_{B_2,k}$	k'th eigenvalue of matrix $\mathbf{B}_2$
μ_i	Modal mass of eigenmode i in subsystem 1, $\mathbf{\Phi}_i$
σ_i	Modal mass of eigenmode i in subsystem 2, $\mathbf{\Psi}_i$
$\mathbf{\Phi}_i$	i'th eigenmode of subsystem 1.
$\phi_i(P_j)$	Coefficient in $\mathbf{\Phi}_i$ corresponding to degree of freedom P_j
$\mathbf{\Psi}_i$	i'th eigenmode of subsystem 2.
$\psi_i(Q_j)$	Coefficient in $\mathbf{\Psi}_i$ corresponding to degree of freedom Q_j
ω	Angular frequency

Acronyms

ATPA	Advanced transfer path analysis
FD	Finite differences
FEM	Finite element method
FRF	Frequency response function
GTDT	Global transfer Direct transfer

Chapter 1

Introduction

1.1 Motivation

This thesis has three parts exploring path theory and one part working on the subsystem synthesis.

Path theory is a 37 years old subject that has already provided interesting results as can be seen in (Guasch and Cortés, 2009; Thompson et al., 2018; Sapena et al., 2012) and more broadly in appendix A.2 but, still, a lot of new knowledge can be gained.

One aspect studied in this thesis is to find out to what extent paths are able to give a complete description of a linear system. In other words, is it always possible to express the solution of a linear system as a sum of paths?

Although it seems reasonable to assume that the paths are a complete solution, there are mathematical arguments to suppose that this is not true. Solving this apparent contradiction between intuition and mathematics has been one of the motivations for writing this thesis.

It is clear that this motivation does not attempt to solve an specific practical problem, but rather it is aimed at completing the frame that supports the theory of transmission paths according to the definitions in Magrans (1981).

Another aspect of the paths, assessed in a second work of this thesis (Chapter 3), is the possibility of defining and quantifying the subsystems and the intensity of the coupling between them.

A subsystem has been defined in many ways. In general, the definitions highlight

a certain aspect that indicate that their behaviour is barely affected by the rest of the system.

Efforts have also been made to define when a subsystem is weakly coupled and to automatically identify possible subsystems.

This thesis explores the possibility of identifying subsystems and assessing the degree of coupling using the path concept (Chapter 3).

The reason for this is that it seems logical that the systems formed by weakly coupled subsystems have paths that mainly pass through the interior of the subsystems. On the other hand the paths that connect these subsystems are likely to be much weaker in number and magnitude than the internal paths.

The path theory has been widely studied at a theoretical level and has also been applied experimentally in the industry under the name of ATPA (Advanced Transfer Path Analysis). However, there are aspects of the theory that are difficult to prove at an experimental level. Thus, the motivation of the third work concerning paths is the interest of demonstrating some aspects using numerical methods (Chapter 4). Just to highlight some of the problems of difficult demonstration at the experimental level, it is worth mentioning; to show that the prediction of the contributions for the less influential subsystems was correct. If we have 70 dB in the microphone and one of the many subsystems contributes 69 dB to this level, another contributes 65 dB, a third 55 dB and the others add up to 45 dB, we have to assume that if we eliminate the first and second subsystems, the total level will fall to 55 dB. This shows that although the third subsystem contributes almost nothing to the total level, it is of fundamental importance to know to what extent we can reduce noise by modifying only two subsystems. If the forecast of the third subsystem contribution is wrong it will compromise the success of the modifications. Experimentally demonstrating that , having a total noise of 70 dB, the third subsystem contributes with 55 dB without altering the total system is very complex while numerically it is easily demonstrable. Also check the influence on the connectivity of degrees of freedom normally not measured such as rotations it is easy numerically and very difficult from an experimental point of view.

A fourth work is independent of the path problem but nevertheless some results will be useful in future path models. The research presented in chapter 5 deals with modal synthesis and complements the algebraic developments with physical interpretation.

The algebraic approach focuses on how to find the eigenvectors and eigenvalues of a system made up by two subsystems given the eigenvectors and eigenvalues of each subsystem.

The physical approach is focused on solving practical problems. Indeed, lots of commercial products consist of a structure and attached auxiliary equipment. Examples are a compressor in a freezer, the brake compressor in a train wagon as well as the frequency converter, HVAC equipment, electrical generators, gearbox etc. Other cases are the transformer in wind turbines or its engines, fans, pumps etc. The attachment of a mechanical subsystem is normally done using elastic supports that can be assimilated to a spring.

Another frequent situation is found when machines are supported by a separate structure. Examples are cooling towers on terraces, oil extraction and storage equipment on oil sea platforms etc. Knowing the vibratory response of both, added subsystem and supporting structure, we want be able to predict the vibratory response of the whole set.

1.2 Objectives and layout of this thesis

This section briefly describes the objectives of this thesis. Concepts linked to the transmission paths are assumed to be known. Some references are Magrans (1981); Magrans et al. (2005); Magrans (1993); Aragonès et al. (2015); Zafeiropoulos et al. (2013); Wang et al. (2017); Sapena et al. (2012).

1. **The first objective developed in Chapter 2 is to prove that the solution of any linear system can be expressed as a linear combination of signal transmission paths weighted with the appropriate coefficients**.

   This proves that the concept of the path and its mathematical definition allows us to fully explain the behaviour of any linear system and in particular the vibroacoustic problems. As a direct consequence, the completeness of the method of Transmission Paths is proven (Magrans et al., 2017)

   This can be applied to the acceleration of the Jacobi's method, i.e. its convergence rate is improved.

2. **The second goal of the thesis is to explore the possible identification of subsystems by means of paths**. The possibility to bound the error

made when calculating the response of each subsystem as an isolated system is considered. The results obtained show the extent to which eigenvectors are independent of the presence of other subsystems .

A paper with the results of this research (Magrans et al., 2018) explains and demonstrates how to find the subsystems and how to evaluate the coupling force.

3. **The third topic related to paths is a comparison of experimentation and numerical simulation**.

   This comparison makes it possible to obtain results with the simulation that are difficult to obtain at an experimental level.

   First the suitability of the numerical model by comparing it with the experimentation is verified.

   In addition, the influence on the reconstructed signals of the modifications in the excitation (i.e. perturbation on the application point, use of random forces, consideration of a more realistic operational excitation)are also considered in the analysis.

   The validity of the measure should be checked for minor contributions whose effect on the total signal can be neglected but which establish a lower limit to the improvement that can be obtained by means of a system redesign and modification that reduces the most important contributions.

   A paper with the results of this research has been published in (Aragonès et al., 2019)

4. **In a fourth objective, equations are obtained that allow to find the eigenvectors and eigenvalues of a system made up of two others coupled by springs, when the eigenvectors and eigenvalues of both subsystems are known**. To the best of my knowledge it is the first eigenvalue and eigenvectors synthesis approach for elastic (rather than rigid) coupled subsystems based on eigenvalues and eigenvectors of the subsystems.

   A paper with the results of this research has been published in (Magrans and J.Poblet-Puig, 2018)

Chapters 2 to 4 deal with issues related to transmission paths. The concepts needed to follow developments related to transmission paths are set out mainly in Chapter 2 and in the appendix A.2.

Chapter 5 is not related to the previous three chapters and the necessary information is self contained.

Finally, chapter 6 gives the conclusions of this thesis, related publications and proposal of future work.

Independently of the content of the PhD dissertation, an explanation of the basic ideas of the transmission paths is given in appendix A.2, providing, also, explanations related to their usefulness and future work.

Chapter 2

The solution of linear mechanical systems in terms of path superposition[1]

2.1 Introduction

Vibroacoustic problems are very often not easy to visualise and understand. Moreover, the availability of experimental measurements is limited by operational costs and times. For these reasons the intuition of engineers/physicists/acousticians has always played an important role during the design process. A key concept is the *transmission path* of sound and vibrations. This has remained an intuitive idea rather than a properly defined and well established concept.

The first attempts to quantify the contribution of subsystems, even if they never spoke about paths, can be found in Koss and Alfredson (1974b) and later works Bendat (1976b,a); Potter (1977); Alfredson (1977); Koss and Alfredson (1974a). They were motivated by the need in the automotive industry to characterise how the noise generated by the engine or in the moving parts of the vehicle were transmitted to the cabin. This method is nowadays known as Operational Transfer Path Analysis (OTPA), Lohrmann (2008); de Klerk and Ossipov (2010).

The first document concerning the paths in a vibroacoustic system is a technical

[1]Chapter based on the paper Magrans et al. (2017)

report Gillard (1980) from the company Keller. The title of the document "Method of measurement for determining the transmission paths and the contributions of the different excitation forces simultaneously applied to a linear mechanic system" highlights two aspects of it, identification of transmission paths and identification of force contributions. This technical document was the result of the analysis that a group of experts in the field of car Vibro–Acoustics made of a previous version of Magrans (1981).

Paths and contributions are implicitly defined and quantified in Magrans (1981). This method is known as Global Transfer Direct Transfer (GTDT) method in the scientific publications or as Advanced Transfer Path Analysis (ATPA) in the industry, where it has been widely used in many applications, such as railways, see for example Sapena et al. (2012).The role of paths in more specific situations was analysed in Guasch and Magrans (2004a), where the interest is focused in the characterisation of the connectivity between system parts. Some academic tests can be also found in Zafeiropoulos et al. (2013); Guasch et al. (2013). A comprehensive classification of the methods and historical overview can be found in Van der Seijs et al. (2016). Paths have also been defined and quantified in a Statistical Energy Analysis (SEA) framework Luzzato and Ortola (1988); Craik (1990); Magrans (1993).

Other applications of the path concept can be found in the literature. An analysis of the paths that contribute more to the system response by means of graph theory is presented in Aragonès et al. (2015); Guasch and Aragonès (2011). Path analysis was simplified considering forward paths only in Magrans (1993). A comparison of path analysis with other methods was reported in Wilson (2014).

Some efforts have been employed to systematize methods based on the path concepts to evaluate the final response that a modification will produce.

Guasch (2009), studies the effects of blocking some paths. More recently Wang et al. (2017) have studied the prediction potential of the method specially linked at FEM results. This has also been studied in Tan, Xu, and Sui (Tan et al.) dealing with multiple points subsystems responses. In Jové and Guasch (2017) the same schema is studied including the forces transmission through the paths.

Another recent application of the method has been developed in Jalali Mashayekhi and Behdinan (2017) where the use of the Direct Transfer is made in the bond graphs environment extending the use of the Direct Transfer to new sectors as the hydraulic and electrical machines. Also new expressions to find the Direct Transfer are obtained

in Jalali Mashayekhi and Behdinan (2017) .

Under the framework of the EU funded Roll2Rail contract No. H2020 636032 D7.4 a study Malkoun, Sapena, Arcas, and Magrans (Malkoun et al.) has been made to split the noise made by the train lane from the noise made by the wheels in a train. The moving boogies of a train make that the noise in a microphone may be studied knowing the transfer functions from the lane to a row of microphones. The change of global transfer functions between different microphones will be equivalent to the train movement.

Also Thompson et al. (2018) studies the results obtained by several methods to asses several measurement-based methods for separating wheel and track contributions including the ATPA method.

In spite of the clear applicability of path analysis to practical situations, a theoretical question remains open: a proof of completeness. In other words, the possibility of fully describing the solution of a mechanical transfer problem by means of the superposition of transmission paths. This theoretical question is addressed here, by using concepts and tools of numerical linear algebra (see textbooks Demmel (1997); Trefethen and Bau (1997) for background material).

It was clearly demonstrated in Magrans (1984, 1993) that a solution of a mechanical problem can be described by means of the Neumann series[2] of the transfer matrix $\mathbf{T}$ (the powers of $\mathbf{T}$ are a representation of paths of different order in the mechanical system). The series has strict convergence conditions, which in practise mean that the solution description through transmission paths and Neumann series[3] is not always possible.

The issue of the completeness of the solution description has also been addressed in Guasch and Cortés (2009); Bessac (1996); Aragonès et al. (2015); Finnveden (2011). Guasch and Cortés (2009) relates the convergence of the series with the damping of the systems because the energy of undamped systems permanently excited would grow indefinitely. However, this does not explain the situations when, even with damping, the series diverge. For this reason Aragonès et al. (2015) claims that other conditions to ensure the convergence are required in addition to the existence of damping. The drawback of the divergence of the solution expressed as a series also appears if the problem is not strictly formulated in terms of the transfer matrix and

[2]In honour of Karl Gottfried Neumann (1832-1925)
[3]A Neumann series has the form $\sum_{k=0}^{\infty} \mathbf{T}^k$.

its powers. This can be seen in Bessac (1996) for the matrix of coupling loss factors and in Finnveden (2011) for the coupling eigenvalues.

The goals and achievements of this research are as follows:

- To provide a definition of what a path is.
- To prove the possibility of expressing the solution of all linear problems in terms of paths (especially applied to vibroacoustic). The proof is done in the framework of the Direct and Global Transfer Matrix formulation of the problem. The final result is a generalisation of the Neumann series.
- To derive a practical recursive methodology that allows the computation of the solution based on the transfer matrix of the problem. The goal is also to provide a closed-form expression of the solution as simple as possible.
- To illustrate this methodology with numerical examples.
- To explore the relationship between the proposed approach and Jacobi iterative method for linear systems. The generalised Neumann series can be understood as an acceleration (i.e. convergence speedup) of the Jacobi method.

The remainder of the chapter is organised as follows. Some key concepts such as the notion of path and the transfer matrix are defined in Section 2.2. A precise and explicit definition of path is given. The theoretical core of the research is presented in Section 2.3. It includes the proof of the existence of an expression of the system solution based on a linear combination of paths. A general methodology to compute the combination factors in the generalised Neumann series is provided. Numerical examples that illustrate the theoretical results are shown in Section 2.4. The concluding remarks of Section 2.5 close the chapter.

2.2 Definitions

2.2.1 Physical considerations on the 'path' concept

Various methods based on path analysis are useful to find engineering solutions in vibroacoustic problems Van der Seijs et al. (2016). Nevertheless the 'path' concept is often not defined in a rigorous way.

Our goal here is to provide this explicit definition of 'path'. It will help later in Section 2.3 in order to develop the core of this research. The definition must be consistent with these three intuitive ideas:

1. *A path is something different from a contribution.* It must provide information on how the system behaves, instead of being understood as a black box with an input and an output. In techniques such as Transfer Path Analysis (TPA, Gajdatsy et al. (2010)) the output is a product of multiple contributions that arrive through different uncharacterised paths. This is not the case of ATPA (GTDT) or OTPA, which are based on the path concept.

2. *A path is not only defined by the topology of the problem.* In addition, the physical behaviour of the system must be considered. Clear examples of this are: *i)* a beam, where the deflection of a point is linked not only with the deflection of other points but also with the rotations Guasch and Magrans (2004a); or *ii)* an SEA description of the sound transmission between two rooms, where coupling loss factors due to forced or resonant transmissions must be considered in the same single wall Hopkins (2012). For the case *i)* see the simple sketch in Figure 2.1 where a supported beam is represented. Three different points in the beam are considered ($i = 1, 2, 3$). Each of them is characterised by its displacement x_i. However, this is not enough in order to study the signal transmission between 1 and 3 because an imposed displacement at 1 causes a displacement at 3 even if the displacement at 2 is blocked. The signal can pass from 1 to 3 not only through the displacement in 2 but also through the rotation in 2. So, two different transmission paths must be considered in order to properly characterise the mechanical system response. It is clearly shown in the path diagram of Figure 2.1.

3. *A path is the edge of a weighted graph including the physical characteristics of the problem.* The quantity that characterises the link between two nodes must be related with the physics of the problem.

2.2.2 Definition of paths

Let $N = \{1, 2, \ldots, n\}$ be a set of n nodes. The nodes may represent single points in a continuous system, a degree of freedom associated to that point, single masses

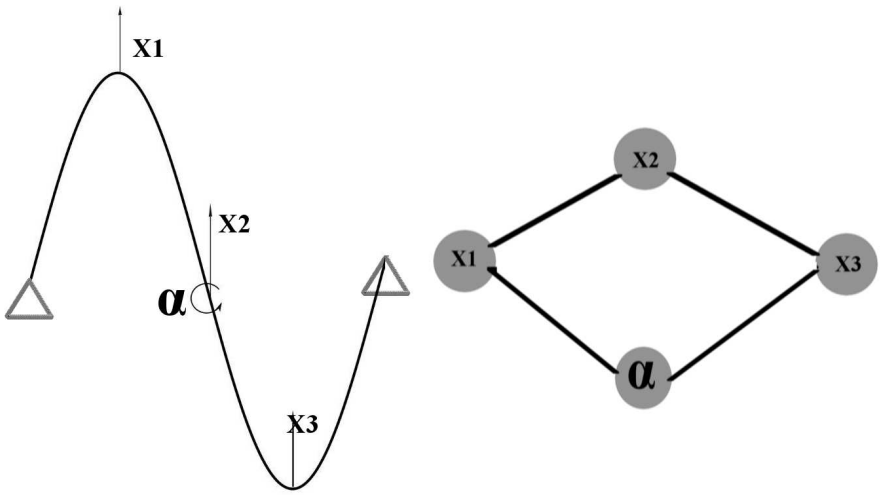

Figure 2.1: Path representation of a simply supported beam. Four degrees of freedom are considered: three displacements x_i and one rotation α.

.

in a discrete system of masses and springs or disjoint parts of a continuous system. Their intersection must be null. Let x_i be a physical signal and b_i an excitation, both associated to node i.

The behaviour of the mechanical system is properly described by the following linear system of equations:

$$\mathbf{Ax} = \mathbf{b} \qquad x_i, b_i, a_{ij} \in \mathbb{C} \tag{2.1}$$

A direct path between nodes i and j exists and is represented by coefficient p_{ij} if the following conditions are satisfied:

1. $p_{ij} \neq 0$ links signals x_i and x_j caused by an excitation in node i while all other nodes are blocked:

$$x_j = p_{ij} x_i \quad \forall j \neq i, \text{ for } x_k = 0, \forall k \neq i,\ j,\ b_i \neq 0 \text{ and } b_j = 0 \tag{2.2}$$

   The non-zero coefficient p_{ij} will be called *direct transfer* between nodes i and j.

2. It is possible to express the solution of the system as a superposition of paths of arbitrary order.
   A k-order path $p_{ij}^{(k)}$ is as a chain of k direct paths that starts at node i and ends at node j with $j \neq i$ or $j = i$ such that: $p_{ij}^{(k)} = \underbrace{p_{ir}p_{rs}\ldots p_{qj}}_{k}$.
   That is, it must be possible to express every signal x_j as

$$x_j = \sum_{i=1}^{n} \sum_{\substack{\text{all paths} \\ k=1}}^{\infty} \gamma_k p_{ij}^{(k)} x_i \tag{2.3}$$

   where γ_k are combination factors that depend on the order of the path (see Section 2.3 where γ_k are defined in Eq. (2.42)).

Several models used to describe the response of mechanical systems can fit in the definition of the path concept presented here, see for example Magrans (1981); Bessac (1996); Finnveden (2011); Jove and Guasch (2012).

2.2.3 The Global Transfer Direct Transfer (GTDT) frame for paths

The basic concepts of the GTDT method Magrans (1981) are briefly reviewed here.

2.2.3.1 Problem statement

Consider the linear system of equations (2.1), where $\mathbf{A}$ is a (in general complex but possibly real) invertible matrix of dimension n. Matrix $\mathbf{A}$ may be expressed as

$$\mathbf{A} = \mathbf{D} + \mathbf{L} + \mathbf{U} \tag{2.4}$$

where $\mathbf{D}$, $\mathbf{L}$ and $\mathbf{U}$ are the diagonal, strict lower and strict upper parts of matrix $\mathbf{A}$. By assuming that $\mathbf{D}$ is invertible, system (2.1) may be recast as

$$\mathbf{x} = \mathbf{D}^{-1}\mathbf{b} + \mathbf{T}\mathbf{x} \tag{2.5}$$

where

$$\mathbf{T} = -\mathbf{D}^{-1}(\mathbf{L} + \mathbf{U}) \tag{2.6}$$

is the transfer matrix. This matrix is the transpose of the Direct Transfer Matrix, $\mathbf{T}^D$ defined in Magrans (1981) with zeros in the diagonal. Note that $\mathbf{T}$ is not symmetrical

in general and that it takes into account the coupling between the unknowns: for $\mathbf{T} = \mathbf{0}$, the system is diagonal and the solution is simply $\mathbf{x} = \mathbf{D}^{-1}\mathbf{b}$.

The coefficients of the matrix $\mathbf{T}$ will be called Direct Transfers. T_{ij}^D will be the direct transfer from i to j. The diagonal elements of $\mathbf{D}^{-1}$ are the direct transfers from i to i, T_{ii}^D

From Eq. (2.5), the solution of system (2.1) may be expressed as

$$\mathbf{x} = (\mathbf{I} - \mathbf{T})^{-1}\mathbf{D}^{-1}\mathbf{b} \tag{2.7}$$

Finally, we define the Global Transfer Matrix

$$\mathbf{T}^G = (\mathbf{I} - \mathbf{T})^{-1}\mathbf{D}^{-1} \tag{2.8}$$

Note that the definition of the Global Transfer Matrix in Magrans (1981) contains a diagonal scaling matrix not included here. This allows a change between forces and displacements as main variables. In an experimental research it is often more advantageous to work with displacements because they can be measured more easily. On the contrary, in the context of the present work it is more convenient to think in terms of a force-displacement formulation. This diagonal scaling matrix implies that the coefficients of $\mathbf{T}^G$ have the physical meaning of receptance Frequency Response Functions (FRF).

The expression 2.5 allows to calculate the signals as a sum of the effects of the force and the contributions of the movements of the other nodes. This expression is the basis for calculating the contributions on a subsystem coming from the other subsystems in the ATPA.

Previously it is necessary to know the Direct transfers. The measurement or calculus of the Global transfers allows, using 2.8 to compute the Direct transfers. Direct Transfers are the quantification of the paths.

Finally 2.7 allows the calculus at the forces when the signals in the nodes are known by a simple matrix inversion. The problem anyway is usually ill-conditioned. This is the method used for the called TPA to identify the forces. Also when the forces are identified the method allows to calculate the signals coming from each force but going through all the paths.

2.2.3.2 Transfer matrices: physical meaning

Note that, under the assumptions of Eq. (2.2), equation j of the linear system (2.5) is

$$x_j = t_{ji} x_i \quad \forall j \neq i, \text{ for } x_k = 0, \forall k \neq i,\, j,\, b_i \neq 0 \text{ and } b_j = 0 \tag{2.9}$$

where t_{ji} are the entries of matrix $\mathbf{T}$. This means that matrix $\mathbf{T}$ contains all the information on the direct signal transmission from one node to another when all the rest are blocked. This the first requirement in Section 2.2.2. The main goal of this research is to prove that matrix $\mathbf{T}$ also satisfies the second requirement.

The formulation of the problem in terms of the transfer matrix is valid for the modelling of mechanical systems by means of different techniques such as: *i)* Statistical Energy Analysis Hopkins (2012), in which case the system matrix $\mathbf{A}$ is created from the coupling loss factors that relate the subsystems and their damping coefficient; *ii)* the Finite Element Method (FEM Ihlenburg (1998)), in which case the system matrix $\mathbf{A} = \mathbf{K} - \omega^2\mathbf{M}$, where $\mathbf{K}$ and $\mathbf{M}$ are the stiffness and mass matrices (damping can also be considered); or *iii)* models or methods where $\mathbf{T}$ can be indirectly obtained by means of experimental measurements in a laboratory as described in Magrans (1981).

Matrix $\mathbf{T}$ contains information of the system connectivity and its successive powers are a representation of the k-order paths. This can be deduced from the graph theory and the properties of the powers of the adjacency matrix, see for example Biggs (1993).

The recursive substitution of Eq. (2.5) in itself leads to the following identity:

$$\mathbf{x} = (\mathbf{I} + \mathbf{T} + \mathbf{T}^2 + .. + \mathbf{T}^{k-1})\mathbf{D}^{-1}\mathbf{b} + \mathbf{T}^k\mathbf{x} \tag{2.10}$$

This makes evident the relationship between the Neumann series, the re-formulation of the problem in terms of the transfer matrix and the solution of the original linear problem. When the spectral radius (i.e. largest modulus of eigenvalues, see Ciarlet et al. (1989); Demmel (1997); Trefethen and Bau (1997)) of $\mathbf{T}$ is less than one, the limit for k tending to infinity of vector $\mathbf{T}^k\mathbf{x}$ is zero and the solution of the problem is the Neumann series. In other words, the solution of the problem is the simplest (all combination coefficients equal one) linear combination of k-order paths. The order k starts at zero and the series makes sense when k tends to infinity. This case is more rigorously considered later in Section 2.3.1.

The coefficients of the Global Transfer Matrix $\mathbf{T}^G$, as defined in Eq. (2.8), express the signal in node j exciting the node i when the rest of the nodes are not blocked. Consequently, the signal at node j includes the contributions of all the paths. $\mathbf{T}^G$ is more easily measurable in the laboratory than $\mathbf{T}$, which must be indirectly measured by means of laborious tests like the strip method Lebresne (1975).

Finally, matrix $\mathbf{D}^{-1}$ is the matrix of direct transfers from node i to node i: d_{ii}. It accounts for the part of the signal in node i that does not come from the other nodes but from the external applied forces.

Eq. (2.5) can be premultiplied by $\mathbf{x}^t\mathbf{D}$ leading to

$$\mathbf{x}^t\mathbf{D}\mathbf{x} = \mathbf{x}^t\mathbf{b} + \mathbf{x}^t\mathbf{D}\mathbf{T}\mathbf{x} \tag{2.11}$$

This new expression can be interpreted in energetic terms. The left-hand-side represents the kinetic and potential energy of individual elements and $\mathbf{x}^t\mathbf{b}$ is the external work. Consequently, the transfer matrix $\mathbf{T}$ plays the role of an interaction potential.

2.3 Solution based on paths superposition: mathematical proof

The mathematical proof for the existence of a linear combination of paths that leads to the solution of the problem is given here. The methodology is based on the framework presented in Section 2.2, so, the proof is valid for a wide variety of models that satisfy a very usual algebraic structure: linear system of equations reformulated in terms of the transfer matrix.

In those cases the mathematical expression of path addition is Eq. (2.10). However, the convergence of the series cannot always be ensured. It depends on very different factors related with the physical properties or the modelling technique, such as the damping distribution in the mechanical system, how are the SEA subsystems defined, which points are chosen in order to define a transfer matrix, etc. Divergence is found if the spectral radius of the transfer matrix is not less than one, $\rho(\mathbf{T}) \not< 1$. This situation, which in fact is the motivation of the discussion and the main goal of the research, is analysed in Section 2.3.2.

The main question to be answered here, linked with the second aspect of the path definition in Section 2.2.2, is if it is possible to express $(\mathbf{I} - \mathbf{T})^{-1}$ (and, hence, the solution $\mathbf{x}$) as a linear combination of powers of the transfer matrix $\mathbf{T}$ also in the

case when the spectral radius of $\mathbf{T}$ is larger than one. This non-trivial case will be analysed afterwards in Section 2.3.2.

2.3.1 Some useful well-known results

Theorem

Let $\mathbf{B}$ be a square matrix. The following conditions are equivalent (see for example Theorem 1.5-1 in Ciarlet et al. (1989)):

1. $\lim_{k\to\infty} \mathbf{B}^k = \mathbf{0}$
2. $\lim_{k\to\infty} \mathbf{B}^k\mathbf{v} = \mathbf{0}$ for any vector $\mathbf{v}$
3. $\rho(\mathbf{B}) < 1$, where $\rho(\cdot)$ is the spectral radius

Neumann series, spectral radius less than one

If $\mathbf{T}$ verifies the conditions above, then

$$(\mathbf{I} - \mathbf{T})^{-1} = \sum_{k=0}^{\infty} \mathbf{T}^k \tag{2.12}$$

To show this, we consider the partial sum $\mathbf{S}_{0,m} = \sum_{k=0}^{m} \mathbf{T}^k$. Subscript m denotes the upper limit of the summation, whereas subscript 0 indicates that it is the original Neumann series. Then,

$$\lim_{m\to\infty} (\mathbf{I} - \mathbf{T})\mathbf{S}_{0,m} = \lim_{m\to\infty} \left(\sum_{k=0}^{m} \mathbf{T}^k - \sum_{k=0}^{m} \mathbf{T}^{k+1} \right) = \mathbf{I} - \lim_{m\to\infty} \mathbf{T}^{m+1} = \mathbf{I} \tag{2.13}$$

Note that for $\rho(\mathbf{T}) < 1$,

$$\lim_{m\to\infty} \mathbf{S}_{0,m} = (\mathbf{I} - \mathbf{T})^{-1} \tag{2.14}$$

2.3.2 Transfer matrices with spectral radius larger than one

The remainder of the section shows that Eq. (2.12) can be always generalised to deal with transfer matrices $\mathbf{T}$ such that $\rho(\mathbf{T}) \not< 1$. In other words, the solution of a linear system of equations representing a mechanical system can be expressed as a linear combination of paths of different order as defined in Section 2.2.3.

2.3.2.1 One-parameter modification

Consider the sequence of matrices $\{\mathbf{P}_{1,k}\}$ with

$$\mathbf{P}_{1,0} = \alpha_1 \mathbf{T}^0 \text{ and } \mathbf{P}_{1,k} = (1-\alpha_1)\mathbf{T}^{k-1} + \alpha_1 \mathbf{T}^k \text{ for } k \geq 1 \tag{2.15}$$

where α_1 is a free parameter to be determined later, and the modified partial sum

$$\begin{aligned} \mathbf{S}_{1,m} &= \sum_{k=0}^{m} \mathbf{P}_{1,k} = \alpha_1 \mathbf{T}^0 + (1-\alpha_1)\mathbf{T}^0 + \alpha_1 \mathbf{T}^1 + \cdots + (1-\alpha_1)\mathbf{T}^{m-1} + \alpha_1 \mathbf{T}^m \\ &= \mathbf{S}_{0,m-1} + \alpha_1 \mathbf{T}^m \end{aligned} \tag{2.16}$$

Note that, for $\alpha_1 = 1$, one retrieves the Neumann series (2.12). The question here is to know, for the case $\alpha_1 \neq 1$, under what conditions does the partial sum (2.16) converge to the inverse of $(\mathbf{I} - \mathbf{T})$:

$$\begin{aligned} \lim_{m\to\infty} (\mathbf{I}-\mathbf{T})\mathbf{S}_{1,m} &= \lim_{m\to\infty} (\mathbf{S}_{1,m} - \mathbf{T}\mathbf{S}_{1,m}) \\ &= \lim_{m\to\infty} (\mathbf{S}_{0,m-1} + \alpha_1 \mathbf{T}^m - \mathbf{T}\mathbf{S}_{0,m-1} - \alpha_1 \mathbf{T}^{m+1}) \\ &= \mathbf{I} - \lim_{m\to\infty} \left((1-\alpha_1)\mathbf{T}^m + \alpha_1 \mathbf{T}^{m+1} \right) \end{aligned} \tag{2.17}$$

The equality $(\mathbf{I}-\mathbf{T})\mathbf{S}_{0,m-1} = \mathbf{I} - \mathbf{T}^m$ is used for the last step. Eq. (2.17) shows that $\mathbf{S}_{1,m}$ converges to $(\mathbf{I}-\mathbf{T})^{-1}$ if and only if

$$\lim_{m\to\infty} \left((1-\alpha_1)\mathbf{T}^m + \alpha_1 \mathbf{T}^{m+1} \right) = \lim_{m\to\infty} \mathbf{P}_{1,m+1} = \mathbf{0} \tag{2.18}$$

This condition is less restrictive (and includes) the usual condition $\lim_{m\to\infty} \mathbf{T}^{m+1} = \mathbf{0}$.

2.3.2.2 Two-parameter modification

The modification strategy of section 2.3.2.1 can be applied again. Consider the sequence of matrices $\{\mathbf{P}_{2,k}\}$ with

$$\mathbf{P}_{2,0} = \alpha_2 \mathbf{P}_{1,0} \text{ and } \mathbf{P}_{2,k} = (1-\alpha_2)\mathbf{P}_{1,k-1} + \alpha_2 \mathbf{P}_{1,k} \text{ for } k \geq 1 \tag{2.19}$$

and the modified partial sum

$$\mathbf{S}_{2,m} = \sum_{k=0}^{m} \mathbf{P}_{2,k} = \mathbf{S}_{1,m-1} + \alpha_2 \mathbf{P}_{1,m} \tag{2.20}$$

The question here is to know under what conditions does the partial sum (2.20) converge to the inverse of $(\mathbf{I}-\mathbf{T})$:

$$\lim_{m\to\infty}(\mathbf{I}-\mathbf{T})\mathbf{S}_{2,m}=\lim_{m\to\infty}\left(\mathbf{S}_{2,m}-\mathbf{T}\mathbf{S}_{2,m}\right)=\mathbf{I}-\lim_{m\to\infty}\mathbf{P}_{2,m+1} \tag{2.21}$$

To obtain the second equality in Eq. (2.21), one takes into account the definition of the partial sums $\mathbf{S}_{0,m}$, $\mathbf{S}_{1,m}$ and $\mathbf{S}_{2,m}$. Eq. (2.21) shows that $\mathbf{S}_{2,m}$ converges to $(\mathbf{I}-\mathbf{T})^{-1}$ if and only if

$$\lim_{m\to\infty}\mathbf{P}_{2,m+1}=\lim_{m\to\infty}\left((1-\alpha_2)\mathbf{P}_{1,m}+\alpha_2\mathbf{P}_{1,m+1}\right)=\mathbf{0} \tag{2.22}$$

This condition is less restrictive (and includes, for $\alpha_2=1$) the condition $\lim_{m\to\infty}\mathbf{P}_{1,m+1}=\mathbf{0}$ derived in section 2.3.2.1.

2.3.2.3 Multi-parameter modification

In fact, the modification strategy can be applied recursively. Consider the sequence of matrices $\{\mathbf{P}_{j,k}\}$ with

$$\mathbf{P}_{j,0}=\alpha_j\mathbf{P}_{j-1,0}\text{ and }\mathbf{P}_{j,k}=(1-\alpha_j)\mathbf{P}_{j,k-1}+\alpha_j\mathbf{P}_{j-1,k}\text{ for }k\geq 1 \tag{2.23}$$

and the modified partial sum

$$\mathbf{S}_{j,m}=\sum_{k=0}^{m}\mathbf{P}_{j,k}=\mathbf{S}_{j-1,m-1}+\alpha_j\mathbf{P}_{j-1,m} \tag{2.24}$$

The following limit is considered to show under what conditions does the partial sum (2.24) converge to the inverse of $(\mathbf{I}-\mathbf{T})$:

$$\lim_{m\to\infty}(\mathbf{I}-\mathbf{T})\mathbf{S}_{j,m}=\lim_{m\to\infty}\left(\mathbf{S}_{j,m}-\mathbf{T}\mathbf{S}_{j,m}\right)=\mathbf{I}-\lim_{m\to\infty}\mathbf{P}_{j,m+1} \tag{2.25}$$

Eq. (2.25) shows that $\mathbf{S}_{j,m}$ converges to $(\mathbf{I}-\mathbf{T})^{-1}$ if and only if

$$\lim_{m\to\infty}\mathbf{P}_{j,m+1}=\lim_{m\to\infty}\left((1-\alpha_j)\mathbf{P}_{j-1,m}+\alpha_j\mathbf{P}_{j-1m+1}\right)=\mathbf{0} \tag{2.26}$$

For the reasons discussed next, this recursion is applied at most n times, where n is the problem dimension.

2.3.2.4 Selection of parameters

Once the less restrictive convergence conditions of Eqs. (2.18), (2.22) and (2.26) are available, an strategy to select the optimal values of the parameters $\alpha_1, \alpha_2, \ldots, \alpha_n$ is required.

Consider the basis $\{\mathbf{u}_i\}_{i=1}^n$ of eigenvectors of matrix $\mathbf{T}$, associated to eigenvalues $\{\lambda_i\}_{i=1}^n$ (over the complex field $\mathbb{C}$, any matrix $\mathbf{T}$ either *i)* diagonalises or *ii)* is arbitrarily close to one with distinct eigenvalues that does).

By expressing an arbitrary vector $\mathbf{v}$ (see condition 2 in theorem of section 3.1) in this eigenvector basis, $\mathbf{v} = a_1\mathbf{u}_1 + a_2\mathbf{u}_2 + \cdots a_n\mathbf{u}_n$, one gets

$$\mathbf{T}^k\mathbf{v} = a_1\lambda_1^k\mathbf{u}_1 + a_2\lambda_2^k\mathbf{u}_2 + \cdots a_n\lambda_n^k\mathbf{u}_n \tag{2.27}$$

If $|\lambda_i| < 1$ for $i = 1, \ldots, n$, then theorem in section 3.1 applies. Assume now that eigenvalue λ_1 violates this condition, $|\lambda_1| > 1$, so the Neumann series does not converge. Then, for the one-parameter modification of section 2.3.2.1,

$$\mathbf{P}_{1,m+1}\mathbf{v} = a_1\Big((1-\alpha_1) + \alpha_1\lambda_1\Big)\lambda_1^m\mathbf{u}_1 + \cdots a_n\Big((1-\alpha_1) + \alpha_1\lambda_n\Big)\lambda_n^m\mathbf{u}_n \tag{2.28}$$

To cancel out the divergent term $\lambda_1^m\mathbf{u}_1$, the accompanying scalar should be zero:

$$(1-\alpha_1) + \alpha_1\lambda_1 = 0 \Longrightarrow \alpha_1 = \frac{1}{1-\lambda_1} \tag{2.29}$$

By applying the same argument recursively for each additional eigenvalue that violates the constraint, one gets

$$\alpha_1 = \frac{1}{1-\lambda_1}\,;\ \alpha_2 = \frac{1}{1-\lambda_2}\,;\cdots;\,\alpha_n = \frac{1}{1-\lambda_n} \tag{2.30}$$

Remarks:

1. If $|\lambda_i| < 1$, the modification step with coefficient α_i is not strictly necessary for convergence, but it does accelerate the convergence. This can also be seen in Appendix A.

2. In fact, $\alpha_i = 1/(1-\lambda_i)$ are the eigenvalues of $(\mathbf{I}-\mathbf{T})^{-1}$; it is not surprising that incorporating this information into the iterative algorithm improves the convergence.

2.3.3 Analysis of different cases

2.3.3.1 Real transfer matrix

If the transfer matrix $\mathbf{T}$ is real, then its eigenvalues are either real or complex conjugate. Note that, in any case, matrices $\mathbf{I}-\mathbf{T}$ and $(\mathbf{I}-\mathbf{T})^{-1}$ are real.

2.3.3.1.1 All eigenvalues real If $\{\lambda_i\}_{i=1}^n \in \mathbb{R}$, then $\{\alpha_i\}_{i=1}^n \in \mathbb{R}$, and the weighted sum of powers of $\mathbf{T}$ indeed results in a *real* matrix $(\mathbf{I}-\mathbf{T})^{-1}$.

2.3.3.1.2 Some complex conjugate eigenvalues Assume now that matrix $\mathbf{T}$ has one pair of complex conjugate eigenvalues, $\lambda_2 = \overline{\lambda}_1$. Then the corresponding factors are also complex conjugate, $\alpha_2 = \overline{\alpha}_1$. The two-parameter modification of section 2.3.2.2 results in

$$\begin{aligned}\mathbf{S}_{2,m} &= \mathbf{S}_{1,m-1} + \alpha_2\mathbf{P}_{1,m} = \mathbf{S}_{0,m-2} + \alpha_1\mathbf{T}^{m-1} + \alpha_2\Big((1-\alpha_1)\mathbf{T}^{m-1} + \alpha_1\mathbf{T}^m\Big)\\ &= \sum_{k=0}^{m-2}\mathbf{T}^k + \big[\alpha_1 + \alpha_2(1-\alpha_1)\big]\mathbf{T}^{m-1} + \alpha_2\alpha_1\mathbf{T}^m\\ &= \sum_{k=0}^{m-2}\mathbf{T}^k + 2\frac{1-\Re(\lambda_1)}{1-2\Re(\lambda_1)+|\lambda_1|^2}\mathbf{T}^{m-1} + \frac{1}{1-2\Re(\lambda_1)+|\lambda_1|^2}\mathbf{T}^m\end{aligned} \tag{2.31}$$

Note that, as expected, the weights are again real. The same argument applies if $\mathbf{T}$ has more pairs of complex conjugate eigenvalues.

2.3.3.2 Complex transfer matrix

If the transfer matrix $\mathbf{T}$ is complex, all the relevant objects are also complex (i.e. the eigenvalues λ_i, the parameters α_i, the weights in the weighted sum of powers of $\mathbf{T}$, matrix $\mathbf{I}-\mathbf{T}$ and its inverse...).

2.3.4 Recursive method

The modified partial sums of order j can be computed once the modified partial sums of order $j-1$ and the correction parameter α_j are known. From the definition in Eq. (2.16),

$$\mathbf{S}_{j-1,m} = \sum_{k=0}^{m-1}\mathbf{P}_{j-1,k} + \mathbf{P}_{j-1,m} = \mathbf{S}_{j-1,m-1} + \mathbf{P}_{j-1,m} \tag{2.32}$$

from where $\mathbf{P}_{j-1,m}$ can be obtained and substituted in the definition of $\mathbf{S}_{j,m}$ in Eq. (2.24):

$$\mathbf{S}_{j,m} = \alpha_j \mathbf{S}_{j-1,m} + (1-\alpha_j)\,\mathbf{S}_{j-1,m-1} \tag{2.33}$$

2.3.5 Explicit expression

An explicit expression of the solution can be obtained now by means of the repeated use of Eq. (2.33). It must be first particularised for $j = 1$,

$$\mathbf{S}_{1,m} = \alpha_1 \mathbf{S}_{0,m} + (1-\alpha_1)\,\mathbf{S}_{0,m-1} \tag{2.34}$$

For $j = 2$ one gets

$$\begin{aligned}\mathbf{S}_{2,m} &= \alpha_2 \mathbf{S}_{1,m} + (1-\alpha_2)\,\mathbf{S}_{1,m-1} \\ &= \alpha_1\alpha_2 \mathbf{S}_{0,m} + [\alpha_1\,(1-\alpha_2) + (1-\alpha_1)\,\alpha_2]\,\mathbf{S}_{0,m-1} + (1-\alpha_1)\,(1-\alpha_2)\,\mathbf{S}_{0,m-2}\end{aligned} \tag{2.35}$$

and, for $j = 3$

$$\mathbf{S}_{3,m} = \beta_{3,0}\mathbf{S}_{0,m} + \beta_{3,1}\mathbf{S}_{0,m-1} + \beta_{3,2}\mathbf{S}_{0,m-2} + \beta_{3,3}\mathbf{S}_{0,m-3} \tag{2.36}$$

where

$$\begin{aligned}\beta_{3,0} &= \alpha_1\alpha_2\alpha_3 \\ \beta_{3,1} &= \alpha_1\alpha_2\,(1-\alpha_3) + \alpha_1\,(1-\alpha_2)\,\alpha_3 + (1-\alpha_1)\,\alpha_2\alpha_3 \\ \beta_{3,2} &= \alpha_1\,(1-\alpha_2)\,(1-\alpha_3) + (1-\alpha_1)\,\alpha_2\,(1-\alpha_3) + (1-\alpha_1)\,(1-\alpha_2)\,\alpha_3 \\ \beta_{3,3} &= (1-\alpha_1)\,(1-\alpha_2)\,(1-\alpha_3)\end{aligned} \tag{2.37}$$

Inspecting the structure of Eqs. (2.35), (2.36) and (2.37) carefully, it is possible to derive a generic expression for $\mathbf{S}_{j,m}$ and coefficients $\beta_{j,i}$:

$$\mathbf{S}_{j,m} = \sum_{i=0}^{j} \beta_{j,i}\mathbf{S}_{0,m-i} \tag{2.38}$$

with $\beta_{j,i}$ expressed, in multi-index notation, as

$$\beta_{j,i} = \sum_{k=1}^{\binom{j}{i}} \boldsymbol{\alpha}^{\boldsymbol{\omega}_k}(\mathbf{1}-\boldsymbol{\alpha})^{\mathbf{1}-\boldsymbol{\omega}_k} \tag{2.39}$$

Eq. (2.39) has a conveniently compact expression thanks to the use of multi-index notation. For instance, for coefficient $\beta_{3,1}$ shown in Eq. (2.37),

$$\begin{aligned}\beta_{3,1} &= \alpha_1^1\alpha_2^1\alpha_3^0\,(1-\alpha_1)^0\,(1-\alpha_2)^0\,(1-\alpha_3)^1 \\ &+ \alpha_1^1\alpha_2^0\alpha_3^1\,(1-\alpha_1)^0\,(1-\alpha_2)^1\,(1-\alpha_3)^0 \\ &+ \alpha_1^0\alpha_2^1\alpha_3^1\,(1-\alpha_1)^1\,(1-\alpha_2)^0\,(1-\alpha_3)^0 \\ &= \boldsymbol{\alpha}^{\boldsymbol{\omega}_1}(\mathbf{1}-\boldsymbol{\alpha})^{\mathbf{1}-\boldsymbol{\omega}_1} + \boldsymbol{\alpha}^{\boldsymbol{\omega}_2}(\mathbf{1}-\boldsymbol{\alpha})^{\mathbf{1}-\boldsymbol{\omega}_2} + \boldsymbol{\alpha}^{\boldsymbol{\omega}_3}(\mathbf{1}-\boldsymbol{\alpha})^{\mathbf{1}-\boldsymbol{\omega}_3}\end{aligned} \tag{2.40}$$

with $\boldsymbol{\alpha} = (\alpha_1, \alpha_2, \alpha_3)$ and $\boldsymbol{\omega}_1 = (1,1,0)$, $\boldsymbol{\omega}_2 = (1,0,1)$, $\boldsymbol{\omega}_3 = (0,1,1)$.

Finally, Eq. (2.38) can be reorganised in order to express the partial sum in terms of the powers of the transfer matrix $\mathbf{T}$. This is, in fact, the main goal of the research: to show that the solution of the mechanical problem can be expressed as a linear combination of transmission paths. Indeed,

$$\boxed{\mathbf{S}_{j,m} = \sum_{k=0}^{m-j} \mathbf{T}^k + \sum_{k=m-j+1}^{m} \gamma_{m-k}\mathbf{T}^k} \tag{2.41}$$

with

$$\gamma_p = \sum_{i=0}^{p} \beta_{j,i} \qquad p = 0, \ldots, j-1 \tag{2.42}$$

Note that the first $m-j+1$ terms of $S_{j,m}$ are those of the original Neumann series, whereas the last j terms are weighted with the correction factors γ. These modifications are the higher-order paths.

A possible physical interpretation of Eq. (2.41) is that the first sum (lower-order paths) represents the action of the forces on the system, while the second sum (corrected higher-order paths) represents the reaction of the system. The important aspect here is that both response types have been expressed as addition of paths within the system. The whole Eq. (2.41) represents the steady equilibrium state of the mechanical system. At that point the external excitation and the movement of the mechanical system are coordinated in such a way that the excitation does not cause an increase of response.

If the spectral radius is larger than one, it leads to two infinites that compensate each other. If the spectral radius is less than one, the second sum is not relevant anymore. This agrees well with the fact that if the response is controlled by damping (which in general leads to spectral radius less than one), the high-order paths can be neglected because energy is lost in the passage through every path. In terms

of Eq. (2.41) this means that the correction (second sum) is not required to ensure convergence.

If $j = n$ terms of the series are modified (n is the problem dimension), the series convergence is ensured,

$$\lim_{m\to\infty} \mathbf{S}_{n,m} = (\mathbf{I} - \mathbf{T})^{-1} \tag{2.43}$$

This is because in the worst scenario all the matrix eigenvalues have a module larger than one. In this critical situation n modified terms of the series need to be added in order to treat the n eigenvalues. In practice, the inverse of $(I - T)$ is approximated by the partial sum $S_{n,m}$ for a finite value of m.

2.4 Numerical examples

The results of Section 2.3 are illustrated here by means of the simple system of Figure 2.2. It is a one-dimensional mechanism composed of eight masses: $m_1 = 100$ kg, $m_2 = 200$ kg, $m_3 = 300$ kg, $m_4 = 400$ kg, $m_5 = 500$ kg, $m_6 = 630$ kg, $m_7 = 700$ kg, $m_8 = 800$ kg. They are linked by means of springs with stiffnesses: $k_1 = 10^9$ N/m, $k_2 = 3\ 10^9$ N/m, $k_3 = 1.1\ 10^9$ N/m, $k_4 = 4\ 10^9$ N/m, $k_5 = 10^9$ N/m, $k_6 = 5\ 10^9$ N/m, $k_7 = 10^9$ N/m, $k_8 = 3\ 10^9$ N/m and $k_9 = 4\ 10^9$ N/m. The frequencies at which matrix $\mathbf{D}$ is singular are listed in Table 2.1. They can be understood as the vibration frequencies of each single mass when all the others are blocked. Table 2.1 also shows the coupled eigenfrequencies of the mechanical system (matrix $\mathbf{A}$). The dynamic stiffness matrix of the mechanical system is

$$\begin{bmatrix}
m_1\omega^2-(k_1+k_2+k_5) & k_2 & 0 & 0 & & & & \\
k_2 & m_2\omega^2-(k_2+k_3) & k_3 & 0 & & & & \\
0 & k_3 & m_3\omega^2-(k_3+k_8+k_4) & k_4 & & & & \\
0 & 0 & k_4 & m_4\omega^2-k_4 & \dots & & & \\
k_5 & 0 & k_8 & 0 & & & & \\
0 & 0 & 0 & 0 & & & & \\
0 & 0 & 0 & 0 & & & & \\
0 & 0 & 0 & 0 & & & &
\end{bmatrix}$$

$$\begin{bmatrix}
0 & k_5 & 0 & 0 \\
0 & 0 & 0 & 0 \\
k_8 & 0 & 0 & 0 \\
0 & 0 & 0 & 0 \\
\dots\ m_5\omega^2-(k_5+k_8+k_6) & k_6 & 0 & 0 \\
k_6 & m_6\omega^2-(k_6+k_7) & k_7 & 0 \\
0 & k_7 & m_7\omega^2-(k_7+k_9) & k_9 \\
0 & 0 & k_9 & m_8\omega^2-k_9
\end{bmatrix} \tag{2.44}$$

The accuracy of the iterative procedure described in Section 2.3.5 is measured by means of the error parameter

$$e = \frac{||\mathbf{A}^{-1}_{\text{approx}}\mathbf{A} - \mathbf{I}||_{\text{F}}}{n} = \frac{||\mathbf{S}_{j,m}(\mathbf{I} - \mathbf{T}) - \mathbf{I}||_{\text{F}}}{n} \tag{2.45}$$

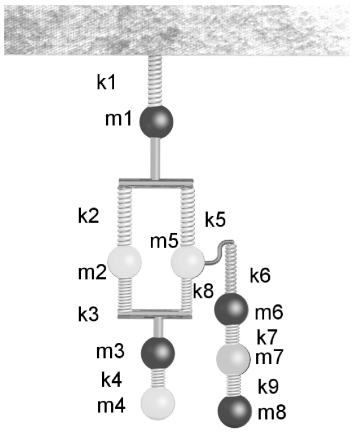

Figure 2.2: Sketch of the discrete system with eight masses.

matrix	1	2	3	4	5	6	7	8
D	355.9	425.4	491.2	503.3	675.2	720.6	827	1125
A	61.91	167.5	369.9	489.5	542.9	743.4	953.3	1250

Table 2.1: Eigenfrequencies of matrices **D** and **A** (in Hz).

where $||\bullet||_F$ is the Frobenius norm.

The reduced dimension of this toy problem allows a detailed study of its spectral properties. Their evolution with frequency f (with f a real number) is shown in Figure 2.3 for the undamped case. **A** can always be inverted (rank equals $n = 8$) except for the eigenfrequencies shown in Table 2.1. Matrix **T** is only singular if one node is completely detached from the others.

Another relevant aspect is the number of eigenvalues of the matrix **T** with modulus larger than one. In practice, it means that the spectral radius of matrix **T** is also larger than one and the Neumann series does not converge. In this system, it happens for a frequency range between 61.91 Hz and 1250 Hz. Figure 2.3 also provides information on the number of conjugate pairs of eigenvalues, linked with the modification of parameters of Section 2.3.3.1.2.

The results in Figure 2.4 illustrate how the solution of the mechanical problem can be obtained by the modified series proposed in Section 2.3. This means that the solution can be computed as a linear superposition of paths. The error measure e, defined in Eq. (2.45), is shown for several series depending on the number of modified

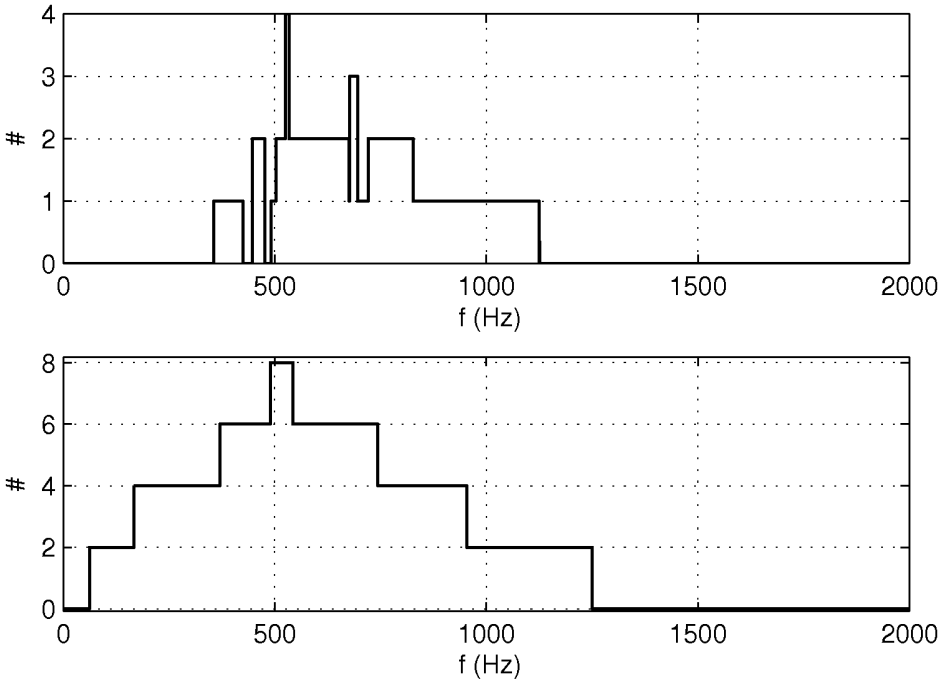

Figure 2.3: Description of the spectral properties of matrix **T**: number of conjugate pairs of eigenvalues (top); number of eigenvalues with modulus larger than one (bottom). Undamped case.

parameters (0, 4 or 8). The total length $m + 1$ of the series is 13.

The first thing to be noted is a strong correlation between the convergence of the series (small values of e) and the fact that the number of modified parameters is equal to or larger than the number of eigenvalues with modulus larger than one. See for example, the improvement obtained for the series with four modified parameters below 350 Hz and above 900 Hz. This is in agreement with the fact that in this frequency range four eigenvalues of matrix **T** have modulus larger than one. When (all) eight parameters are modified, the convergence is improved in the whole frequency range. Note, however, that the error is large around the frequencies where **D** is singular. For larger frequencies all the series converge as expected, even if no parameter is modified. However, even modifying only some parameters largely reduces the error at high frequencies where e has a very small value close to the numerical tolerance.

The non-convergent frequencies are also improved.

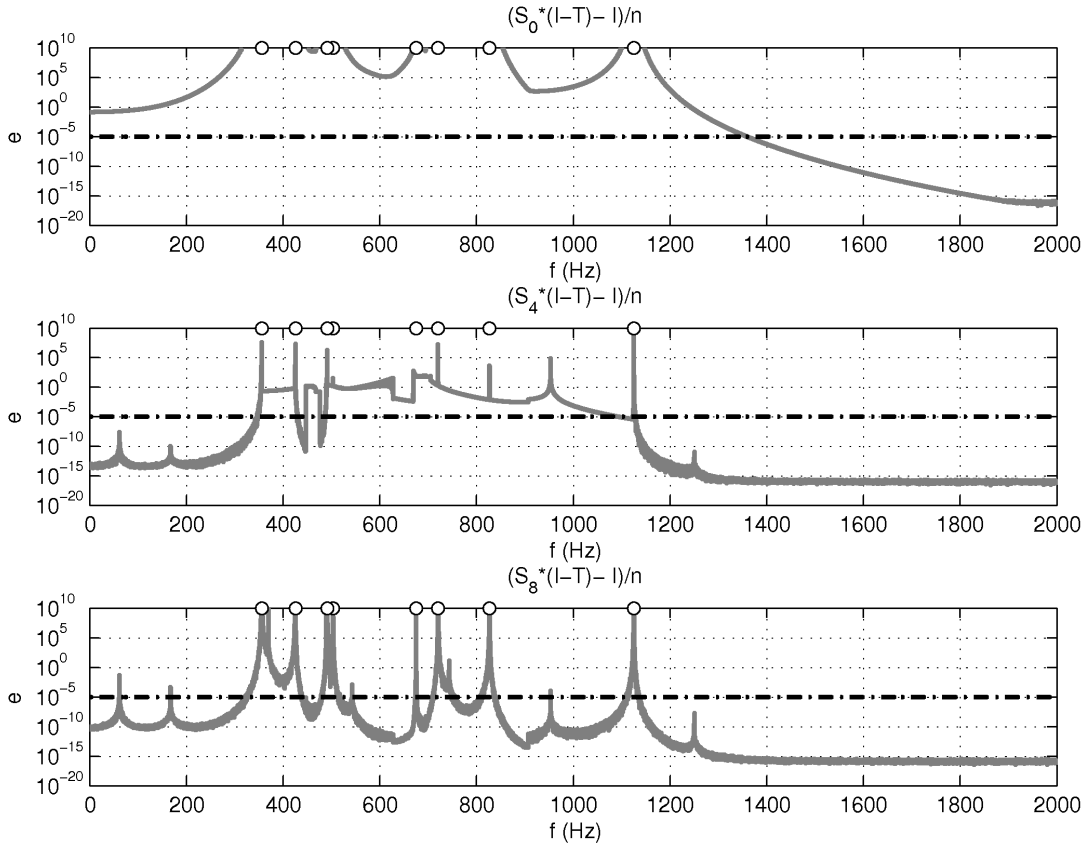

Figure 2.4: Difference between the exact solution and the solution obtained with the series. Influence of the number of modified parameters: 0 (unmodified Neumann series), 4 and 8. The total length $m+1$ is 13. The system is undamped.

The same mechanical system but with a hysteretic damping of 4% in all the springs is considered. Figure 2.5 shows the spectral characteristics of the damped transfer matrix. Two important differences must be noted: *i)* the matrix is not singular at any real frequencies; *ii)* the eigenvalues are not complex conjugate. The frequency range where some eigenvalues have modulus larger than one is very similar to the undamped case.

Figure 2.6 shows the influence of damping in the results. The general trend is similar to the undamped case. However, the effect of the eigenfrequencies of the matrices $\mathbf{D}$ and $\mathbf{A}$ is less important.

Figure 2.7 shows a comparison between the exact value of the global transfer

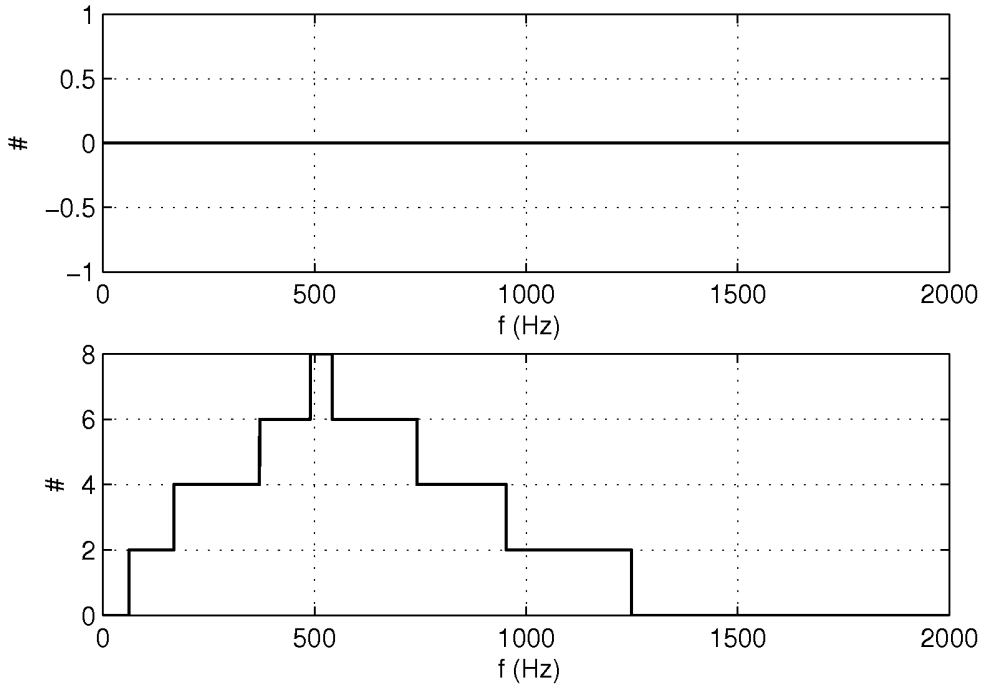

Figure 2.5: Description of the spectral properties of matrix $\mathbf{T}$: number of conjugate pairs of eigenvalues (top); number of eigenvalues with modulus larger than one (bottom). With an hysteretic damping of 4% in all the springs.

matrix $\mathbf{T}^G$ and the approximation obtained with the unmodified Neumann series and the Neumann series with all required correction parameters ($n = 8$). The coefficient t^G_{14} is shown. It represents the displacement of mass number 4 for an unity force at mass 1. The exact value is obtained as detailed in Magrans (1981). The unmodified Neumann series diverges in the frequency interval where the spectral radius of the system matrix is larger than one. On the contrary, the modified Neumann series performs a very good reconstruction of the exact value. The inaccuracies of the modified series are mainly found at the frequencies where the matrix $\mathbf{D}$ is singular and the system is undamped. The error peaks around the eigenfrequencies of the mechanical system (matrix $\mathbf{A}$ singular) are smaller. Damping drastically reduces the error peaks of both types.

The error measure of Eq. (2.45) is global. However it is interesting to note that

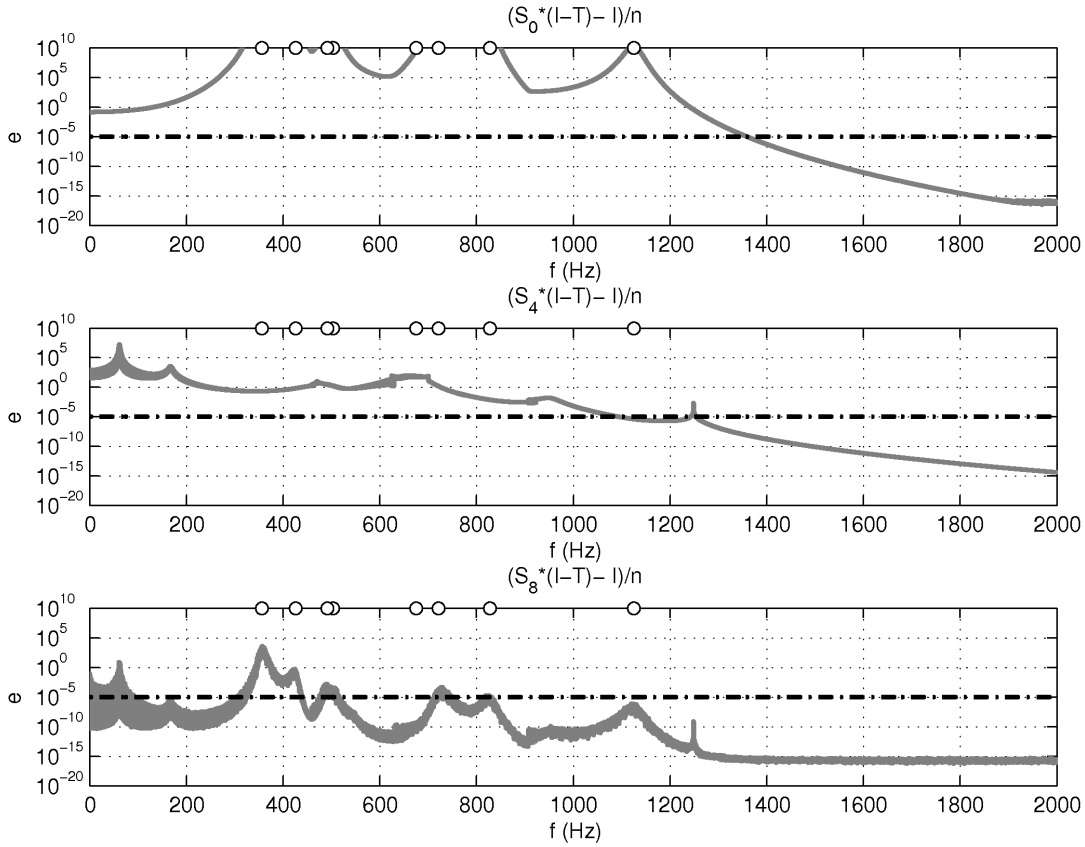

Figure 2.6: Difference between the exact solution and the solution obtained with the series. Influence of the number of modified parameters: 0 (unmodified Neumann series), 4 and 8. The total length $m+1$ is 13. The system has hysteretic damping of 4% in all the springs.

for most of the cases with large error, it is caused by only a few entries of the matrix $\mathbf{T}^G$ while the approximation of the others remains good enough. See for example Figure 2.8 where only the coefficients with significant error have been highlighted with a grey square.

2.5 Conclusions

The main interest of this research is theoretical and focused on the possibility of fully describing the solution of a mechanical problem by means of the superposition of transmission paths. It is conceived in the field of mechanics but the results, could be

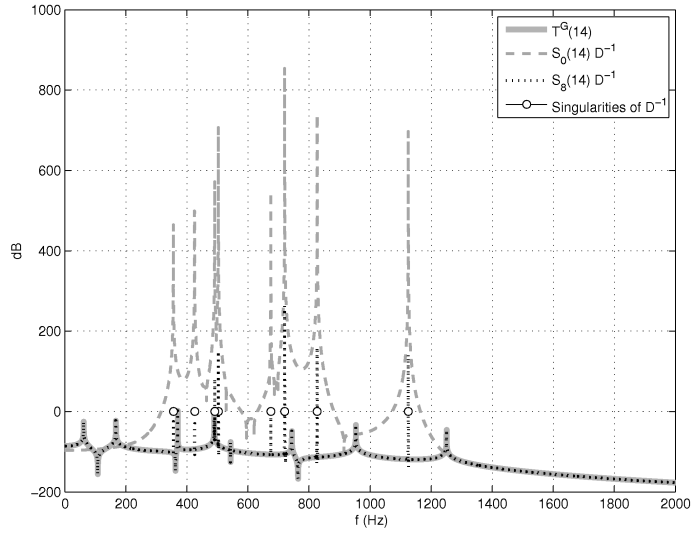

(a)

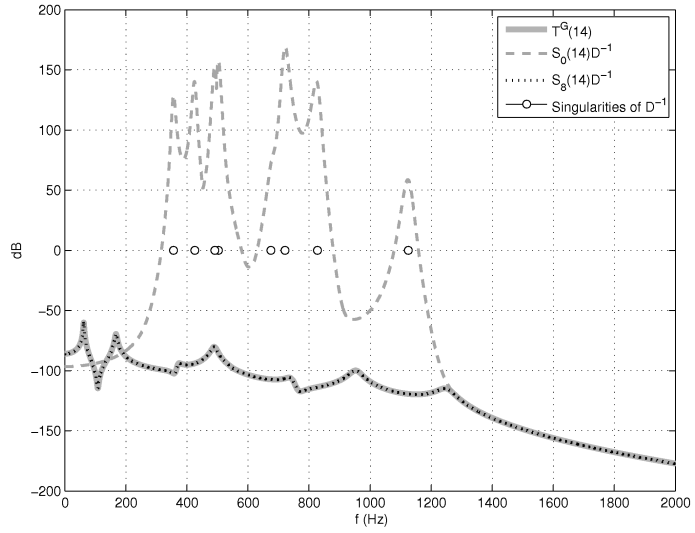

(b)

Figure 2.7: Value of the entry t_{14} of the global transfer matrix $\mathbf{T}^G$. Comparison between: exact computation; approximation obtained with the unmodified Neumann series; and approximation obtained with the modified Neumann series including all the required correction parameters ($n = 8$): (a) undamped mechanical system; (b) mechanical system with hysteretic damping of 4% in all the springs.

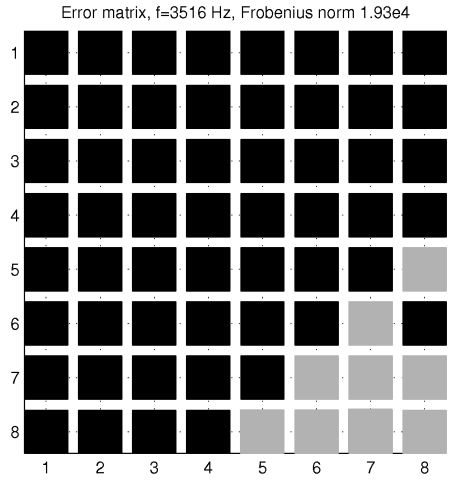

(a)

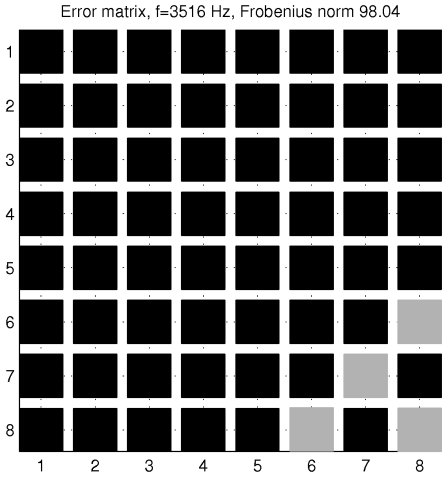

(b)

Figure 2.8: Representation of the 64 global transfer matrix $\mathbf{T}^G$ coefficients with an error larger than one (grey squares) in the comparison between the exact computation and approximation obtained with the modified Neumann series. Reconstruction of the matrix done for a frequency of 351.6 Hz: (a) Undamped mechanical system; (b) The mechanical system has hysteretic damping of 4% in all the springs.

used in other fields of science because the framework of analysis is very general. It is only required that the problem remains linear, formulated in terms of a linear system of equations and where the path concept has some physical meaning.

In the current form, the final results cannot be taken as a calculation tool. Some aspects such as the matrix powers and series are very useful for theoretical proofs but may have some numerical drawbacks (i.e. rounding errors, large number of operations, filling of matrices). For this reason, a way to apply the main theoretical conclusions to the practical use in systems with a large number of unknowns is required. The algorithms can only be directly applied for calculation in mechanical systems with not many unknowns or in the low-frequency range. The applicability depends on the specific physical problem and the modelling technique used (it is not the same if the signals are the unknowns in every node of a FE mesh or just a few measurements in key points of a structure to generate a direct or global transfer matrix).

The main achievements of the work are the formal definition of path and the proof of completeness of the description of the system behaviour by means of paths. The former establishes a framework where other modelling techniques can be identified; it is not only valid when working with transfer matrices. The latter leads to a generalisation of the Neumann series that converges whatever the spectral radius of the transfer matrix is. Moreover, a simplified recursive expression of the generalised series is provided.

The theoretical findings presented here are important by themselves because it was not clear that any solution of a mechanical system could be described by means of paths. Moreover, they also open a door for improvement of simulation techniques in mechanics.

2.A A link with iterative solvers: the acceleration of the Jacobi method

The Jacobi method Ciarlet et al. (1989) for the iterative solution of linear systems of equations is:

$$\mathbf{x}_{k+1} = \mathbf{D}^{-1}\mathbf{b} + \mathbf{D}^{-1}\left(-\mathbf{L} - \mathbf{U}\right)\mathbf{x}_k \tag{2.46}$$

It can be seen how its algebraic structure is the same as Eq. (2.5) and $\mathbf{T}$ plays the role of iteration matrix. A parallelism between the developed theory in the frame of the GTDT and the Jacobi method can be established.

The approximation $\mathbf{x}_{k+1}$ at the k iteration in the Jacobi method can be obtained directly from a Neumann series like in Eq. (2.10). So, the correction of the series proposed in Section 2.3.2 can be applied in order to modify the Jacobi iteration algorithm.

The method is applied to the solution of linear systems with matrices of dimension 300 that have the second largest eigenvalue not close to one. So, the discussion can be done by comparison of the standard Jacobi method with the proposed modification with only one parameter. As an example, see the results in Figure 2.9. There is a comparison between the conventional Jacobi method and its modification, taking into account the dominant eigenvalue in a one-parameter correction. The solution obtained with a direct solver is used as reference in order to compute the relative error. We can see how the correction always accelerates the convergence. This is more relevant when the dominant eigenvalue is close to one because in that case, the convergence of the Jacobi method is very slow and it makes the practical applicability of the solver very poor.

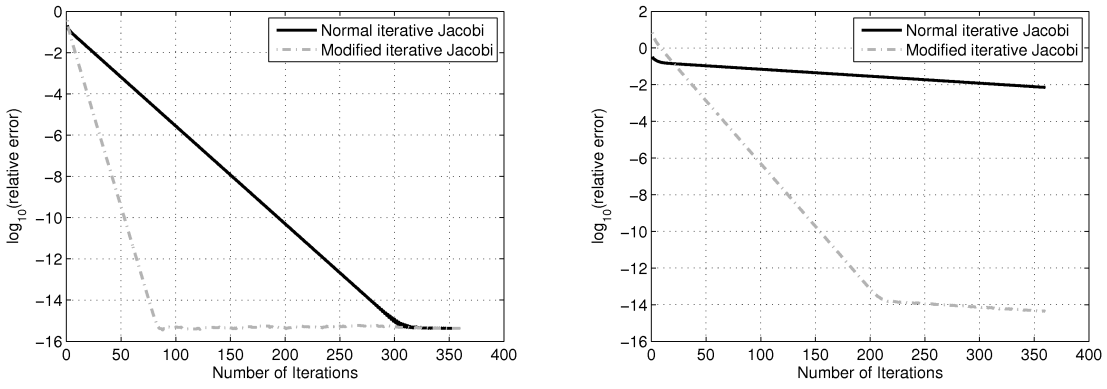

(a) (b)

Figure 2.9: Convergence of the Jacobi method compared with its one-parameter modification. The dimension of the matrix is 300 and the two eigenvalues of largest modulus are:(a) $|\lambda_1| = 0.89012$ and $|\lambda_2| = 0.66415|$; (b) $|\lambda_1| = 0.99129$ and $|\lambda_2| = 0.78518$.

Chapter 3

A subsystem identification method based on the path concept with coupling strength estimation[1]

3.1 Introduction

The subdivision of a mechanical system into subsystems according to their vibroacoustic response is a task required in several modelling methods or in order to better understand the behaviour of the mechanical system. A clear example is Statistical Energy Analysis (SEA, Le Bot (2015); Lyon (1975)) that requires, as a preliminary step, the definition of subsystems which satisfy several physical properties (high modal density, equipartition of energy between modes, equal probability of mode excitation, weak coupling between subsystems Culla and Sestieri (2006); Lafont et al. (2014, 2017)). Also from an experimental viewpoint it can be interesting to know which parts of a large system (train coach, building, airplane) can be tested in the laboratory isolated from the other parts and the results will still be meaningful. A proper subsystem identification determines the quality in the estimation of modal parameters in the experimental or operational modal analysis Reynders and De Roeck (2008), a review of techniques for parameter and system identification from measured data can be found in Reynders (2012). Finally, the knowledge about subsystem plays

[1] Chapter based on the paper Magrans et al. (2018)

also an important role in the transfer path analysis and can determine which is the more appropriate technique to apply as well as the quality of the solution de Sitter et al. (2010); Gajdatsy et al. (2010); Oktav et al. (2017).

In this work we apply cluster analysis Magrans et al. (2016) in order to automatically define the subsystems in a vibroacoustic problem. The core of the method is based on the transfer matrices and their powers. This is representative of transmission paths inside the system.

Another goal of the proposal is to quantify the coupling strength between subsystems. To do this we define the coupling strength as the error committed if coupling is disregarded and each subsystem is solved isolatedly from the rest of subsystems: the larger the error, the larger the coupling strength. We do not attempt to give a strict definition of "weak coupling", because whether coupling between subsystems may be disregarded or not depends on the type of analysis: a certain relative error may be admissible for an industrial pre-project but not for the final design.

Some brief background concepts and the core idea of the method are explained in Section 3.3. The theoretical aspects and approach are illustrated by the numerical examples of Section 3.4. The concluding remarks of Section 3.5 close the chapter.

3.2 State of the art

As far as the identification of subsystems is concerned, several papers can be cited, all of them outside the field of paths.

Automatic subsystem identification in statistical energy analysis. First one is ref.Kassem et al. (2011). A vibro–acoustic local energy model is introduced based on the observation of the homogeneous vibroacoustic behaviour of the energy model throughout a given zone. Using this model an scalar valued centred quadratic mean criterion is defined allowing to evaluate the error if using the sub–structured problem. A second paper ref.Kovalevsky and Langley (2012). The paper proposal is to built a matrix with the squared Green functions. This matrix is supposed to be by blocks and with each block totally homogeneous in the ideal uncoupled case. From this point, the eigenvectors of A are evaluated and their degree of coincidence with the perfect uncoupled hypotheses is used to evaluate the subsystems.

Another, ref.Gagliardini et al. (2005),defines a transfer function from injected energy in one degree of freedom to energy on another degree of freedom. Based on

it and in a iterative way sets of similar points are selected changing the excitation point in each step. After to obtain groups of degrees of freedom obtained by this way two methods, first about the Entropy and the other on a called attraction force are used to refine the groups. The paper extends to find also the coupling factors in SEA. ref.Totaro and Guyader (2006) makes a detailed study about to characterize a mechanical system with only the kinetic energy based in a supposed equipartition of the energy with the strain energy. The conclusion is that both need to be used because in curved parts the strain energy may be more important and the kinetic energy can be more important in the free parts of the structure, corners, holes , etc. Then a matrix **E** (with N rows and M columns) composed by N energy transfer functions and M frequency lines is considered and each row is projected on the the P main eigenvectors of the cross correlation matrix coming from E. The components on this base for each row will be P numbers. From this P numbers a cluster strategy is used to find the subsystems and a called MIR value defining the similarity between two subsystems is used to decide the validity of the obtained subsystems classification . Finally in ref.Díaz-Cereceda et al. (2015) the system it is subdivided in cells with a size bigger than a semi wave length in the frequency being studied. Then each cell become a sample valued for each mode by the energy in the cell, normalized with the average energy in the system. A cluster analysis allows then choose the sets of samples with a minimum distance to get the subsystems.

3.3 Methodology

Our approach to automatically identify the subsystems is based on a combination of the powers of the transfer matrix **T** and a standard cluster analysis. $\mathbf{T}^k$ is a representation of the transmission paths inside the mechanical system. Detailed developments can be found in Magrans et al. (2017); Magrans (1984, 1993); Van der Seijs et al. (2016) and the main concepts required in this section are overviewed in Section 3.3.1. The main idea of the identification method is exposed in Section 3.3.3.1. This is done in a conceptual way that is sustained latter by the numerical examples of Section 3.4. Section 3.3.3.2 explains the relation between this path-based method and other more widely used criteria. Finally, an important aspect is addressed in Section 3.3.4: the estimation of the coupling strength between subsystems.

3.3.1 Overview of path analysis

The basic concepts of the GTDT method Magrans (1981) are briefly reviewed in Section 2.2.3

It has been proved in Magrans et al. (2017) that the inverse of the matrix $(\mathbf{I} - \mathbf{T})$ can be expressed as the limit of a matrix series as

$$(\mathbf{I} - \mathbf{T})^{-1} = \lim_{m \to \infty} \left(\sum_{k=0}^{m-n} \mathbf{T}^k + \sum_{k=m-n+1}^{m} \gamma_{m-k} \mathbf{T}^k \right) \tag{3.1}$$

The series in Eq. (3.1) is unconditionally convergent, without any constraint on the value of $||\mathbf{T}||$, if coefficients γ_{m-k} are properly chosen. For $||\mathbf{T}|| \geq 1$, Eq. (3.1) with the optimal choice of γ_{m-k} is convergent, whereas the standard Neumann series with $\gamma_{m-k} = 1$ diverges. For $||\mathbf{T}|| < 1$, on the other hand, both series are convergent, but the convergence is faster with the optimal γ_{m-k}. These aspects are discussed in detail in Magrans et al. (2017).

Eq. (3.1) as well as expressions for the coefficients γ_{m-k} are the main results in Magrans et al. (2017). They allow the generalisation of the path superposition idea to any linear mechanical system (and not only to those with convergent Neumann series). So, a theoretical procedure based on the path concept has now a solid basis. In the present research, this idea is applied to the formulation of an algorithm for automatic sub-structuring of mechanical systems.

3.3.2 Subsystems and transfer matrices

We define a subsystem as a set of nodes with similar path behaviour. The concept of node is very general, see Magrans et al. (2017): it may refer to a point in a continuous system, to a degree of freedom associated to that point, to a mass in a discrete system of masses and springs, to a subdomain of a continuous system,... In a computational model, for instance, "node" refers to the actual nodes of the finite element mesh, whereas in the laboratory a "node" is a point of excitation or measurement.

The transfer matrix $\mathbf{T}$ describes the *direct* signal transmission between nodes (that is, the first-order paths). How this matrix is obtained depends on the context: in a computational model, for instance, $\mathbf{T}$ is computed from the system matrix $\mathbf{A}$, or from a few selected nodes, see Section 3.4.4, whereas in the laboratory $\mathbf{T}$ is determined experimentally.

The powers $\mathbf{T}^k$ of the transfer matrix represent the k-order paths. If a k-order path remains inside a strongly connected zone, it is not attenuated: the entries in $\mathbf{T}^k$ that relate nodes in the same subsystem are large. On the contrary, if a k-order path passes through weakly connected subsystems it is attenuated, and the associated entries in $\mathbf{T}^k$ are small.

3.3.3 Subsystem identification by means of cluster analysis

3.3.3.1 How it works?

Based on the above discussion about the information carried by $\mathbf{T}^k$, our approach to identify subsystems consists of three simple steps:

1. Obtain (i.e. compute or measure) the transfer matrix $\mathbf{T}$.
   Iterative loop
   Set $k = 2$

2. Compute power $\mathbf{T}^k$ of the transfer matrix, $\mathbf{T}^k = \mathbf{T}^{k-1}\mathbf{T}$.

3. Perform a cluster analysis of the rows of $\mathbf{T}^k$.
   Set $k = k + 1$ and go to step 2.

The iterative loop is stopped when the clustering process is stable, that is, when the clusters of rows do not change as the power k increases. To attain a stable clustering in fewer iterations, power k may jump s units at each iteration, $\mathbf{T}^{k+s} = \mathbf{T}^k\mathbf{T}^s$. In the numerical example of Section 3.4.1, for instance, we have taken $s = 5$.

The clustering algorithm is similar to the one described in Díaz-Cereceda et al. (2015), but with one important difference: the elements are simply the rows of $\mathbf{T}^k$, and there is no need to divide the problem domain into cells nor to compute energies associated to those cells. The clustering process is hierarchical; this means that the rows of $\mathbf{T}^k$ are grouped progressively into sets of rows according to their correlation distance. As this distance increases, small sets of rows are grouped into larger sets. This clustering process can be graphically depicted as a tree diagram or dendrogram, see Figs. 3.7 and 3.19. The output of the algorithm is *i)* the optimal number of clusters, corresponding to the widest range of correlation distance (i.e. the longest branches in the dendrogram) and *ii)* the rows of $\mathbf{T}^k$ in each cluster. The clustering algorithm is described in the three companion videos of Figure 3.1.

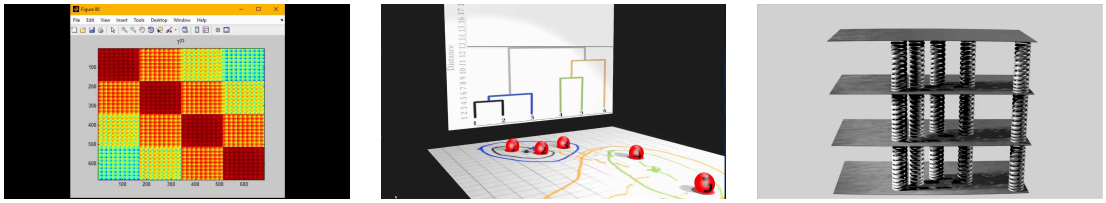

(a) (b) (c)

Figure 3.1: Screenshots of the three companion videos: (a) Relationship between the powers of the transfer matrix and the high-order paths; (b) Explanation of the dendrogram concept and the clustering process; (c) Illustration of the clustering algorithm by means of an example.

3.3.3.2 Why it works?

A simple explanation. The analysis is restricted here to systems composed of two subsystems. Consider first the case where these two subsystems are completely uncoupled, Figure 3.2(a). The transfer matrix is

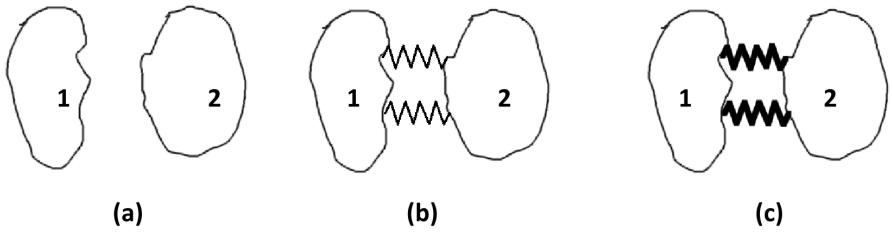

Figure 3.2: (a) Uncoupled subsystems; (b) Weakly coupled subsystems; (c) Strongly coupled subsystems

$$\mathbf{T} = \begin{pmatrix} \mathbf{T}_1 & \mathbf{0} \\ \mathbf{0} & \mathbf{T}_2 \end{pmatrix} \tag{3.2}$$

Note that the off-diagonal blocks in the transfer matrix (3.2) are zero because there is no coupling between subsystems 1 and 2. The transfer matrices $\mathbf{T}_1$ and $\mathbf{T}_2$ are typically sparse because not all nodes in subsystem 1 (or 2) are directly connected, by means of a first-order path, to all nodes in subsystem 1 (or 2). The k power of matrix $\mathbf{T}$ is

$$\mathbf{T}^k = \begin{pmatrix} \mathbf{T}_1^k & \mathbf{0} \\ \mathbf{0} & \mathbf{T}_2^k \end{pmatrix} \tag{3.3}$$

For k large enough, the block $\mathbf{T}_1^k$ and $\mathbf{T}_2^k$ (k-order paths in subsystems 1 and 2) are full matrices, so the sparsity pattern of matrix $\mathbf{T}^k$ is:

$$\text{pattern}\left(\mathbf{T}^k\right) = \begin{pmatrix} \bullet & \bullet & \bullet & \bullet & & & \\ \bullet & \bullet & \bullet & \bullet & & & \\ \bullet & \bullet & \bullet & \bullet & & & \\ \bullet & \bullet & \bullet & \bullet & & & \\ & & & & \bullet & \bullet & \bullet \\ & & & & \bullet & \bullet & \bullet \\ & & & & \bullet & \bullet & \bullet \end{pmatrix}$$

A cluster analysis of the rows of $\mathbf{T}^k$ readily detects that there are two different types of rows, namely

$$\begin{pmatrix} \bullet & \bullet & \bullet & \bullet & & & \end{pmatrix} \text{ and } \begin{pmatrix} & & & & \bullet & \bullet & \bullet \end{pmatrix}$$

and identifies the two subsystems. Note that this approach also works if the system nodes are not ordered (first nodes in subsystem 1, then nodes in subsystem 2). Indeed for an arbitrary ordering the sparsity pattern of $\mathbf{T}^k$ is

$$\text{pattern}\left(\mathbf{T}^k\right) = \begin{pmatrix} \bullet & & \bullet & \bullet & & & \bullet \\ & \bullet & & & \bullet & \bullet & \\ \bullet & & \bullet & \bullet & & & \bullet \\ \bullet & & \bullet & \bullet & & & \bullet \\ & \bullet & & & \bullet & \bullet & \\ & \bullet & & & \bullet & \bullet & \\ \bullet & & \bullet & \bullet & & & \bullet \end{pmatrix}$$

and the two different types of rows are now

$$\begin{pmatrix} \bullet & & \bullet & \bullet & & & \bullet \end{pmatrix} \text{ and } \begin{pmatrix} & \bullet & & & \bullet & \bullet & \end{pmatrix}$$

Consider now the case of two weakly coupled subsystems, see Figure 3.2(b). The transfer matrix is

$$\mathbf{T} = \begin{pmatrix} \mathbf{T_1} & \epsilon\mathbf{T}_{12} \\ \epsilon\mathbf{T}_{21} & \mathbf{T}_2 \end{pmatrix} \tag{3.4}$$

Where the factor $0 < \epsilon < 1$ in the off-diagonal blocks reflects the weak coupling. Power 2 of matrix $\mathbf{T}$ is

$$\mathbf{T}^2 = \begin{pmatrix} \mathbf{T}_1^2 + \epsilon^2\mathbf{T}_{12}\mathbf{T}_{21} & \epsilon\mathbf{T}_{12,2} \\ \epsilon\mathbf{T}_{21,2} & \mathbf{T}_2^2 + \epsilon^2\mathbf{T}_{21}\mathbf{T}_{12} \end{pmatrix} \simeq \begin{pmatrix} \mathbf{T}_1^2 & \epsilon\mathbf{T}_{12,2} \\ \epsilon\mathbf{T}_{21,2} & \mathbf{T}_2^2 \end{pmatrix} \tag{3.5}$$

where $\mathbf{T}_{12,2} = \mathbf{T}_1\mathbf{T}_{12} + \mathbf{T}_{12}\mathbf{T}_2$ and $\mathbf{T}_{21,2} = \mathbf{T}_{21}\mathbf{T}_1 + \mathbf{T}_2\mathbf{T}_{21}$. Note that only the leading term in the diagonal blocks is retained in the approximate expression of $\mathbf{T}^2$. It is straightforward to show that power k is

$$\mathbf{T}^k = \begin{pmatrix} \mathbf{T}_1^k & \epsilon\mathbf{T}_{12,k} \\ \epsilon\mathbf{T}_{21,k} & \mathbf{T}_2^k \end{pmatrix} \tag{3.6}$$

with appropriate definitions of $\mathbf{T}_{12,k}$ and $\mathbf{T}_{21,k}$. Eq. (3.6) shows that the weak coupling between subsystems 1 and 2 is visible in k-order paths. For k large enough, all four blocks in $\mathbf{T}^k$ are full matrices and the sparsity pattern of $\mathbf{T}^k$ is

$$\text{pattern } \left(\mathbf{T}^k\right) = \begin{pmatrix} \bullet & \bullet & \bullet & \bullet & \circ & \circ & \circ \\ \bullet & \bullet & \bullet & \bullet & \circ & \circ & \circ \\ \bullet & \bullet & \bullet & \bullet & \circ & \circ & \circ \\ \bullet & \bullet & \bullet & \bullet & \circ & \circ & \circ \\ \circ & \circ & \circ & \circ & \bullet & \bullet & \bullet \\ \circ & \circ & \circ & \circ & \bullet & \bullet & \bullet \\ \circ & \circ & \circ & \circ & \bullet & \bullet & \bullet \end{pmatrix}$$

where the black dots $\bullet$ represent larger numerical values than the void dots $\circ$. A cluster analysis of the rows of $\mathbf{T}^k$ detects the different types of rows, irrespective of the node ordering. As the coupling between the two subsystems increases, the block structure of $\mathbf{T}^k$ becomes less clear. In the limit case of two strongly coupled subsystems, see Figure 3.2 (c), they are regarded as a monolithic system.

Local vs global eigenmodes. Different definitions of coupling may be found in the literature Le Bot (2015); Ungar (1966). Some of them Fahy and Gardonio (2007) are based on the nature of the eigenmodes: subsystems 1 and 2 are regarded as weakly coupled if the vibration eigenmodes are localised in subsystems 1 or 2, see Figure 3.3(b), whereas they are considered to be strongly coupled if vibration eigenmodes are global, see Figure 3.3(c). We show here that our approach based on the cluster analysis of the powers of $\mathbf{T}$ is consistent with this definition of coupling based in eigenmodes. Consider the basis $\{\mathbf{v}_i\}_{i=1}^n$ of eigenvectors of the transfer matrix $\mathbf{T}$, associated to eigenvalues $\{\lambda_i\}_{i=1}^n$,

$$\mathbf{T}\mathbf{v}_i = \lambda_i\mathbf{v}_i \qquad i = 1, \ldots, n \tag{3.7}$$

and the corresponding eigendecomposition

$$\mathbf{T} = \mathbf{V}\mathbf{\Lambda}\mathbf{V}^{-1} \tag{3.8}$$

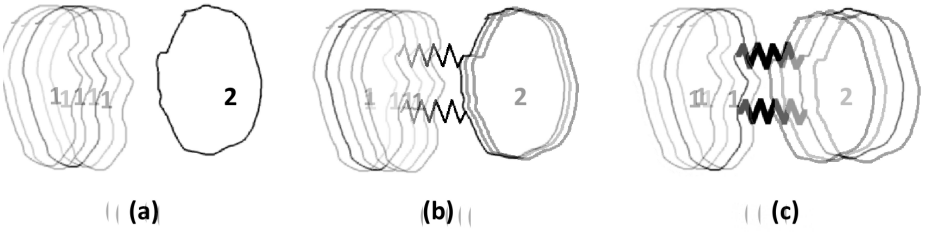

Figure 3.3: (a) Uncoupled subsystems modes; (b) Weakly coupled subsystems modes; (c) Strongly coupled subsystems modes

where $\mathbf{\Lambda}$ is a diagonal matrix of eigenvalues and $\mathbf{V}$ is the matrix of eigenvectors:

$$\mathbf{\Lambda} = \begin{pmatrix} \lambda_1 & & & \\ & \lambda_2 & & \\ & & \ddots & \\ & & & \lambda_n \end{pmatrix}; \quad \mathbf{V} = \begin{pmatrix} | & | & \dots & | \\ | & | & \dots & | \\ \mathbf{v}_1 & \mathbf{v}_2 & \dots & \mathbf{v}_n \\ | & | & \dots & | \end{pmatrix} \tag{3.9}$$

From Eq. (3.8), the powers of matrix $\mathbf{T}$ can be expressed as

$$\mathbf{T}^k = \left(\mathbf{V}\mathbf{\Lambda}\mathbf{V}^{-1}\right)\left(\mathbf{V}\mathbf{\Lambda}\mathbf{V}^{-1}\right)\cdots\left(\mathbf{V}\mathbf{\Lambda}\mathbf{V}^{-1}\right) = \mathbf{V}\mathbf{\Lambda}^k\mathbf{V}^{-1} \tag{3.10}$$

Eq. (3.8) and Eq. (3.10) show that any block structure that matrix $\mathbf{T}$ or $\mathbf{T}^k$ may have is associated to matrix $\mathbf{V}$, because matrix $\mathbf{\Lambda}$ is diagonal. By taking into account that the inverse of any (almost) block-diagonal matrix is another (almost) block-diagonal matrix, one can conclude that:

- For two uncoupled subsystems, the pattern of $\mathbf{V}$ is

$$\text{pattern } (\mathbf{V}) = \begin{pmatrix} \bullet & \bullet & \bullet & \bullet & & \\ \bullet & \bullet & \bullet & \bullet & & \\ \bullet & \bullet & \bullet & \bullet & & \\ \bullet & \bullet & \bullet & \bullet & & \\ & & & & \bullet & \bullet & \bullet \\ & & & & \bullet & \bullet & \bullet \\ & & & & \bullet & \bullet & \bullet \end{pmatrix} \tag{3.11}$$

  so eigenvectors of $\mathbf{T}$ are fully local.

- For two weakly coupled subsystems, the pattern of $\mathbf{V}$ is

$$\text{pattern } (\mathbf{V}) = \begin{pmatrix} \bullet & \bullet & \bullet & \bullet & \circ & \circ & \circ \\ \bullet & \bullet & \bullet & \bullet & \circ & \circ & \circ \\ \bullet & \bullet & \bullet & \bullet & \circ & \circ & \circ \\ \bullet & \bullet & \bullet & \bullet & \circ & \circ & \circ \\ \circ & \circ & \circ & \circ & \bullet & \bullet & \bullet \\ \circ & \circ & \circ & \circ & \bullet & \bullet & \bullet \\ \circ & \circ & \circ & \circ & \bullet & \bullet & \bullet \end{pmatrix} \tag{3.12}$$

  so eigenvectors are localised, see Figure 3.3(b).

- For two strongly coupled subsystems, matrix $\mathbf{V}$ does not have a clear block structure, so eigenvectors of $\mathbf{T}$ are global, see Figure 3.3(c).

Note that the above discussion is based on the eigenvectors of $\mathbf{T}$, not on the eigenmodes of the mechanical system. However, as discussed in Appendix A, these two sets of vectors are closely related.

Contrast of the transfer matrix. Consider the transfer matrix for a system composed of two subsystems

$$\mathbf{T} = \begin{pmatrix} \mathbf{T}_1 & \alpha\mathbf{T}_{12} \\ \alpha\mathbf{T}_{21} & \mathbf{T}_2 \end{pmatrix} \tag{3.13}$$

with $\alpha = 0$ for uncoupled subsystems $0 < \alpha = \epsilon < 1$ for weakly coupled subsystems and $\alpha \simeq 1$ for strongly coupled subsystems. We assume that the blocks $\mathbf{T}_1$ and $\mathbf{T}_2$ are invertible and define the contrast of $\mathbf{T}$ as

$$\text{contrast}_{12} = \frac{1}{\|\mathbf{T}_1^{-1}\alpha\mathbf{T}_{12}\|} = \frac{1}{\alpha\|\mathbf{T}_1^{-1}\mathbf{T}_{12}\|} \tag{3.14}$$

$$\text{contrast}_{21} = \frac{1}{\|\mathbf{T}_2^{-1}\alpha\mathbf{T}_{21}\|} = \frac{1}{\alpha\|\mathbf{T}_2^{-1}\mathbf{T}_{21}\|} \tag{3.15}$$

The contrast provides a simple, scalar measure of the strength of the coupling between subsystems: the greater the contrast, the weaker the coupling. Note that the contrast of a matrix is invariant under scalar multiplication,

$$\text{contrast}(a\mathbf{T}) = \text{contrast}(\mathbf{T}) \quad \text{for any} \quad a \neq 0 \tag{3.16}$$

so it provides an scale-independent measure of the block diagonal dominance of a matrix. We examine now the contrast of matrix $\mathbf{T}^k$. Eq. (3.10) can be recast as

$$\mathbf{T}^k = \mathbf{V}\mathbf{\Lambda}^k\mathbf{V}^{-1} = \sum_{i=1}^{n} \lambda_i^k \mathbf{v}_i \mathbf{u}_i^T \approx \lambda_n^k \mathbf{v}_n \mathbf{u}_n^T \tag{3.17}$$

where λ_i and $\mathbf{v}_i$ are respectively the eigenvalues and the eigenvectors of $\mathbf{T}$, see Eq. (3.9), and $\mathbf{u}_i^T$ are rows of the matrix $\mathbf{V}^{-1}$. Note that $\mathbf{T}$ may be approximated, for k large enough, by the term associated to the dominant eigenvalue λ_n.

From Eqs. (3.16) and (3.17), it follows that

$$\text{contrast}\left(\mathbf{T}^k\right) \approx \text{contrast}\left(\lambda_n^k \mathbf{v}_n \mathbf{u}_n^T\right) = \text{contrast}\left(\mathbf{v}_n \mathbf{u}_n^T\right) \tag{3.18}$$

Equation (3.18) shows that irrespectively of the dominant eigenvalue λ_n, the contrast of $\mathbf{T}^k$ tends to a limit when k growths. From a practical point of view, this means that there is not need to fine-tune the value of k: any value large enough may be used. Furthermore, even if $\mathbf{T}^k$ tends to ∞ when its norm is larger than one, the contrast will not: the method is stable.

3.3.4 Estimation of the coupling strength

An important aspect is to quantify the degree of coupling between subsystems. In other words, the correctness of the solution obtained if a subsystem is considered as isolated from the other parts.

Several definitions of the weak coupling between subsystems exist, see for example Le Bot (2015); Ungar (1966). Consider a mechanical system described as

$$\begin{pmatrix} V_1 \\ V_2 \end{pmatrix} = \begin{pmatrix} Y_{11} & Y_{12} \\ Y_{21} & Y_{22} \end{pmatrix} \begin{pmatrix} F_1 \\ F_2 \end{pmatrix} \tag{3.19}$$

where Y are the admittances, V the velocities and F the forces, and the admittance integrals defined by integration of the whole frequency range

$$I_{jk} \equiv \int_{-\infty}^{\infty} |Y_{jk}|^2 d\omega \tag{3.20}$$

Ungar Ungar (1966) defines that two systems are weakly coupled if the transfer admittance integrals are equal, $I_{12} = I_{21}$, and their values are smaller than those of the self-admittance integrals I_{11} and I_{22}. Moreover, the transfer impedances and admittances $Z_{12}, Z_{21}, Y_{12}, Y_{21}$, must not affect the values of I_{11} and I_{22} significantly. That definition is provided in terms of the energy and integrated in the frequency domain. This is less restrictive that conditions that must be satisfied at each frequency.

An estimation of the coupling between subsystems can also be done through the analysis of the largest eigenvalue of a coupling matrix Gagliardini and Guyader (2000).

The matrix representation of the mechanical system must be reorganised as proposed in Maidanik (1976) which allows a separation of the coupling part. A similar block matrix structure, combined with the path concept, is considered here in order to define the coupling strength between subsystems. We consider a linear system of equations partitioned in coupled blocks

$$\begin{pmatrix} \mathbf{A}_{11} & \mathbf{A}_{12} \\ \mathbf{A}_{21} & \mathbf{A}_{22} \end{pmatrix} \begin{pmatrix} \mathbf{x}_1 \\ \mathbf{x}_2 \end{pmatrix} = \begin{pmatrix} \mathbf{b}_1 \\ \mathbf{b}_2 \end{pmatrix} \tag{3.21}$$

where $\mathbf{A}_{11}$ and $\mathbf{A}_{22}$ are the dynamical matrices of two sets of degrees of freedom and $\mathbf{A}_{12}$ and $\mathbf{A}_{21}$ their coupling matrices. Our purpose is to establish which is the difference between the fully coupled solution and the solution of the uncoupled system

$$\begin{pmatrix} \mathbf{A}_{11} & \mathbf{0} \\ \mathbf{0} & \mathbf{A}_{22} \end{pmatrix} \begin{pmatrix} \mathbf{x}_1^{'} \\ \mathbf{x}_2^{'} \end{pmatrix} = \begin{pmatrix} \mathbf{b}_1 \\ \mathbf{b}_2 \end{pmatrix} \tag{3.22}$$

The linear system in (3.21) can be rewritten in terms of transfer matrices

$$\begin{pmatrix} \mathbf{x}_1 \\ \mathbf{x}_2 \end{pmatrix} = \begin{pmatrix} \mathbf{A}_{11} & \mathbf{0} \\ \mathbf{0} & \mathbf{A}_{22} \end{pmatrix}^{-1} \begin{pmatrix} \mathbf{b}_1 \\ \mathbf{b}_2 \end{pmatrix} - \begin{pmatrix} \mathbf{0} & \mathbf{A}_{11}^{-1}\mathbf{A}_{12} \\ \mathbf{A}_{22}^{-1}\mathbf{A}_{21} & \mathbf{0} \end{pmatrix} \begin{pmatrix} \mathbf{x}_1 \\ \mathbf{x}_2 \end{pmatrix} \tag{3.23}$$

which is useful in order to relate the difference between the coupled solution in the subsystem 1, $\mathbf{x}_1$ and the uncoupled solution $\mathbf{x}_1^{'}$

$$\mathbf{x}_1 = \mathbf{x}_1^{'} - \mathbf{A}_{11}^{-1}\mathbf{A}_{12}\mathbf{x}_2 \tag{3.24}$$

If the force is applied on subsystem 1 and there is no local resonance on subsystem 2, $\|\mathbf{x}_1\| > \|\mathbf{x}_2\|$ and then

$$\frac{\|\mathbf{x}_1 - \mathbf{x}_1^{'}\|}{\|\mathbf{x}_1\|} \leq \|\mathbf{A}_{11}^{-1}\mathbf{A}_{12}\| = \frac{1}{\text{contrast}_{12}} \tag{3.25}$$

It is clear from Eq. (3.25) that the contrast of matrix $\mathbf{A}$ is a measure of the coupling between subsystems 1 and 2: the greater the contrast, the more accurate the isolated solution.

3.4 Numerical examples and analysis

The ideas exposed in Section 3.3 are illustrated by means of mechanical and acoustic problems solved in the frequency domain (steady harmonic).

3.4.1 Example 1: Two plates connected by means of five (soft) springs

The first example consists of two plates of different size and linked through five springs, see Figure 3.4. The geometric and mechanical properties of the plates are listed in Table 3.1 and the stiffness of the springs and their positions are summarized in Table 3.2 ('x' and 'y' coordinate axes shown in Figure 3.7). The results are shown for an excitation frequency of 100 Hz. The system matrix **A** is obtained with finite differences, using a regular grid (spacing 0.1 m) in both plates.

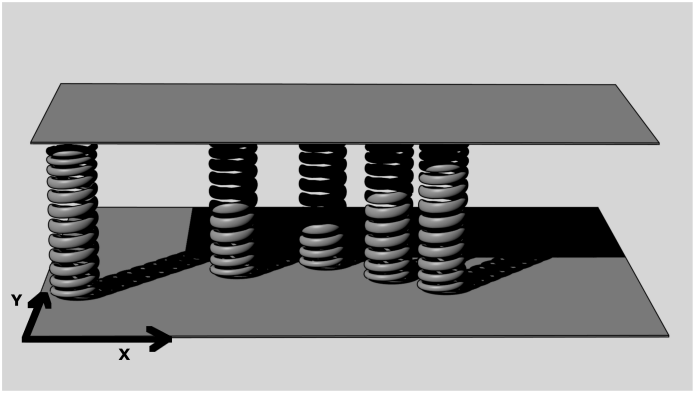

Figure 3.4: Two plates and five springs as described in Table 3.2. Computation at 100 Hz.

Material	ρ_v (kg/m^3)	ν	E (Pa)	L_x (m)	L_y (m)	h (m)
Concrete	2000	0.2	$2 \cdot 10^{10}$	2	2	0.03
Concrete	2000	0.2	$2 \cdot 10^{10}$	1	2	0.03

Table 3.1: Geometric and mechanical properties of the two plates (ρ_v is the volumetric density, ν is the Poisson's ratio, E is the Young modulus, L_x, L_y the plate dimensions and h the plate thickness).

Figure 3.5 shows the sparsity pattern of the transfer matrix of the system **T**. Note that a natural nodal ordering is used (first the nodes in the bottom plate, then the nodes in the top plate). This facilitates the interpretation of results, but, as discussed in Section 3.3.3.2, is not required by the clustering algorithm.

Figure 3.6 shows power $k = 21$ of the transfer matrix that clearly presents a block structure. The coefficients of the diagonal blocks are representative of paths that start

Spring	K (N/m)	x (m)	y (m)
1	$2 \cdot 10^5$	0.3	0.4
2	$2 \cdot 10^5$	0.6	0.1
3	$2 \cdot 10^5$	0.2	0.4
4	$2 \cdot 10^5$	0.5	0.5
5	$2 \cdot 10^5$	0.1	0.1

Table 3.2: Stiffness K and position of each spring that connects the plates.

and end at the same plate. On the contrary, the coefficients in the out-of-diagonal or coupling blocks represent paths that begin and end in different plates. In this case the nodal ordering helps to see the block structure.

Figure 3.7 illustrates the clustering process. The dendrogram identifies two clusters of nodes, coloured in red and blue, that correspond to the two plates. Note that the lower part of the dendrogram is barely visible, because the correlation distance between nodes in the same plate is much smaller than the correlation distance between the two plates.

We have checked that the vibration fields in plate 1 subject to random forces are virtually identical for the coupled and uncoupled cases. This is a consequence of the large contrast of $1.1 \cdot 10^3$.

We can conclude that the method allows us to identify the subsystems in agreement with the concept that a subsystem is a set of nodes with similar behaviour.

3.4.2 Example 2: Four plates connected by springs

The second example consists of four plates of equal size (1 m $\times$ 2 m) and linked by means of springs, see Figure 3.8.

The positions of the springs in the plates are the same as in Section 3.4.1 and the spring properties are given in Table 3.4. The springs linking plates 2 and 3 are more flexible than the ones linking plates 1 and 2 and plates 3 and 4. With this configuration we expect to find two subsystems composed of two plates each.

Material	ρ_v (kg/m^3)	ν	E (Pa)	L_x (m)	L_y (m)	h (m)
Concrete	2000	0.2	$2 \cdot 10^{10}$	1	2	0.03

Table 3.3: Mechanical properties of the four plates linked by means of springs.

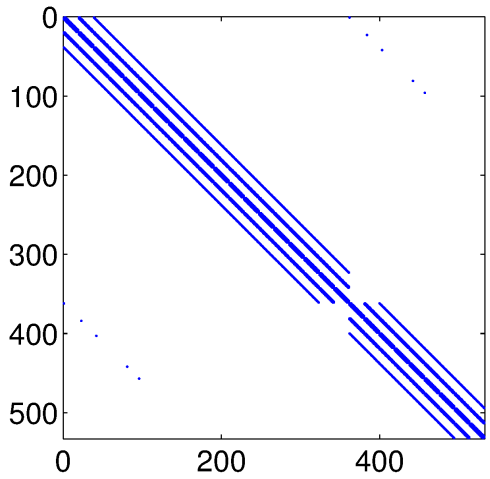

Figure 3.5: Sparsity pattern of the transfer matrix of the example with two plates and five springs as described in Table 3.2.

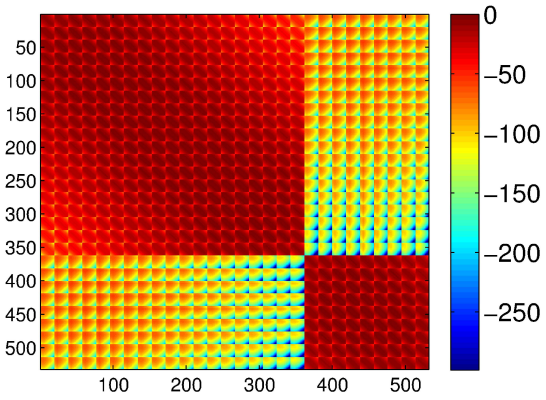

Figure 3.6: Block structure of matrix $\mathbf{T}^{21}$. The colour represents the normalised entries in the dB scale, $10\log_{10}\left(\left|t_{ij}^{21}\right| / \max(\left|t_{ij}^{21}\right|)\right)$.

Plates	Spring	K (N/m)	x (m)	y (m)
$1-2$	$1-5$	$2\cdot\ 10^{10}$	As in example 1	As in example 1
$2-3$	$6-10$	$2\cdot\ 10^{5}$	As in example 1	As in example 1
$3-4$	$11-15$	$2\cdot\ 10^{10}$	As in example 1	As in example 1

Table 3.4: Properties of the five springs that link contiguous plates.

Figure 3.9 shows the transfer matrix $\mathbf{T}$ of the four plates. Figure 3.10(a) shows

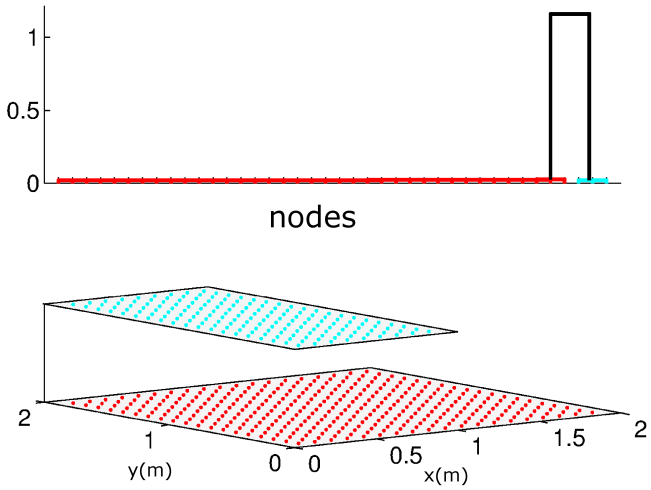

Figure 3.7: Top: Dendrogram obtained with $\mathbf{T}^{21}$. Bottom: Dendrogram nodes assigned to the plates.

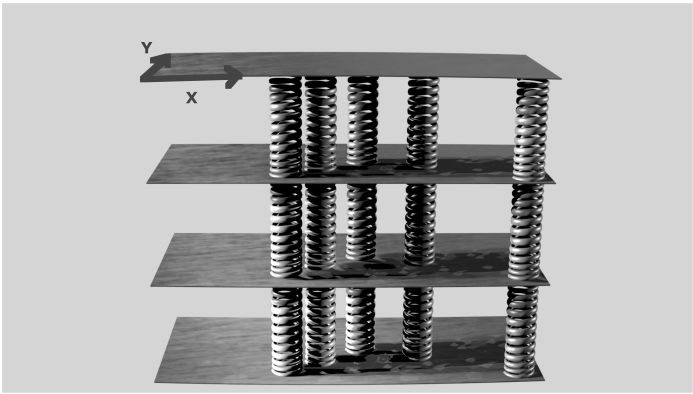

Figure 3.8: Four plates connected by springs as described in Table 3.4. Computation at 100 Hz.

$\mathbf{T}^k$, with $k = 28$. A 4×4 block structure can be clearly seen. Moreover the colour plot allows the visual identification of two mechanical subsystems (plates 1–2 and plates 3–4). Two different degrees of coupling exist. On the one hand a clearly weak coupling between subsystems. This is caused by the flexible springs that link plates 2 and 3. On the other hand we can see that inside each subsystem there is a much stronger coupling between the two plates. This causes the cluster analysis to define two subsystems instead of four. The two subsystems are also clearly visible in matrix $\mathbf{V}$ of eigenvectors of the direct transfer matrix $\mathbf{T}$, see Figure 3.10(b).

Figure 3.11 shows the dendrogram of the cluster analysis. It is clear regarding the length of the branches that it suggests the definition of only two subsystems instead of four.

A comparison of the solutions obtained by solving the whole problem (four plates) or an isolated subsystem (two plates) is made. A measure of the difference is

$$e = \frac{||\mathbf{u}_{\text{iso}} - \mathbf{u}_{\text{all}}||}{||\mathbf{u}_{\text{all}}||} \tag{3.26}$$

where $||\bullet||$ is the Euclidean norm, $\mathbf{u}_{\text{iso}}$ is the vector of nodal displacements in the isolated solution and $\mathbf{u}_{\text{all}}$ is the vector of nodal displacements in the coupled solution.

If the subsystem formed by plates 1 and 2 is analysed isolatedly, a very low error of $e = 8.7 \cdot 10^{-7}$ with respect to the coupled solution is obtained. This is related to the very high contrast of 147.

If the subsystems identified by the cluster analysis are not respected and plate 1 is analysed isolatedly, a large error of $e = 0.6$ is committed. This is explained by the low contrast of 0.21.

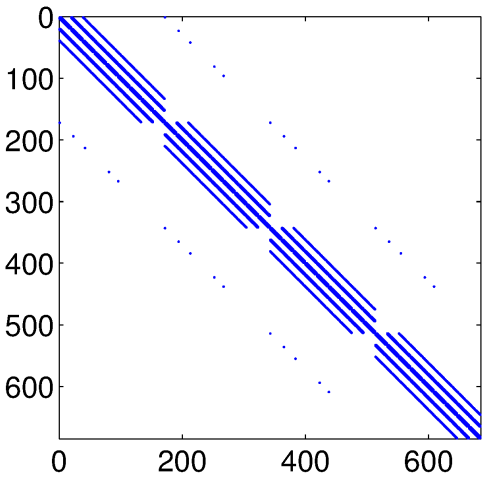

Figure 3.9: Sparsity pattern of the transfer matrix. Four plates connected by springs as described in Table 3.4.

Figure 3.12 shows the evolution of the contrast of $\mathbf{T}^k$ with respect to power k. Note that the contrast between plates 2 and 3, linked by soft springs, is much larger than the contrast between plates 1 and 2 or plates 3 and 4, linked by much stiffer springs. Figure 3.12 also shows that the contrasts stabilise as k increases, to values that can be accurately estimated from the dominant eigenvectors, see Eq. (3.18).

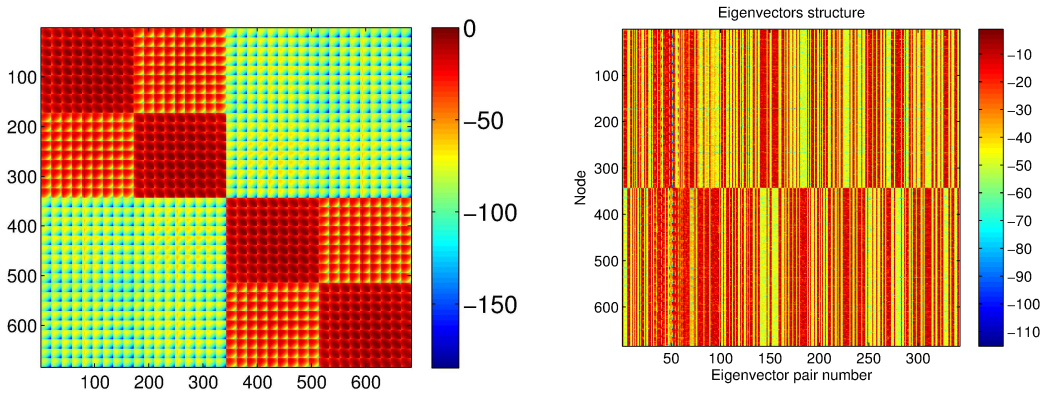

(a) (b)

Figure 3.10: (a) Block structure of matrix $\mathbf{T}^{28}$. The colour represents the normalised entries in the dB scale; (b) matrix $\mathbf{V}$ of eigenvectors of the direct transfer matrix.

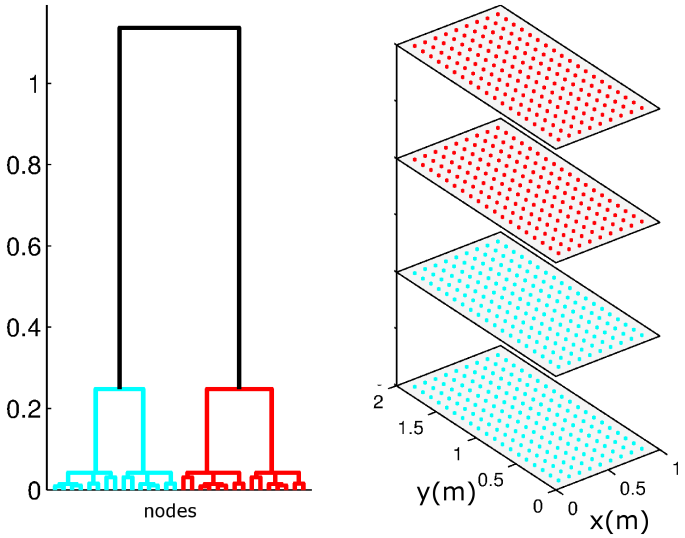

Figure 3.11: Left: Dendrogram obtained with $\mathbf{T}^{28}$. Right: Dendrogram nodes assigned to the plates

3.4.3 Two acoustically coupled rooms

The clustering method is applied to a two-dimensional acoustic problem: two rectangular rooms connected through a one-dimensional hole, see Figure 3.13. The room sizes are 20 $u \times 23$ u and 25 $u \times 23$ u (u is a unit length). Two different situations are considered. In the first one, the hole length is 5 u, and the acoustic wavelength (ratio

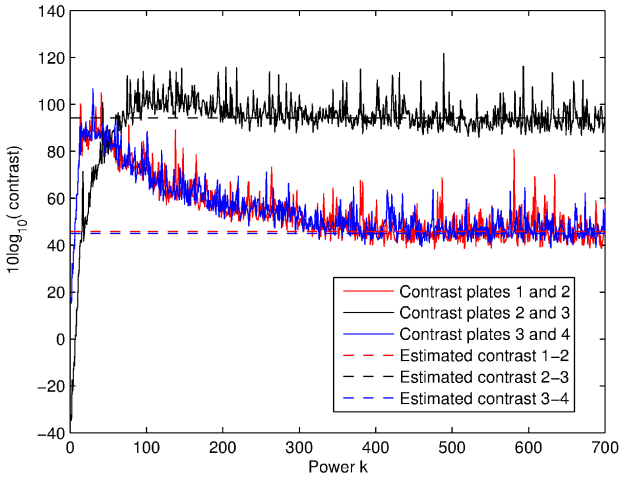

Figure 3.12: Evolution of contrast of matrix $\mathbf{T}^k$ with power k (solid lines) vs value estimated according to Eq. (3.18) (dashed lines).

between the speed of sound and frequency, $\lambda_{ac} = c/f$) satisfies $\lambda_{ac} = 1.26 \times 5\ u$. This is the case of hole size which is similar to the acoustic wavelength. In the second one, the hole length is 1 u, and the acoustic wavelength satisfies $\lambda_{ac} = 76.3 \times 1\ u$. This is the case of hole size very different to the acoustic wavelength. The system matrix $\mathbf{A}$ is obtained by discretising the Helmholtz equation by means of finite volume-based technique.

The degree of coupling between the two rooms is controlled by the ratio of the wavelength to the hole size. Two different cases are shown here with ratios 1.26 and 76.3 respectively. Weak coupling is only expected in the second case due to the large difference between the acoustic wavelength and the hole width.

The outputs of the clustering process for the case the small ratio are shown in Figs. 3.14 and 3.15. In that case, the hole size is very similar to the acoustic wavelength. As expected, the dendrogram in Figure 3.15 identifies only one system. The interaction between both rooms is very important due to the large width of the hole with respect to the wavelength.

If the rooms are analysed isolatedly, the error computed according to Eq. (3.26) is 208% for the left room and 191% for the right room, with contrasts $4.8 \cdot 10^{-2}$ and $2.8 \cdot 10^{-2}$ respectively. It is clear that considering both rooms as independent subsystems is not a valid option.

Figs. 3.16 and 3.17 show the outputs of the clustering process for the large ratio of

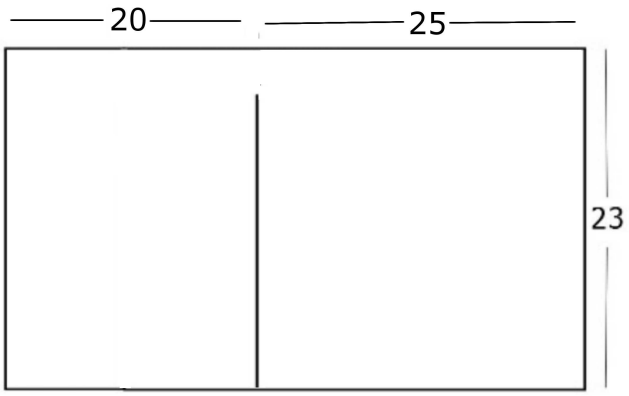

Figure 3.13: Sketch of the two rectangular rooms connected by means of a hole. The room sizes are 20 $u \times 23$ u and 25 $u \times 23$ u (u is a unit length). Two different holes have been considered: 1 u and 5 u in length.

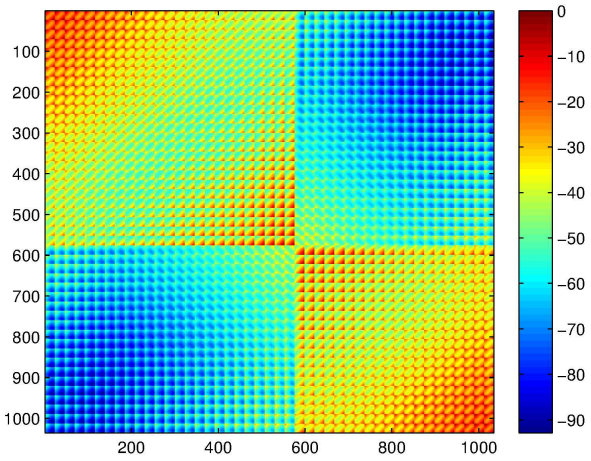

Figure 3.14: Block structure of matrix $\mathbf{T}^{343}$. The colour represents the normalised entries in the dB scale. Wavelength to hole size ratio: 1.26.

wavelength to hole size: 76.3. Now, both rooms are identified as almost independent subsystems. This can be concluded by the aspect of the dendrogram and is corroborated by the error measure. In that case, Eq. (3.26) provides values of 9% for the left room and 11% for the right one, which were expected due to the smaller value of

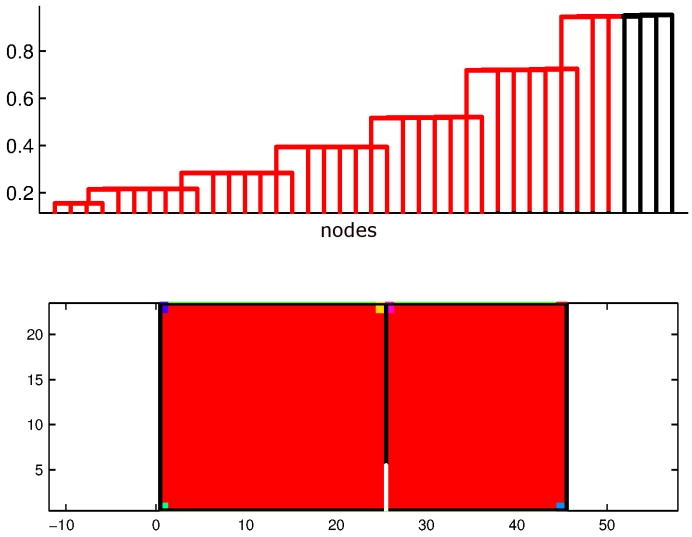

Figure 3.15: Top: Dendrogram . Wavelength to hole size ratio: 1.26; Bottom: Identified groups of nodes assigned to the room.

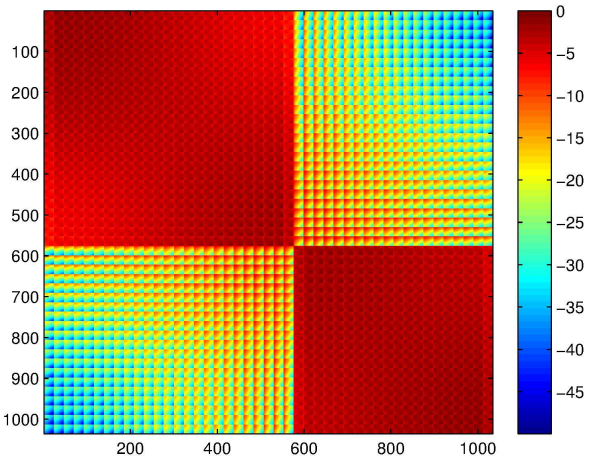

Figure 3.16: Block structure of matrix $\mathbf{T}^{343}$. The colour represents the normalised entries in the dB scale. Wavelength to hole size ratio: 76.3.

the contrasts (0.27 for both).

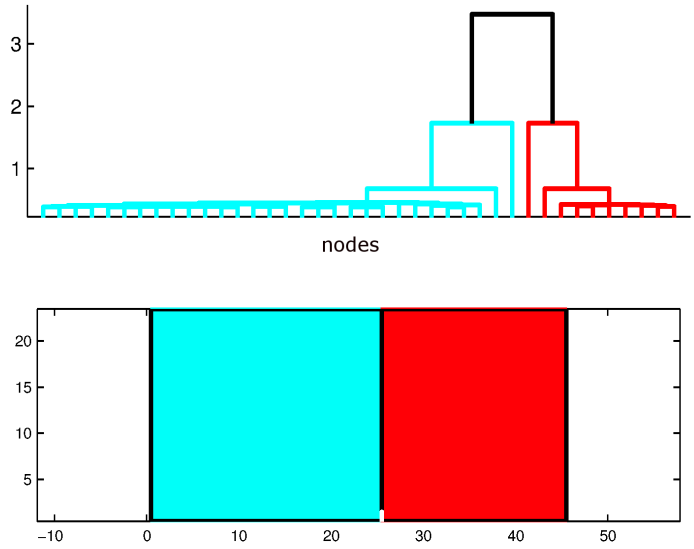

Figure 3.17: Top: Dendrogram. Wavelength to hole size ratio: 76.3; Bottom: Identified groups of nodes assigned to the room.

3.4.4 Degrees of freedom selection: problem size reduction

In the previous examples, the transfer matrix is directly obtained from the dynamical matrix of the system. The dynamical matrix was generated by means of numerical techniques. The number of unknowns is quite large because the discretisation of a mechanical or acoustic system must be done according to physical criteria. Enough nodes must be considered in order to properly describe the displacement or acoustic waves. Consequently, the transfer matrix $\mathbf{T}$ is a large matrix.

This has two important implications. On the one hand, when applying the proposed substructuring method, the cluster analysis has to deal with a large amount of data. This makes the process slow. On the other hand, a large power k of matrix $\mathbf{T}$ must be considered. $\mathbf{T}^k$ is representative of the k-order paths. First-order paths in the numerical techniques are very short, because they link contiguous nodes. The clustering method requires paths that explore all the problem geometry; hence, a large value of k is required.

What it is proposed here is to consider a more elaborated (post-processed) transfer matrix. This accounts only for some strategically chosen nodes on the system. They can be uniformly distributed all around the geometry or intuitively chosen as it would be done in a laboratory experiment where it is needed to choose a reduced num-

ber of measuring points (this is often limited by the number of available measuring channels).

The coefficients of the transfer matrix $\mathbf{T}$ are now computed by means of the solution of several problems as

$$t_{ij} = \frac{s_j}{s_i} \tag{3.27}$$

where s_j is the signal at node j when a unit excitation is applied at node i and the signal of all the nodes $r \neq i, j$ is blocked. Note that for each coefficient t_{ij} a problem has to be solved. The whole procedure is detailed in Magrans (1984, 1993).

This transfer matrix with less degrees of freedom it is a full matrix with direct connectivity between all the selected nodes. This drastically reduces the power k of matrix $\mathbf{T}$ required to represent paths that cover the whole geometry.

To illustrate this approach, the problem with four plates of Section 3.4.2 is revisited here. The only difference is that now all the springs have the same stiffness of $2 \cdot 10^7$ N/m. The discretisation of the four plates leads to a system with 684 degrees of freedom. This is later reduced to 48 degrees of freedom, 12 points per plate.

The clusters can be clearly identified from matrix $\mathbf{T}$ itself, with no need of computing powers. This is shown in Figs. 3.18 and 3.19, which show that each plate is identified as one subsystem. These smaller transfer matrices are the ones typically obtained in a laboratory or in situ measurement.

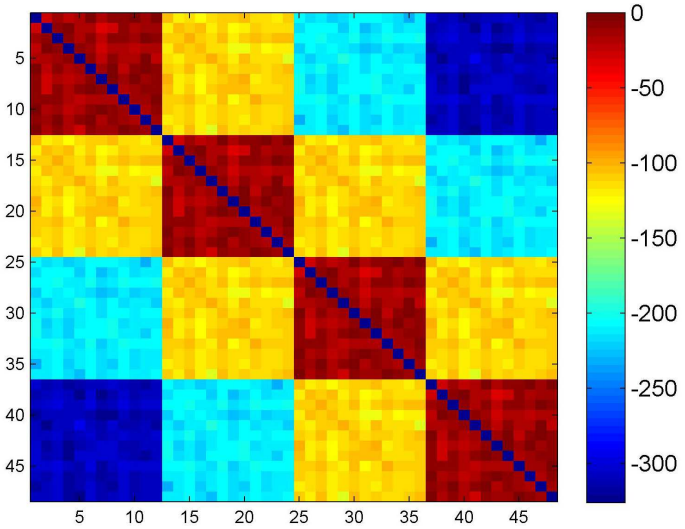

Figure 3.18: Block structure of matrix $\mathbf{T}$. The colour represents the normalised entries in the dB scale, $10 \log_{10} (|a_{ij}| \,/\, \max(|a_{ij}|))$.

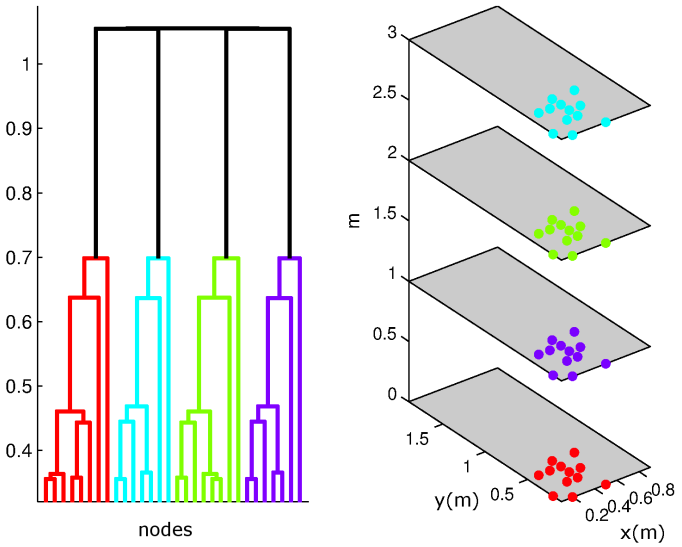

Figure 3.19: Left: Dendrogram obtained with $\mathbf{T}^1$. Right: Grouping of the 12 randomly selected nodes on each of the four plates (one subsystem per plate in this example).

3.5 Conclusions

The main conclusions of the research are as follows:

1. A methodology for the automatic identification of subsystems has been proposed. It is based on the cluster analysis applied to powers of the transfer matrix. It is shown, through numerical examples, how the method works and is able to identify subsystems on its own without additional information or guidelines.

2. The subsystems are more clearly identified when higher powers of the transfer matrix are considered. This agrees with the explanations of Section 3.3.3.2.

3. If the transfer matrix represents all the degrees of freedom in a numerical discretisation of the system, the power required in order to properly identify the subsystems can be quite high. This can be linked with the representation of paths. They must be large enough in order to cover all the domain. On the contrary, if the transfer matrix is manipulated in order to directly represent long paths, as described in Section 3.4.4, a lower powers is required. This sec-

ond option makes the method more efficient for the characterisation of large systems.

4. An important parameter in order to explain the good behaviour of the proposed technique is the contrast of the matrix. It is also used as an estimator of the coupling strength between subsystems.

5. A fast method to estimate the contrast of $\mathbf{T}^k$ is proposed. It is based on the dominant eigenvalue of the transfer matrix $\mathbf{T}$ and the associated eigenvector(s).

3.A Eigenvectors of T vs. vibration eigenmodes

Consider a mechanical system with stiffness matrix $\mathbf{K}$ and mass matrix $\mathbf{M}$. The eigenmodes $\mathbf{\Phi}_i$ and eigenfrequencies ω_i verify

$$\mathbf{K}\mathbf{\Phi}_i = \omega_i^2 \mathbf{M}\mathbf{\Phi}_i \qquad i = 1 \dots n \tag{3.28}$$

If this mechanical system is subject to an harmonic excitation of frequency ω_{exc} and phasor $\mathbf{f}$, the phasor $\mathbf{u}$ of displacements is the solution of

$$\mathbf{A}\left(\omega_{exc}\right)\mathbf{u} = \mathbf{f} \tag{3.29}$$

with

$$\mathbf{A}\left(\omega_{exc}\right) = \mathbf{K} - \omega^2\mathbf{M} \tag{3.30}$$

We are interested in exploring the relation between the eigenmodes $\mathbf{\Phi}_i$ and the eigenvectors $\mathbf{v}_i$ of the transfer matrix $\mathbf{T}(\omega_{exc})$ associated to the linear system (3.29). We start by assuming that the mass matrix is diagonal (i.e. all system mass concentrated at nodes) and that all diagonal entries of $\mathbf{M}$ and $\mathbf{K}$ are equal:

$$\mathbf{M} = m_0\mathbf{I} \tag{3.31}$$

$$\mathbf{K} = k_0\mathbf{I} + \mathbf{L} + \mathbf{U} \tag{3.32}$$

This result in the system matrix

$$\mathbf{A}\left(\omega_{exc}\right) = \left(k_0 - \omega_{exc}^2 m_0\right)\mathbf{I} + \mathbf{L} + \mathbf{U} \tag{3.33}$$

and the transfer matrix

$$\mathbf{T}\left(\omega_{exc}\right) = -\frac{1}{k_0 - \omega_{exc}^2 m_0}\left(\mathbf{L} + \mathbf{U}\right) \tag{3.34}$$

Under these conditions, the vibration eigenmodes $\mathbf{\Phi}_i$ *are equal* to the eigenvectors of $\mathbf{T}(\omega_{exc})$ for any excitation frequency $\omega_{exc} \neq \omega_0 = \sqrt{\frac{k_0}{m_0}}$. Indeed, by combining equations (3.28), (3.31), (3.32) and (3.34), one obtains

$$\begin{aligned} \mathbf{T}(\omega_{exc})\,\mathbf{\Phi}_i &= -\frac{1}{k_0 - \omega_{exc}^2 m_0}\,(\mathbf{L}+\mathbf{U})\,\mathbf{\Phi}_i = -\frac{1}{k_0 - \omega_{exc}^2 m_0}\,(\mathbf{K} - k_0\mathbf{I})\,\mathbf{\Phi}_i \\ &= \frac{\omega_0^2 - \omega_i^2}{\omega_0^2 - \omega_{exc}^2}\mathbf{\Phi}_i = \lambda_i(\omega_{exc})\,\mathbf{\Phi}_i \end{aligned} \tag{3.35}$$

Eq. (3.35) also shows that, contrary to the eigenvectors $\mathbf{v}_i \equiv \mathbf{\Phi}_i$, the eigenvalues λ_i do depend on the excitation frequency.

Without the simplifying assumptions Eq. (3.31) and Eq. (3.32), the vibration eigenmodes are not equivalent to the eigenvectors of $\mathbf{T}$. However, there is still a qualitative relation. Weakly coupled subsystems results in small off-diagonal blocks in the stiffness matrix $\mathbf{K}$ that lead to local vibration eigenmodes; they also result in small off-diagonal blocks in the system matrix $\mathbf{A}(\omega_{exc})$ and in the transfer matrix $\mathbf{T}(\omega_{exc})$ that lead to local eigenvectors.

An example can be seen in the Figure 3.20. Some eigenvectors of $\mathbf{T}$ are compared with the corresponding eigenmodes of a room 12 m wide and 14 m long.

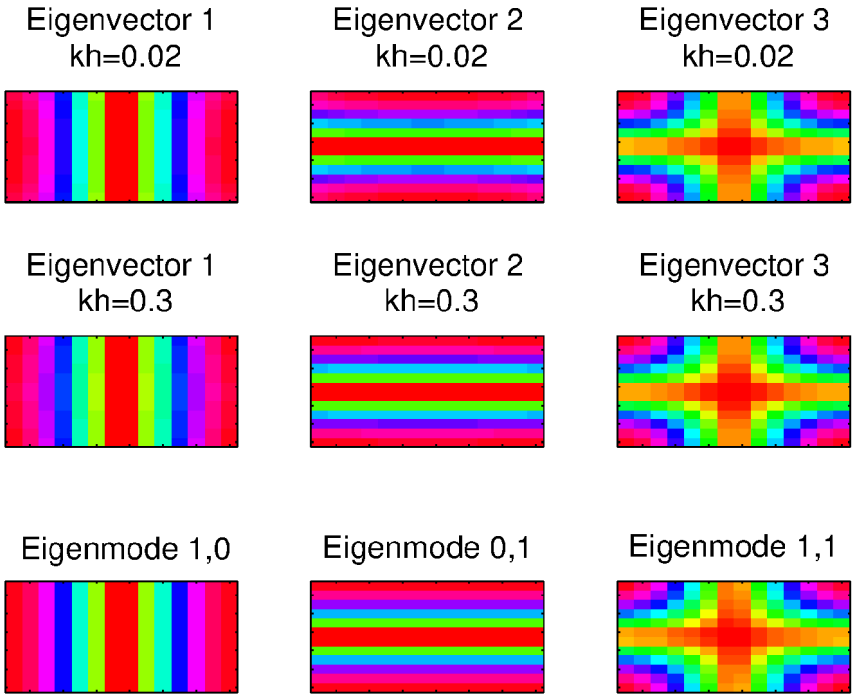

Figure 3.20: Comparison of some eigenvectors of T with the corresponding eigenmodes of a room 12 m wide for 15 m long.

Chapter 4

Experimental and numerical study of Advanced Transfer Path Analysis applied to a box prototype [1]

4.1 Introduction

A major concern when dealing with vibroacoustic systems is to understand how the vibration and noise are transmitted and distributed. A common way to acquire this knowledge is through the path concept. In a network of interconnected nodes we understand that it exists a path between the node i and the node j simply if they are connected. In a vibroacoustic system the nodes are control points, and signals (vibrations or acoustic pressure) are used in order to identify and study the paths. It is not the same a path from i to j as a contribution from i to j. The contribution is the amount of signal that arrives at j due to an excitation on i. But this signal can be transmitted through any path from i to j (regardless of the existence of a direct path between i and j). So, the contributions are descriptions of the inputs and the outputs while paths are a description of the system topology. One formal definition of 'path' can be found in Magrans (1981). More recently, it was shown in Magrans

[1] Chapter based on the paper Aragonès et al. (2019)

et al. (2017) that the solution of a mechanical problem can be expressed in terms of paths. This can be used at both numerical modelling and experimental levels. An application example is to characterise the transmission of vibration and noise from the engine to the passengers cavity or other parts of a car. It is usually generated at the wheels, engine, exhaust and travels through the chassis, axes and insulating layers to the passenger compartment.

The final goal is always to characterise the response of each subsystem (measured in terms of the acceleration of a vibrating element or the acoustic pressure in a zone of interest) caused by a specific excitation. A large amount of experimental methods have been developed during the past decades Van der Seijs et al. (2016). We can distinguish, in a quite general classification: Transfer Path Analysis TPA (Hambric et al. (2016)) and Advanced TPA (ATPA) Magrans et al. (2005); Guasch et al. (2013), see for both Gillard (1980) and Magrans (1981) or also Force contribution analysis Zafeiropoulos et al. (2013)) and OTPA method,Bendat (1976b) and de Klerk and Ossipov (2010). The main difference between the methods grouped under the name TPA and the name ATPA is that traditional TPA characterises only the source contributions from the inputs to some receivers. It is done by combining operational signals (measured while the equipment is working) with transfer functions (frequency response functions, FRF) measured on the empty passive structure where the equipment is installed. For example, the transfer functions can be measured on a car body prior to the engine installation. This body is uncoupled from the engine and passive in the sense that it only acts as transmitter of vibrations that are generated elsewhere. ATPA, as the in-situ TPA procedure, does not require any disassembly of the structure. It characterises furthermore the topology of the mechanical system and thus, the paths and their contribution to any receiver. TPA measures global transfer functions between subsystems while ATPA measures the direct transfer functions. Direct transfer functions provide a more useful information on the system behaviour. Another feature of ATPA is that, contrary to TPA, the measurement of the excitation force is not required which is indeed an advantage. Both ATPA and TPA are adequate if one can act on the exciting forces to control and reduce them. This means that a redesign of the vibroacoustic system acts on the exciting force in order to improve the response in terms of noise emission or vibration levels. However only with ATPA it is possible to quantify the contributions of a passive system (like the interior panels of a train coach or of a vehicle) and with this information decide

which part of this system needs to be modified in order to reduce the noise measured in the receiver position (the redesign acts on the system itself).

If the studied system is understood as a black box with n inputs and m outputs interconnected through the box, TPA and ATPA can predict which is the contribution of each input to each output. This means that both methods are able to decompose the output signal into contributions coming from every input signal. However, TPA is unable to describe how the input and outputs are connected. ATPA is able to characterise, in addition, how the input and output signals are connected inside the black box, discover which is the intrinsic structure of the mechanical system, which and how are the paths. For this reason when a detailed analysis of the mechanical system is needed, the use of ATPA is helpful.

4.1.1 Goals of the research

This work deals with the application of the ATPA method to a simple laboratory prototype. This is a cuboid-shaped box with an air cavity inside. A major control on the laboratory measurements is possible due to the simplicity of the prototype. This allows a more detailed analysis. It also opens some unusual options for the analysis of the method that are not possible in more complex mechanical systems such as a car or a train coach. Experimental methods in vibroacoustic have several common limitations in practice such as: difficulty in the access to the desired control points, limit in the number of sensors to be used, large time required to make the installation of the measurement setup, difficulty in the repetition of tests (i.e. time to measure in a building, car or train is often limited), etc. Most of these drawbacks are non-existent in the box prototype because it is available at the lab, sensors can therefore be placed without problems (the box is lightweight and it can be handled and moved without external machinery).

Other issues such as difficult measurement of the rotation degrees of freedom, finite size of the exciter heads, uncoupling air-structure, measurement of the real contributions, can be solved only by using numerical models.

A numerical model of the box has been developed. The degree of uncertainty of the experiment is more controlled than usual. Consequently a better agreement between the numerical model and the experimental data can be obtained. Once calibrated, the numerical model will allow for a faster execution of virtual experiments, the possibility of doing parametric analyses or a more visual representation of the results. In other

words, to analyse and gain understanding of aspects that are very difficult to visualise and control in the laboratory or in situ test such as: automatic identification of the subsystems, optimisation of the sensor position inside each subsystem, combination of more than one sensor per subsystem, study the influence of the excitation type (point force, rain-on-the roof, acoustic wave, etc.) and the spectrum of the excitation.

The application of the ATPA method in a vibroacoustic mechanical system as well as the comparison with a numerical model have not been reported before.

4.1.2 Contributions of the research

In addition to the application of ATPA to a vibroacoustic problem as the box with cavity inside, the main contributions of the research and results shown here are:

1. To be able to compute any transmission path with ATPA and show that it properly characterises the paths with small contributions (not only the main contributors). This is important because after a redesign oriented to suppress the most contributing paths, these other still remain and are the ones that define the response of the modified system.

2. To verify that two methods of estimation of the direct transfer functions provide equivalent results. One of the methods is used in laboratory and in situ measurements and the other is based on the definition of direct transfer.

3. Numerically prove that the error in the reconstruction of a signal by means of the direct transfer functions can be estimated by the direct field (displacement or pressure field when all the control points are blocked).

4. Study the influence of the excitation type in order to reconstruct operational signals.

4.1.3 Precedents of ATPA

The theoretical bases of the ATPA method were presented in Magrans (1981). The framework of the global and direct transfer matrices as well as their relationship were defined. Later some applications were done, based on theoretical models and experimental measurements of simple systems. The method presented in Magrans

(1981) and also referred to as Global Transfer Direct Transfer (GTDT) was considered in Guasch (2009) to theoretically study a mechanical system made of masses and springs. Later in Guasch et al. (2013), GTDT was similarly applied to a real mechanical device composed of a mass on four springs. The agreement between computed and measured transmissibilities was good. There are other techniques that share with GTDT the determination of direct transmissibilities with an artificial excitation and posterior use of them to simulate the operational response of the system, see for example Roozen and Leclere (2013). The establishment of GTDT as an experimental method for the analysis of mechanical systems was done in Magrans et al. (2005), where the specification of the experimental procedure and main steps were explained. The name given to the measurement procedure based on GTDT was ATPA. It was included in the review of TPA methods Van der Seijs et al. (2016) where some of the similitudes and differences with the other available techniques can be seen.

The laboratory setup and the numerical model are described in Sections 4.1.5 and 4.1.6 respectively. The results are shown in Section 4.2 before the conclusions of Section 4.3.

4.1.4 Application of ATPA in this study

The theoretical base of ATPA, the GTDT, has been explained in Section 2.2.3 and with more extension in chapter A. In this study the method will be applied to a set of accelerations on the box and to the noise in a microphone. Two types of relationships will be used first of all for the calculation of the TD the expression already shown in 2.8. Secondly, for the reconstruction of pressure the formula given in 2.5 will be particularized for the present case as

$$p_T = \sum_{i=1}^{N} x_i \mathbf{T}_{iT} + p_T^e \tag{4.1}$$

where p_T is a signal in the target (i.e. pressure in a microphone placed inside the passenger's compartment of a car), x_i is the measured signal in subsystem i (i.e. acceleration of a vibrating panel), $\mathbf{T}_{iT}$ are the direct transfers between subsystem i and the target and N is the number of subsystems in which the mechanical system has been divided. p_T^e is the direct field of the signal that arrives at T due to an external excitation when all the N nodes are blocked.

Plate	Thickness h [m]
Top	8×10^{-3}
Front	1×10^{-2}
Back	1×10^{-2}
Left	1×10^{-2}
Right	8×10^{-3}

Table 4.1: Box plate thicknesses

4.1.5 Description of the experimental setup

The prototype of the cuboid-shaped box is shown in Figure 4.1. It is made of methacrylate with dimensions $L_x = 0.534$ m, $L_y = 0.426$ m and $L_z = 0.586$ m. In general, it is designed in order to be complex enough to test the ATPA method but also as simple as possible to allow a proper numerical modelling with as few uncertainties as possible. For example, in order to satisfy the first goal, the three box dimensions and also the face thickness (see Table 4.1) are different, to try to decouple as much as possible the vibration and resonances of the rectangular faces. And in order to reduce the uncertainties, all the junctions at the edges are made as homogeneous as possible. The two methacrylate plates are glued to each other at each edge. The bottom part is made of multiple thin steel plates separated by layers of rubber damping material.The solid steel layers provide the stiffness and the mass while the rubber between them ensures large damping. Consequently, its vibration can be neglected when compared with the vibration of the other faces. It also includes several latches that are used to detach and fix the methacrylate part (the box needs to be accessible in order to place the microphones inside).

Twenty control points are considered. Four of them are placed at the centre of each quarter in the five vibrating faces. The notation and position of them is shown in Figure 4.2. An accelerometer is placed at each of these points. At the same time, the excitation is applied also there by means of a hammer impact (in general) or a fixed shaker (only in the calibration phase discussed in Section 4.A.2).

On the one hand, some of the measured data can be unreliable below 100 Hz. The reasons are several: the foam supports of the rectangular plate as commented above(modify the low frequency modes); the cases where the excitation is done by means of the shaker (it is difficult to induce vibrations when rigid-body motion modes are present); the existence of background noise and vibrations at very low frequencies.

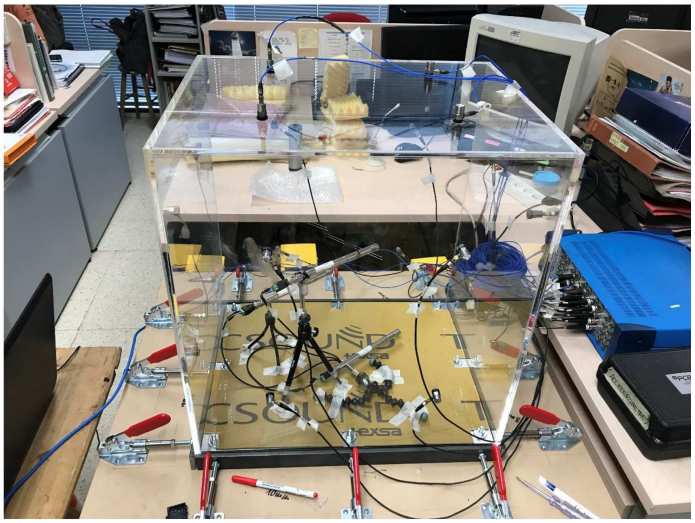

Figure 4.1: Experimental setup including the box, twenty accelerometers (four per face) and three microphones inside.

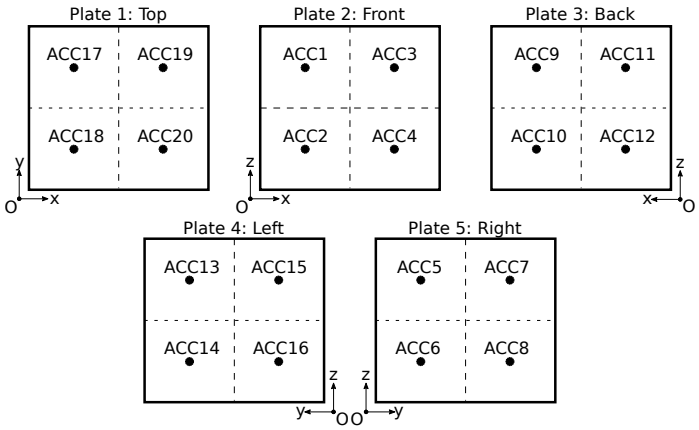

Figure 4.2: Sketch with the distribution of the accelerometers.

On the other hand, the material of the hammer impact zone and the impact velocity limit the validity of experimental data to frequencies below 2000 Hz. So, in order to avoid the use of unreliable data we preferred to keep in the safe side and limit the frequency range of the study from 100 Hz to 2000 Hz.

4.1.6 Description of the numerical model

A virtual setup for the experimental mechanical system described in Section 4.1.5 is developed. It is based on the finite element method (FEM) by means of the software

Code-Aster EDF (2017).

The box is modelled by means of triangular shell elements that use DKT formulation Batoz et al. (1980) to describe the bending behaviour. The nodes in the lower contour of the box are blocked (null displacements and rotations). The material behaviour is linear elastic with hysteretic damping. Perpendicular point and surface forces can be applied on each face. The coupled vibroacoustic problem in the frequency domain is considered. Only the air cavity inside the box is included in the model. The effect of the radiation losses and the air surrounding the box is neglected which is a common assumption in the modelling of this type of vibroacoustic systems.

Code-Aster EDF (2017) is used to solve a single problem (i.e. compute displacement and pressure field due to a point force in a list of given frequencies). However, in order to reproduce all the process of the ATPA method, a script system is required due to the large number of simulations involved. As it will be detailed below in Section 4.2, point forces need to be applied at each control point and boundary conditions modified sometimes at every simulation. For this reason a systematised procedure is required.

The size of structural elements has been determined by means of a convergence test and set to 2×10^{-2} m. The size of acoustical elements has been set to obtain at least 34 elements per wavelength in every 100 Hz frequency band. This is a balance between accuracy and computational costs. The use of variable finite element size in the acoustic part of the problem requires to refine the mesh at several frequencies. This is done as a task inside the frequency loop of the script system. The simulation is split in user-defined frequency-bands and the remeshing is done for each of these steps. In addition, the value of the frequency-dependent parameters is updated.

The mechanical properties considered in the FEM model for the methacrylate are shown in Table 4.2. The procedure that leads to these values is described in Appendix 4.A.

Material	ρ_v (kg/m^3)	ν	E (Pa)	η
methacrylate	1153.2	0.45	$4.3 \cdot 10^9$	$0.07 + \frac{1}{\omega}$

Table 4.2: Mechanical properties of the methacrylate (ρ_v is the volumetric density, ν is the Poisson's ratio, E is the Young modulus and η is the hysteretic damping coefficient).

4.2 Results

The most meaningful results obtained by means of the box analysis are reported here. They are organised in four different sections. Section 4.2.1 mainly shows the efficiency of the ATPA method for characterising all the transmission paths and how the same direct transfers are obtained by means of different procedures. Section 4.2.2 analyses the influence of the imprecisions in the application of point forces, which is one of the key aspects of ATPA. Another very important aspect, the use of direct transfers in order to characterise the operational state, is studied in Section 4.2.3. Finally, the transmission between opposite faces illustrates some other features of the method in Section 4.2.4.

In all the results shown here a variable number of sensors per face have been considered (one, two, three or four). This leads to very similar results in all the cases, which means that for the box, each face behaves like a subsystem and one accelerometer is enough. It is well known that in structures composed of rectangular plates (for example: L-shaped, T-shaped, X-shaped junctions, see Díaz-Cereceda et al. (2015)) each rectangular part acts as a subsystem and the junction makes it difficult to spread the vibration energy in the excited plate to the other plates. At the low frequency range the modes of vibration tend to exhibit much larger displacements in one part than in the others (it is like local resonances). At high frequencies, the vibration is more or less uniform (especially if several frequencies are averaged) and we can distinguish different energy levels in every rectangular plate. So, for this type of structures the behaviour is quite binary: vibrate or not. In this situation ATPA needs information of one control point of the subsystem in order to properly characterise the response and the topology.

This can be different in more complex mechanical systems where the definition of subsystems is not so clear. In that situation the use of a more dense network of control points can be mandatory. All these is related with the proper identification of the subsystems. But in any case, the direct transfer function between two points is not depending on the number of sensors considered. $\mathbf{T}$ is an intrinsic property of the system. The figures show here the case of four sensors per face, which is almost equivalent to the others. Only the result in Figure 4.7 are included to illustrate the unvariability of transfer functions due to the addition of other control points.

4.2.1 Computation of the direct transfer matrix T

The direct transfer matrix $\mathbf{T}$ is usually computed as a post-process of the global transfer matrix $\mathbf{T}^G$ as described in 2.8. The reason is that the coefficients of $\mathbf{T}^G$ can be directly obtained as measurement output while it is difficult and time-consuming to perform a direct measurement of the $\mathbf{T}$ coefficients. Moreover, imposing the boundary conditions would imply a modification of the system. So, it is not clear that in most of the cases this procedure could be done.

To deal with a numerical model helps in order to overcome these difficulties because it is easier and faster to handle the boundary conditions and virtually perform repetitive experiments. Blocking all the subsystems except two is more easily done in a computational model than in a laboratory experiment.

Two procedures to compute $\mathbf{T}$ are considered:

1. *'Mimics the experiment (labelled 'from GT')':* Excitation of the box at points $i = 1, 2, \ldots, N$. Each excitation applied to a node i provides a row of the matrix $\mathbf{T}^G$ and the coefficient ${\mathbf{T}^G}_{iT}$. The direct transfer matrix can be obtained from 2.8. Afterwards, N simulations per frequency are required in order to generate the linear system of equations (4.1).

2. *'Apply the definition of* $\mathbf{T}$ *(labelled 'from definition')':* Excitation of the box at points i with all the other nodes $j \neq i$ blocked. With this simulation type, the coefficients $\mathbf{T}_{iT}$ are obtained. This situation is difficult to consider in the laboratory because it requires time to block all the paths except the one that is studied (from the excitation point i to the target T). Most probably, this procedure cannot be done experimentally because the original system would be altered.

Figure 4.3 shows two representative computations of a direct transfer matrix coefficient: Figure 4.3(a) for the transmission from an excited point to one of the micros inside the cavity and Figure 4.3(b) for points placed on the box structure. In both cases ('from GT' and 'from definition') the values of $\mathbf{T}$ obtained by means of the numerical model are almost equivalent in the whole frequency range. This is the case for all the direct transfer functions to the microphones and between accelerometers as it can be seen in Figure 4.3(a).

However, some difference has sporadically been found as it can be seen in Figure 4.3(b) around 300 Hz. The very few times that this is observed, coincides with the

peaks of the curves. They are associated at some of the system resonances. Numerical models can suffer from small eigenfrequency shifts and it is know that numerical error can be larger around the eigenfrequencies. Also matrices can be ill-conditioned which help in the propagation of possible numerical errors. Both methods to compute **T** use a system with different spectra (due to the modified boundary conditions). So, it is logical to expect some small difference, especially for poorly damped systems. In any case, the agreement between curves that have been found is in general very accurate.

The experimental curve is obtained from the laboratory measurements and the 'from GT' procedure.This is the only of the two procedures to determine the direct transfer functions presented in Section 4.2.1 whose application in a real laboratory experiment does not entail very important difficulties and efforts. Otherwise a large amount of different experiments are required if the option 'from definition' is considered . Moreover, the difficulties to impose and modify the boundary conditions are important. The agreement with the computed values is correct.

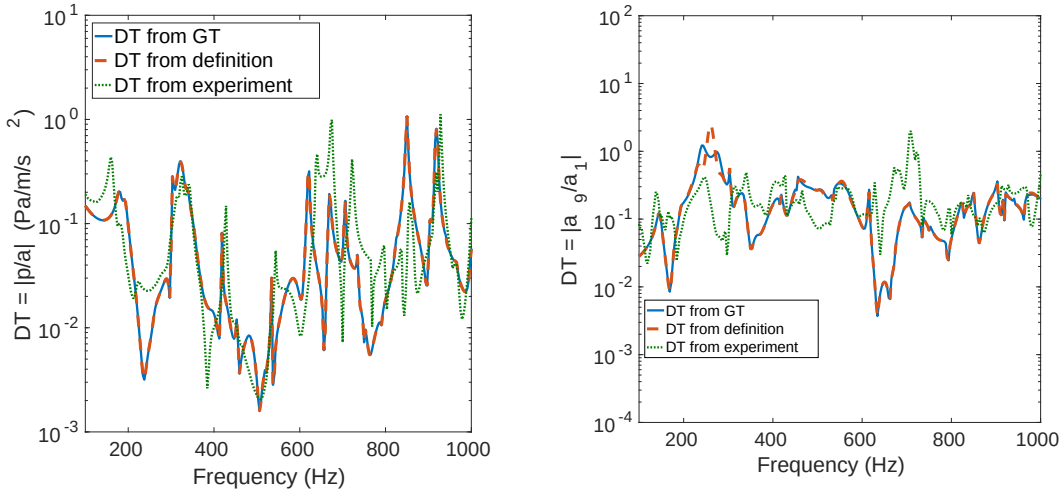

(a) (b)

Figure 4.3: Direct transfer functions (modulus): (a) from the accelerometer ACC1 to the microphone MIC1, pressure divided by acceleration; (b) from the accelerometer ACC1 to another accelerometer of the box (ACC9). Comparison of experiment results (third curve: 'from experiment') with the two methods of obtaining the direct transfers by means of the numerical model (first and second curves).

A similar comment applies for all the 400 structure-to-structure paths (20 sensors

on the box acting as transmitter and receivers at the same time) and the 60 structure-to-air paths (20 sensors on the box acting as transmitter and 3 microphones acting as receivers). This is especially relevant because it means that the ATPA method properly characterises not only the dominant paths but also the ones associated with a smaller **T**. Potential redesigns or modifications in order to suppress the dominant transmission paths require the proper characterisation of these less important paths in order to properly predict the new behaviour of the system.

4.2.2 Influence of the error in the position of the hammer impact in the T computation

As explained above in Section 4.2.1, ATPA requires the excitation of the mechanical system by means of a hammer impact. Moreover, this has to be done multiple times in order to compute the direct transfer matrix **T** (N times, the same as the number of control points). This manual repetitive action is not free of errors and can hinder the reproducibility of the experiment.

The effect of the influence of the precision in the position of the hammer impact on the **T** computation is checked here by comparing two different scenarios. On the one hand, **T** is computed by applying the point force at the nominal position (where the sensor or measure point is placed). On the other hand **T** is computed by applying the point force around this nominal position, approximately, at a distance between 2.5 cm and 4.5 cm. This can be quite representative of deviations in the impacted point in mechanical systems where it is difficult to access and hit with the hammer (i.e. inside a windmill blade).

In the experimental measurement, the hammer impact is not applied at the nominal position. It can be done if adapted acceleration sensors are used (i.e. the accelerometer can be placed on the other side of the plate or it is protected in such a way that is possible to hit directly over the sensor).

An illustrative result is shown in Figure 4.4 for the direct transfer between the accelerometer ACC1 and the microphone MIC1. This figure shows three curves: experimental direct transfer, numerical direct transfer with the point force applied at the nominal position where the sensor is placed and numerical direct transfer with the point force applied close to the position where the sensor is placed. The relation between the curves is quite random, depending on the frequency. This illustrates the importance of the excitation type.

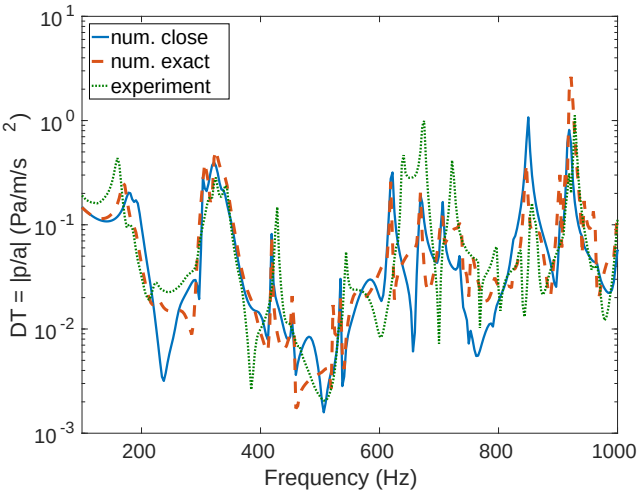

Figure 4.4: Direct transfer function from the accelerometer ACC1 to the microphone MIC1 (pressure to acceleration ratio $|p/a|$). Comparison of experimental results with the **T** values obtained by means of the numerical model with a point force applied close to the accelerometer (as it is done with the hammer impact of the experiment) or in the exact point (nominal position).

More important than the comparison with the experiment is the relation between the two numerical simulations, which shows the influence of the precision in the application of the point force. To do so, the separation between frequency response curves is measured as

$$e = \frac{\sum_i \left(\psi_{\mathrm{FEM1}}(f_i) - \psi_{\mathrm{FEM2}}(f_i)\right)^2}{\sum_i \left(\psi_{\mathrm{exp}}(f_i)\right)^2} \tag{4.2}$$

with ψ_{FEM1} the FEM simulation with the point force applied to the exact point, ψ_{FEM2} the FEM simulation with the point force applied close to the exact point, f_i the central frequency of the third octave band and the sum is done in all the third octave frequency bands between 125 Hz and 1000 Hz, both included. ψ_{FEM1} and ψ_{FEM2} are the result of the frequency average of the signal in the third octave frequency band (i.e. they are the mean response in the band). It is important to note that the outputs are now not averaged in space or excitation cases (only one force position and only one reception point). The results are shown in Figure 4.5. In each plot two sets of data are shown. One of them represents the difference considering the third octave bands in the range 160 Hz to 630 Hz. The other considers also the third octave bands equal or below 1000 Hz. It can be seen that while the difference

is not very large at the lower frequencies (for most of the paths), it becomes more important at high frequencies. Again it must be taken into account that we are dealing with a linear output and that these differences become less important from the engineering point of view when dealing with outputs expressed in dB scale. There exist a difference between the results in Figure 4.5(a) and Figure 4.5(b). We have no clear explanation for this and we can also speculate with an small deviation in the micro position. This affects more at high frequencies where the acoustic wavelength becomes shorter and point outputs (non-averaged) can suffer from larger deviations.

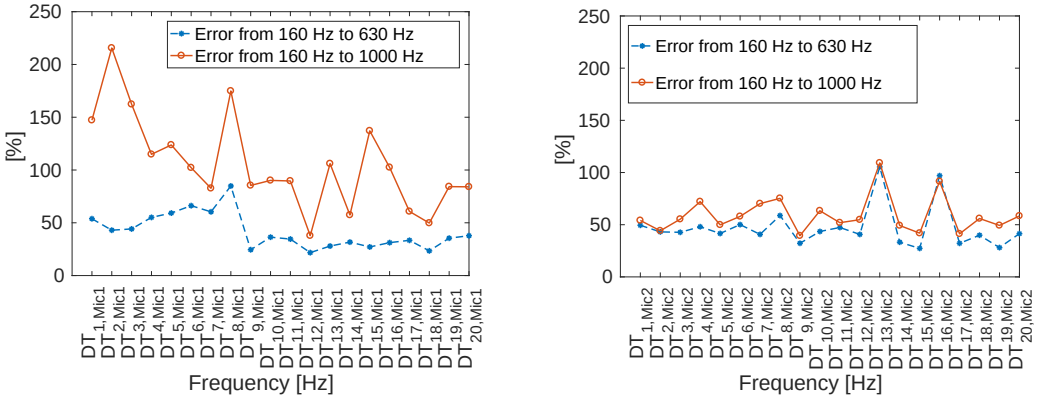

(a) (b)

Figure 4.5: Difference between direct transfer functions when the point force is applied at the nominal position or with an excentricity between 2.5 cm and 4.5 cm. Each curve represents a frequency range where the difference in third octave bands is averaged. All the curves are FEM simulations. Each point in the plot represents the transmission from an accelerometer to a microphone: (a) to MIC1; (b) to MIC2.

4.2.3 Signal reconstruction using the direct transfer matrix

The main output of the ATPA method is the **T** matrix. It concentrates the information about the transmission paths and can be used to quantify the flow of signal (in the form of vibrations or acoustic pressure) through them. In some sense, the matrix **T** is a representation of the mechanical system.

However, an excitation type (here the hammer impact) needs to be chosen in order to compute **T**. The value of **T** is independent of the excitation type. The big question is how the two terms on the right-hand-side of Eq. (4.1) are balanced. On

the one hand, if the signal in the target is properly reconstructed with the sum of contributions through the direct transfers ($\sum_{i=1}^{N} x_i \mathbf{T}_{iT}$), this means that the choice of control points is adequate and the system characterisation is excitation-independent. The operational response can be approximated by means of the information condensed in the direct transfer functions. On the other hand, if the second term (p_T^e) is important, it means that the signal arriving at the target without passing through the control points (direct field) is relevant and the reconstruction cannot be done by only considering the contributions from the direct transfers. In that situation, a redefinition of the control points is recommended. The new configuration should be able to block the direct field ($p_T^e = 0$). In general, an increase in the density of control points (i.e. putting more sensors on a plate) leads to a decrease of the direct field contribution ($p_T^e \to 0$). Of course, this must be understood as a limit situation because it is difficult to completely block a system for all the frequencies by simply adding control points. The determination of the direct field is more complicated and it would make more tedious the whole process. In general, it is much better if the direct field is small with respect to the paths contribution and consequently it can be neglected.

The purpose of ATPA method is to determine $\mathbf{T}$ with a group of excitations that satisfy: *i)* It is comfortable to apply them to the mechanical system in an instrumented experiment or in situ measure; *ii)* Excite all (or as many as possible) the behaviour types of the mechanical system and generate energy in all the zones (at least in one of the excitations); *iii)* Avoid problems of matrix inversion due to the similarity between all the considered excitations which leads to a poor linear independence of the linear systems to solve. Afterwards, the $\mathbf{T}$ matrix information is used to predict the real behaviour of the system.

We will refer as 'operational' output as the signal measured or computed when the mechanical system is excited with the real actions (not a test in the laboratory). In that situation the excitation can be almost random or at least different from the hammer impacts. For the case of the methacrylate box an operational state could be generated by means of a loudspeaker moving around the box. For the case of a train wagon, the operational states are the induced vibrations when the train is moving. We will talk also about 'Reconstructed' outputs. This will refer to the response of the system that is computed by means of $\mathbf{T}$ and the operational signal of the control points. An expression similar to Eq. (4.1) is considered. The direct field p_T^e has been

in most of the cases neglected. The target output can differ from the pressure in a position. This is specified in every shown simulation.

Figure 4.6(a) shows two curves with the absolute value of the pressure in microphone 1 when the point force is applied at ACC1. One of them ('Operational') is the signal directly measured. The other one ('Reconstructed'), is the reconstruction of the pressure in microphone 1 by means of the accelerations in all the control points. $\mathbf{T}$ is computed with hammer impacts in the nominal position (the operational behaviour is caused also by the same point force applied at ACC1).

Both pressure curves are exactly the same. This is because the same excitation type is considered in order to compute $\mathbf{T}$ and generate the operational state. The same coincidence between curves is observed with the point force applied at any of the control points.

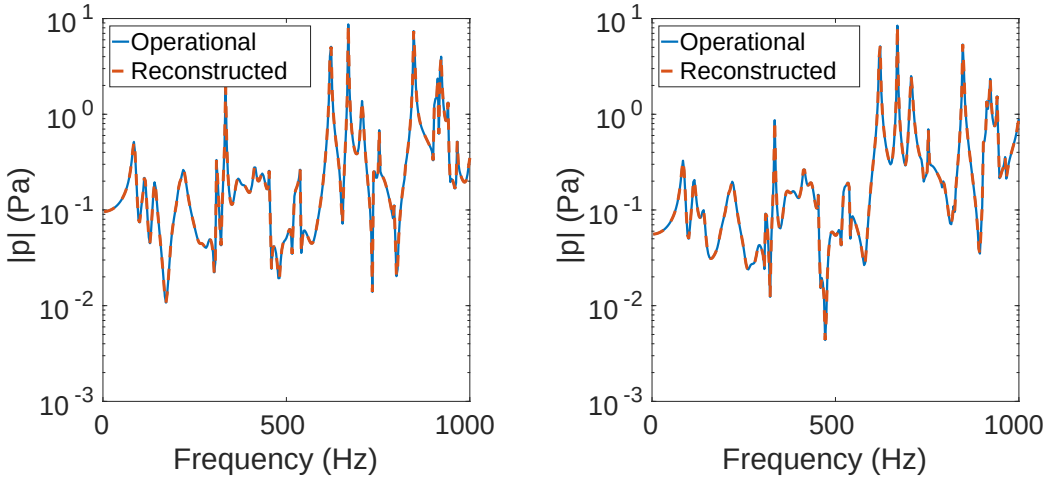

(a) (b)

Figure 4.6: Signal at microphone MIC1 (absolute value of pressure $|p|$) when a point force is exciting at the position of the accelerometer ACC1. All the curves are FEM simulations. Comparison between operational and reconstructed signals. The two curves are overlapped because the reconstruction is exact. Both the point force considered in the operational state and the point force used to compute the $\mathbf{T}$ are placed at: (a) nominal position of the accelerometer; (b) close to accelerometer.

Figure 4.6(b) is exactly the same as Figure 4.6(a) with the difference that the point forces are not applied at the nominal position where the accelerometer is placed but in the surroundings. The agreement between operational and reconstructed signals is again almost exact.

Some differences can be found if the point force used to generate an operational state of the mechanical system is applied at a position that differs from the ones used to compute the $\mathbf{T}$ matrix. Figure 4.8 shows this effect.

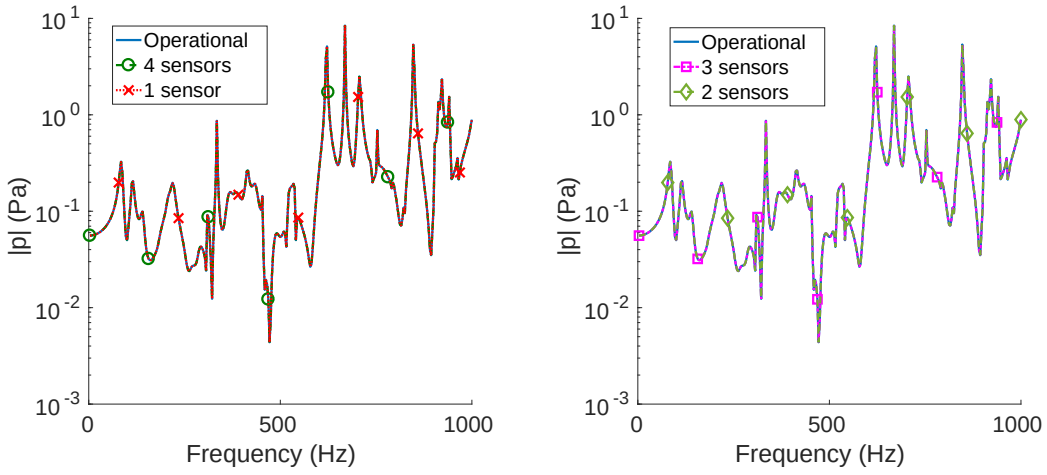

(a) (b)

Figure 4.7: Signal at microphone MIC1 (absolute value of pressure $|p|$) when a point force is exciting at the position of the accelerometer ACC1. Comparison between operational and reconstructed signals (point force close to accelerometer). All the curves are FEM simulations. Influence of the different number of used sensors per face. Each plot contains three overlapped curves because the reconstruction is exact and the result is not dependent on the number of sensors per face used. Operational signal on both plots is overlapped with the reconstructed signal taking into account: (a) 1 and 4 accelerometers per face; (b) 2 and 3 accelerometers per face.

As mentioned before, four accelerometers per face are considered in all the box results shown here. However, the simulations have also been done with only one, two (side by side and symmetrical with respect to the rectangular face diagonal) and three accelerometers per face. The positions in Figure 4.2 are considered and some of the accelerometers are removed. Figure 4.7 shows the same signal reconstruction of Figure 4.6(b) but using a different number of accelerometers per face. As expected, the results are exactly the same. The transfer function between the accelerometer 1 and the microphone 1 is not modified by adding other accelerometers.

The box has also been excited by means of 88 randomly distributed point forces normal to the face with also random modulus and sign (close to rain-on-the-roof excitation in the sense that point forces are distributed all around the plate but with

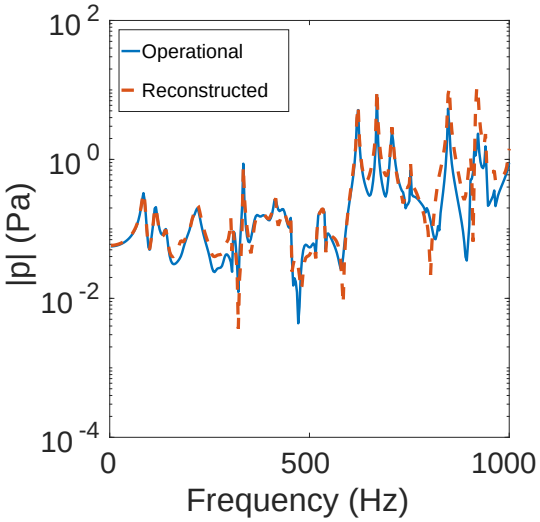

Figure 4.8: Signal at microphone MIC1 (absolute value of pressure $|p|$) when a point force is exciting at the position of accelerometer ACC1. All the curves are FEM simulations. Comparison between operational and reconstructed signals. The point force excitation is placed close to point ACC1 but $\mathbf{T}$ matrix has been computed by means of point forces exciting exactly at points ACCi.

coherent excitation) and a uniform pressure applied at the front face. The results are shown in Figure 4.9(a) and Figure 4.9(b) respectively. It can be seen that in both cases the differences between operational and reconstructed curves are larger than before but they still have a similar trend and modal distribution. This separation of the curves is due to the different excitation type considered when computing the $\mathbf{T}$ and when simulating the operational status.

Figure 4.9(b) contains also a third curve. Its goal is to illustrate the effect of the direct field p_T^e in Eq. (4.1). p_T^e is computed here as the vibration and pressure fields obtained due to the excitation of the mechanical system by means of the operational action but considering the boundary conditions used in the 'from definition' procedure to compute $\mathbf{T}$. Here it is the uniform pressure applied at the front face with all the control points blocked. For this reason p_T^e is known as the direct field (signal that arrived when all the control points are blocked, the signal cannot go through alternative paths). We see that the addition of p_T^e to the reconstructed field exactly complements the reconstructed curve in order to fit the 'operational' simulation. This is important and shows that the relationship (4.1) is exact. p_T^e is usually neglected in the experimental procedures. Among other reasons, because it is very difficult

to measure (all control points should be blocked) and because if control points are properly chosen and enough sensors used, p_T^e tends to be small. This numerical simulation shows also that the inherent errors of the ATPA method by neglecting the direct field can be estimated a priori by means of p_T^e.

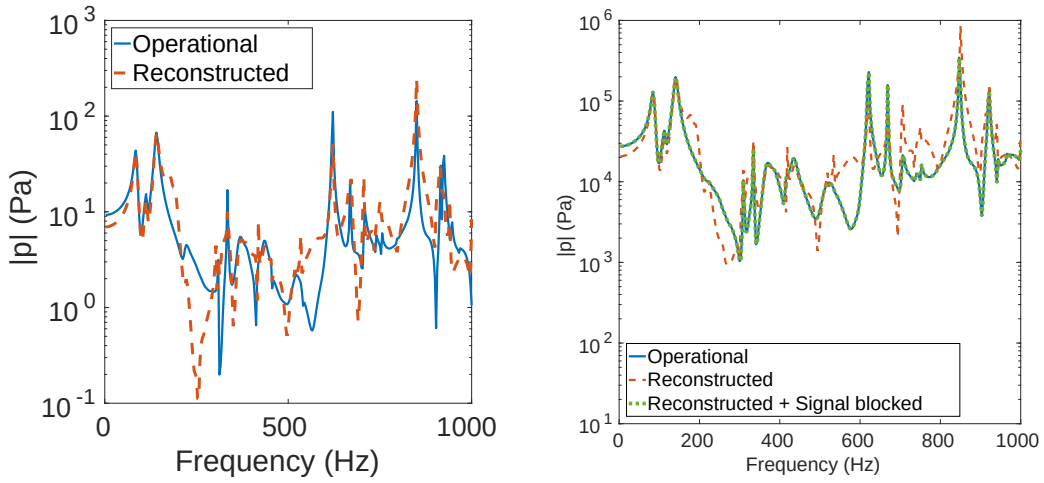

(a) (b)

Figure 4.9: Signal reconstruction at microphone number 1 (MIC1, absolute value of pressure $|p|$): (a) 88 point forces are randomly distributed all over the front face; (b) the front face is excited with a uniform unitary pressure. All the curves are FEM simulations.

It is shown how the hypothesis of excitation-independence for the direct transfer functions is not completely true and sometimes the direct field is relevant. However, the global trend of the signal is properly reconstructed in spite of the differences at specific frequencies.

4.2.4 Vibration transmission between opposite faces of the box

A particular transmission path is analysed in this section: the vibration transmission between opposite (front and back) faces. This is relevant because there is no direct transmission path between the faces. Moreover, the paths are not only through the structure but also across the air cavity. For these reasons, to properly characterise the transmission caused by a chain of first-order paths is a good challenge in order to test the ATPA method and understand the vibroacoustic response of the box.

A first aspect to be considered is the importance of the cavity paths versus the structural ones. Figure 4.10 compares two direct transfers with and without air cavity. In both cases, the values of the function at a specific frequency and the general trend of the curve is very similar. This indicates that the cavity has no important effect on this transmission path and that the coupling air-to-structure is weak. The curve corresponding to the case with cavity shows some more oscillations. This is caused by the increase of modes on the system due to the presence of the cavity. Moreover, the modal density of the cavity is larger than those of the box faces after 500 Hz approximately. At very low frequencies the cavity can produce a more efficient transmission.

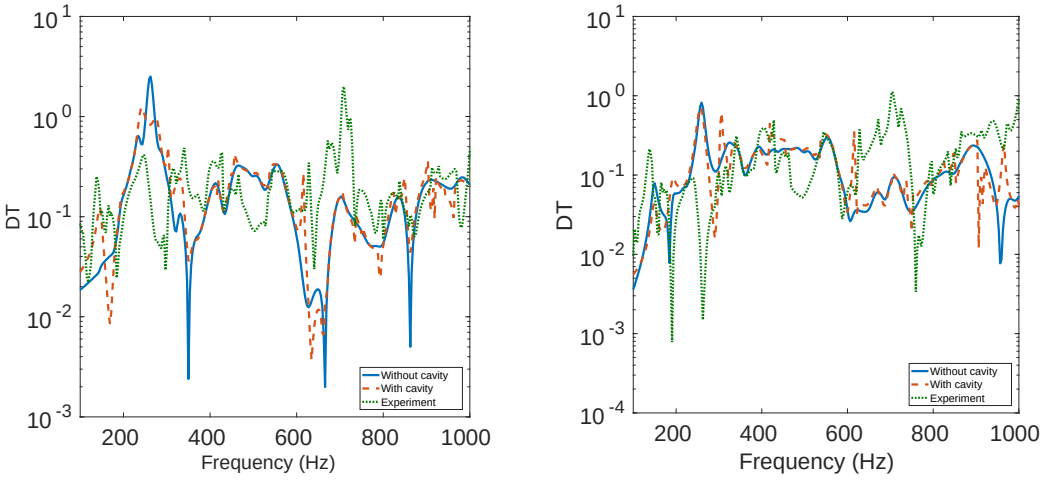

Figure 4.10: Comparison of the direct transfer between opposite faces of the box with and without air cavity inside: (a) $\mathbf{T}_{1,9}$; (b) $\mathbf{T}_{1,10}$.

In all the previous results the control points are characterised by the acceleration in the direction normal to the plate (this is chosen among the six degrees of freedom per node in the shell finite element) . This is a common option because normal acceleration is measured in a natural way, the vibration is mostly caused by bending and the interaction with the cavity is due to normal displacement. However, the ATPA method deals with degrees of freedom in general and allows dealing with more than one variable per control point. See for example Guasch and Magrans (2004a) where it is shown how rotations and displacements are relevant for the transmission path analysis of a beam. Figure 4.11 shows the comparison for the usual case where

only the normal acceleration is considered at each control point and the case where also two rotations are considered. The rotations are the ones with rotation vector in the plane of the plate (i.e. in the control points in the plate with constant X coordinate and acceleration measured in the X direction, the rotations with vectors in the Y and Z directions are considered). These degrees of freedom are chosen as a more detailed an alternative description of the bending response of the plates in the framework of an ATPA analysis. The differences between the two curves are not large and the general trend is the same. This suggests that for the analysis of this box, taking into account the normal acceleration is enough.

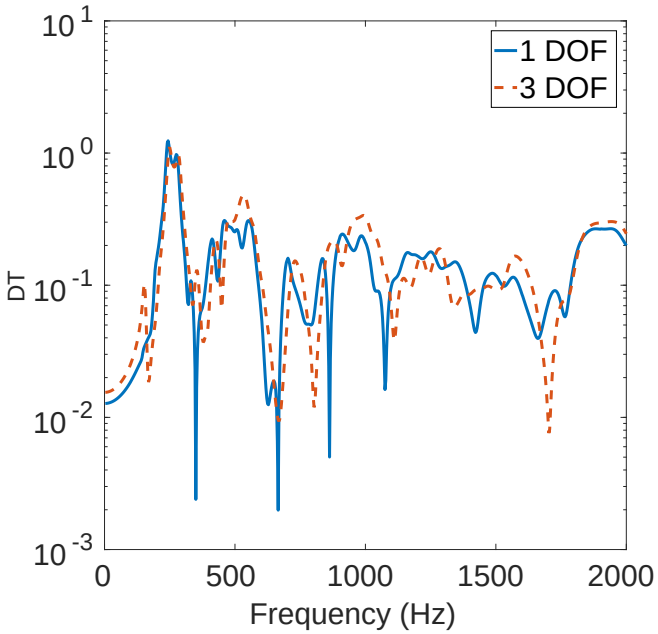

Figure 4.11: Direct transfer function between two accelerometers computed by means of the FEM: $\mathbf{T}_{1,9}$. Comparison between the case when only the normal displacement at each accelerometer (1 DOF: one degree of freedom per control point) is considered or also two rotations are taken into account (3 DOF: three degrees of freedom per control point).

It should be noted that experimental measurement of rotations is not straightforward. On the contrary they can be obtained without difficulties from the numerical model which shows again on of the advantages of virtual experiments.

A good option for determining the importance of a transmission path is to compare its direct and global transfer functions. Even if the low-frequency ATPA method

works with modulus and phase (complex numbers) and individual paths can cancel each other, the comparison of the absolute value of direct and global transfer functions can be a good indicator. A small difference between global and direct transfers means that most of the transmission is done through the path. Figure 4.12 shows this comparison for three different transmissions: between opposite faces, between adjacent faces and between sensors placed at the same face. It is clear how the largest difference between frequency response curves is found for the case of opposite faces. This transmission is not done by means of a direct path from face to face, which does not exist, but through indirect paths.

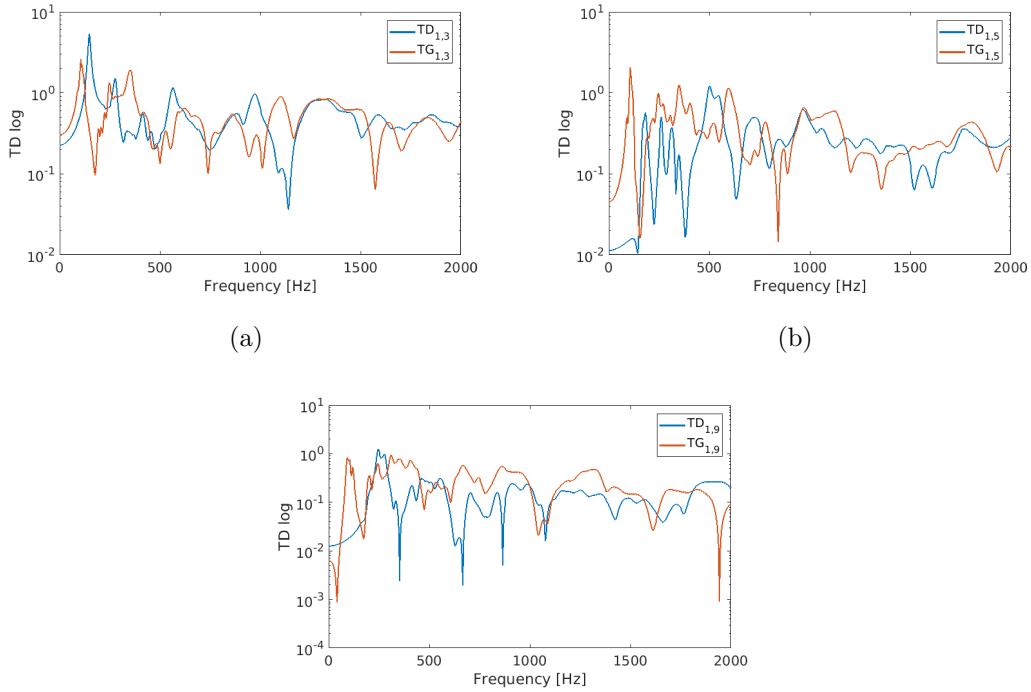

(a) (b)

(c)

Figure 4.12: Comparison between the global transfer (GT) and the direct transfer (DT): (a) $\mathbf{T}_{1,3}$ and $\mathbf{T}^G{}_{1,3}$, points located at the same face; (b) $\mathbf{T}_{1,5}$ and $\mathbf{T}^G{}_{1,5}$, points located at adjacent faces; (c) $\mathbf{T}_{1,9}$ and $\mathbf{T}^G{}_{1,9}$, points located at opposite faces. All the curves are FEM simulations.

ATPA can be used to discover the topology of a system and determine how the signal is transmitted. To do so, all the direct transmission functions are required. They provide information on the direct connection between control points. Figure 4.13 is an example on how by means of the direct transfer matrix the topology of the box

can be recovered. It is based on the outputs of the FEM model for the box without air cavity inside at a frequency of 62.5 Hz. Figure 4.13(b) is a physical interpretation of the signals, taking into account the geometry of the box and the positions of the accelerometers. The box is unfolded in order to draw it in a single plane with the most important paths in nodes 1 and 4. Figure 4.13(a) is a graph map with only the most important transmission paths for all the box. The nodes represent the accelerometers and the arrows the connections. Both figures are just a graphical representation of the direct transfer values of the matrix $\mathbf{T}$ shown in Figure 4.13(c). There the colours indicate the absolute value of the coefficient.

All the coefficients in the matrix $\mathbf{T}$ are ordered (considering their absolute value). In that case, all the paths between nodes i and j with $|\mathbf{T}_{ij}|$ which are less than 20% of the maximum coefficient are neglected. The assumption of this 'neglecting criterion' helps in order to clear all the non-meaningful paths and keep only those that are useful in order to characterise the system response. It is also important in order to draw a plot that can be more easily understood. Figure 4.13(a) shows a graph map of the most important connections between nodes. In red, the four stronger connections of node 1 are highlighted. The same is done in blue for the three stronger connections of node 4. When identifying these connections in the box geometry (see Figure 4.13(b)), it makes sense. In both cases these connections are the path to the closest nodes. This representation can be different at higher frequencies.

This shows how the outputs provided by ATPA can be represented in a graphic way. The plots help in order to understand the the physical behaviour of the system which is always very important in order to propose an improved design or identify noise and vibration problems.

4.3 Conclusions

The main conclusions that can be drawn in view of the results obtained and the experience with the laboratory prototype and the numerical model are as follows:

1. A consistent comparison between the laboratory measurement of a box with air cavity inside and a numerical model of the same box is shown. This validates somehow both the numerical simulations and the reliability of the experimental measurement. To neglect the radiation losses (effect of the air outside) is a reasonable hypothesis if the interest is focused on the box and air cavity inside.

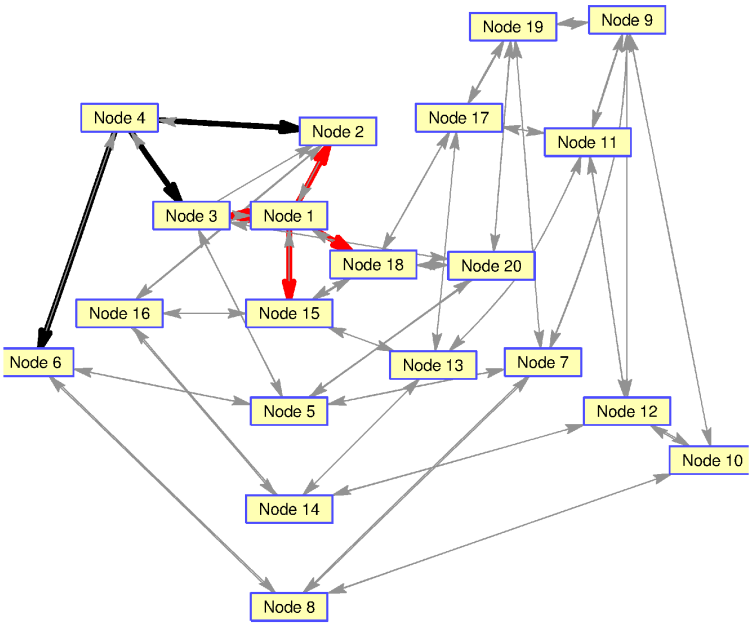

(a)

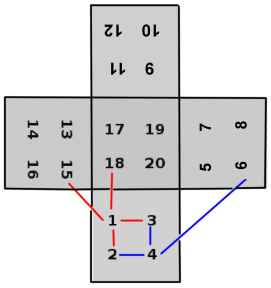

(b)

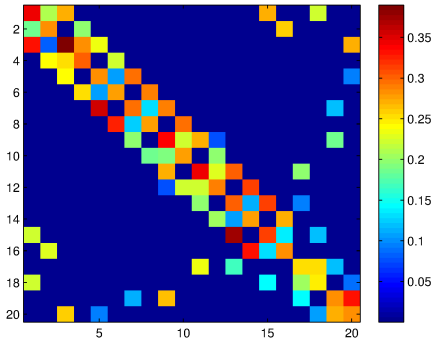

(c)

Figure 4.13: Graphical representation of the box topology through the direct transfer functions obtained by means of ATPA. Results obtained with the FEM model not considering the air cavity at a frequency of 62.5 Hz: (b) Sketch of the unfolded box where the main transmission paths are highlighted; (a) Graph of the most meaningful connectivities between control points; (c) Colour plot of the direct transfer matrix $\mathbf{T}$.

The combination of a multiphysics FEM software (Code Aster EDF (2017) with Gmsh Geuzaine and Remacle (2009)) with an automatic pre and post-processing set of scripts is a valid option to reproduce the ATPA procedures.

2. The numerical results show that ATPA procedure is exact if no experimental imprecisions exist. This can be seen with the coincidence of direct transfer functions computed by means of two different procedures in Section 4.2.1 or the exact reconstruction of the signal for the case of most simple operational excitation shown in Section 4.2.3.

3. ATPA method properly characterises all the transmission paths, not only the dominant ones.

4. The mechanical connectivity of the system can be defined by means of direct transfer functions. This is frequency-dependent and can be influenced by a proper definition of the measured degrees of freedom and points at the beginning of the process. By taking into account the frequencies that are below the first eigenfrequency, the physical structure of the system is identified.

5. Imprecision in the position where point force is applied has no effect on the outputs at low frequencies but it can be important at mid and high frequencies.

6. The difference between operational and reconstructed signals can be computed a priori. It is the solution of the system excited with operational force and all the control points / degrees of freedom blocked.

7. The type of operational excitation causes some differences in the signal reconstruction. However, they are not very large and can be estimated a priori. The difference is the solution of the problem with the control degrees of freedom blocked and the operational excitation.

4.A Calibration of the model and parameter tuning

Two different experimental setups are considered in order to callibrate the model. On the one hand the monitoring of the vibration response of a rectangular plate, see Figure 4.14(a). This is used in order to characterise the material properties of the methacrylate. On the other hand, the cuboid-shaped box which is also made of methacrylate with air cavity. This is the mechanical system where ATPA has been applied.

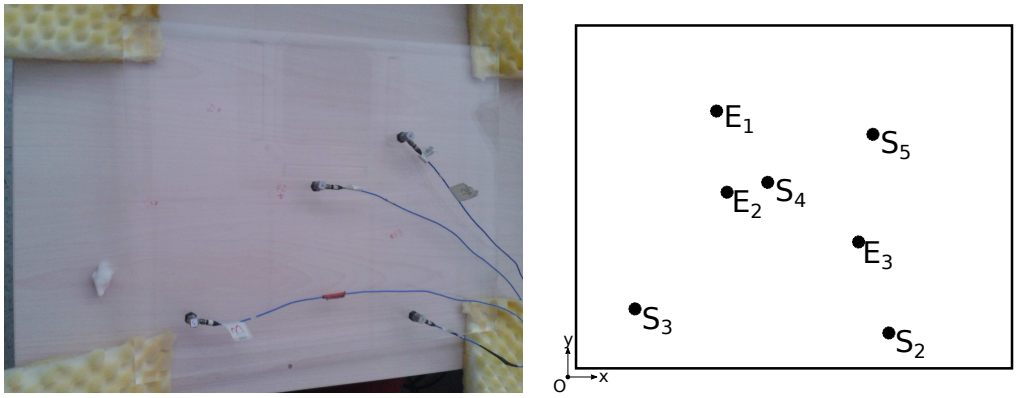

(a) (b)

Figure 4.14: Rectangular plate: (a) Photo of the instrumented plate; (b) Distribution of the excitation and sensor points in the plate.

Point	x [m]	y [m]
E_1	0.170	0.305
E_2	0.180	0.210
E_3	0.335	0.150
S_2	0.370	0.040
S_3	0.070	0.070
S_4	0.230	0.220
S_5	0.355	0.280

Table 4.3: Position of the excitation points E_i and the sensors S_i $(i = 2, \ldots, 5)$ in the plate model.

The rectangular plate, with dimensions 0.515 m $\times$ 0.405 m and 8.1 mm thick, is excited by means of a hammer impact at the positions E_i in Figure 4.14(b). In every of the realisation of the experiment, with the point force in a different position E_i, this input signal (the force measured at the point E_i) is denoted by S_1. Four accelerometers where the signal S_i $(i = 2, \ldots, 5)$ is measured are distributed judiciously (trying to avoid nodal lines, corners or accelerometers placed close to each other) over the plate. The positions of excited and control points are listed in Table 4.3. The plate is supported at the four corners on a very soft foam. Since the stiffness and the mass of the foams is small, the plate is supposed to be tested in free-free conditions. An experimental modal analysis of the plate was done in order to verify this hypothesis. It revealed that the agreement was correct except for the first two modes. For them, the stiffness of the foam had some influence in the response of the plate.

The calibration of the numerical model is done in three stages. First of all, the rectangular plate is used in order to find proper numerical values for the material parameters. It is reasonable to suppose that the methacrylate is a homogeneous and isotropic material. The density is thus obtained from the weight of the plate, see Table 4.2. The thickness of the plate is approximately constant and the measurements done by means of a calliper were in the range ± 0.1 mm. The details on the determination of the other material parameters are described in Section 4.A.1. Second, the vibration transmission through the corner in an L-shaped junction is measured and compared with the FEM simulation with correct agreement. It was concluded that these glued junctions could be properly modelled as homogeneous junctions. Finally a successful comparison of the box model and the measurements is shown in Section 4.A.2.

4.A.1 Material characterization: elasticity modulus and damping

Since the material is supposed to be linearly elastic and the density is known, the required material parameters are the elasticity modulus E, the Poisson's ratio ν and the hysteretic damping η. E and ν are supposed to be frequency-independent and ν is taken from the literature Bhushan and Burton (2005); Wei et al. (2005). It is reasonable since ν does not show a large variation range for this type of material. Once ν is fixed, the strategy is first to determine E and afterwards adjust a frequency-dependent damping law.

E is chosen in order to fit the first eigenfrequencies in the frequency range with modal behaviour (approximately $100 - 600$ Hz). These eigenfrequencies are obtained from an experimental modal analysis of the plate and can also be identified as the peaks in the experimental curve of Figure 4.15. Both eigenfrequency values are very similar and these reference values are listed in Table 4.4. As commented before, only the two lowest eigenfrequencies are affected by the stiffness of the foam used to sustain the plate.

The experimental curve in Figure 4.15 shows the averaged output

$$\psi(f) = \frac{1}{3}\sum_{j=1}^{3}\left|\frac{1}{F_j(f)}\right|\frac{1}{4}\sum_{i=1}^{4}|a_i(f)| \tag{4.3}$$

Mode	1	2	3	4	5	6	7
Eigenfrequency (Hz)	55	61	106	118	137	178	222
Mode	8	9	10	11	12	13	14
Eigenfrequency (Hz)	232	286	320	348	362	394	423

Table 4.4: Eigenfrequencies of the rectangular plate obtained with the experimental modal analysis

where the sum on i is done on all the four sensors of the plate, the sum on j is done on the three impacted positions, a_i and F_j are the phasors of the acceleration and the force registered in the hammer respectively. ψ can be understood as an spatially averaged accelerance. The other curves in Figure 4.15 are the results of the equivalent numerical experiments with different values of E.

The value of E can differ depending on the methacrylate type. Based on several values published in the literature Bhushan and Burton (2005); Wei et al. (2005) a variation range is defined and several discrete values of E between 3.0 GPa and 6.0 GPa are considered in order to feed the numerical model and plot curves like the ones in Figure 4.15. Each curve has a different peak pattern. It can be seen how the value of $E = 4.3$ GPa fits better the position of the peaks when compared with the experimental measurement. An eigenvalue problem has also been solved in order to verify that the undamped eigenfrequencies are in the same positions as the peaks.

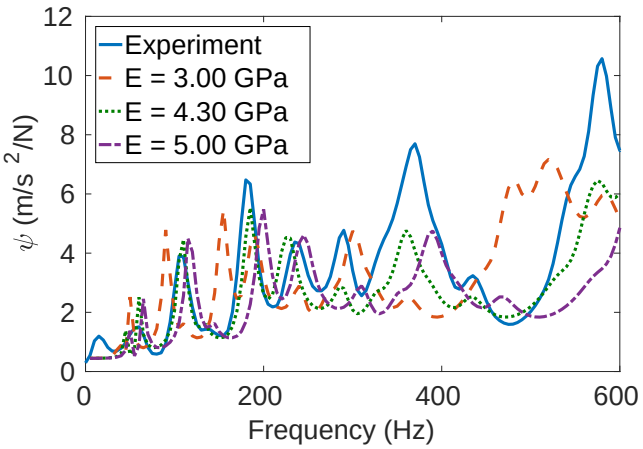

Figure 4.15: Frequency response function (averaged accelerance ψ) for different values of the elasticity modulus. The damping is constant $\eta = 0.07$.

Table 4.5 shows the arithmetic average of the relative error (considering absolute

Elasticity modulus	Mean	Standard deviation
3.00 GPa	17.71%	4.15%
4.00 GPa	5.02%	4.77%
4.30 GPa	3.04%	4.18%
4.60 GPa	4.07%	3.42%
5.00 GPa	7.69%	2.47%
6.00 GPa	16.59%	4.97%

Table 4.5: Mean relative error of the first 14 eigenfrequencies depending on the value of E. The results of the experimental modal analysis are taken as a reference.

value in order to avoid sign compensations) between the numerical and experimental eigenfrequencies. The value $E = 4.3$ GPa minimises these differences.

The damping law $\eta(f)$ is chosen in order to minimise the difference in the low frequency peak values (around the eigenfrequencies in the modal response zone) and also to properly reproduce the trend at high frequencies. Figure 4.16 shows some of the damping laws with the form $\eta = a + \omega^b$, where a and b are constants to fit. A minimisation of the difference between the computed and experimental curve in the whole frequency range (not only at the eigenfrequencies) leads to the following expression of the damping

$$\eta = 0.07 + \frac{1}{\omega} \tag{4.4}$$

4.A.2 Box model validation

Once the material parameters of the methacrylate are calibrated by means of the rectangular plate experiment, the response provided by the numerical model of the box is compared with measured data. The problem is vibroacoustic, including the cavity inside the box. The air parameters for the numerical model are taken from the literature: sound velocity in air $c = 345.23$ m/s and air density $\rho_a = 1.18$ kg/m^3.

A shaker is installed in the position of accelerometer ACC6, see Figure 4.2. This allows a better control of the position where the excitation is applied. The shaker is fixed to the face and the uncertainty of human manipulation of the hammer impact is suppressed. The output defined in Eq. (4.3) is considered for comparison. ψ is computed at every plate taking into account the four accelerometers, with the difference that only one force position is considered (where the shaker is placed). Figure 4.17 shows the parameter ψ for the top plate. The agreement is very good in

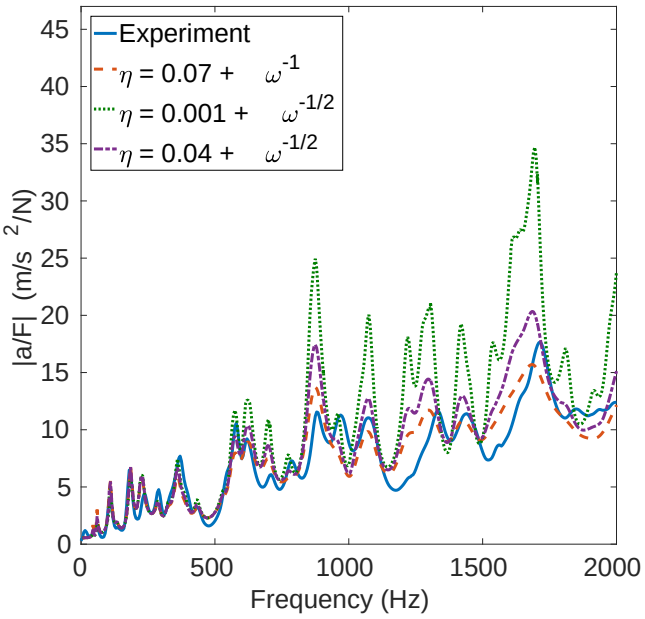

Figure 4.16: Frequency response function (accelerance) between two arbitrary points According to the notation $\eta = a + \omega^b$: $(a = 0.07, b = -1)$, $(a = 0.001, b = -1/2)$ and $(a = 0.04, b = -1/2)$.

Plate	e
Top	14.12%
Front	18.82%
Back	8.40%
Left	8.89%
Right	6.21%

Table 4.6: Difference between the experimental measurement and the simulation in each face of the plate according to Eq. (4.2).

both the shape of the curve and also the magnitude. We have not absolute certainty for the experimental measurements below 100 Hz. The reasons are several as exposed above: difficulty in the proper excitation of rigid-body motion modes and interference with the background noise/vibration. Similar results are obtained for the other faces of the box. A global measure of the error is shown in Table 4.6 where the difference between frequency response curves is measured by means of Eq. (4.2).

Figure 4.18 shows the comparison for the averaged square pressure at the microphones placed inside the cavity. The measure of the difference between experimental

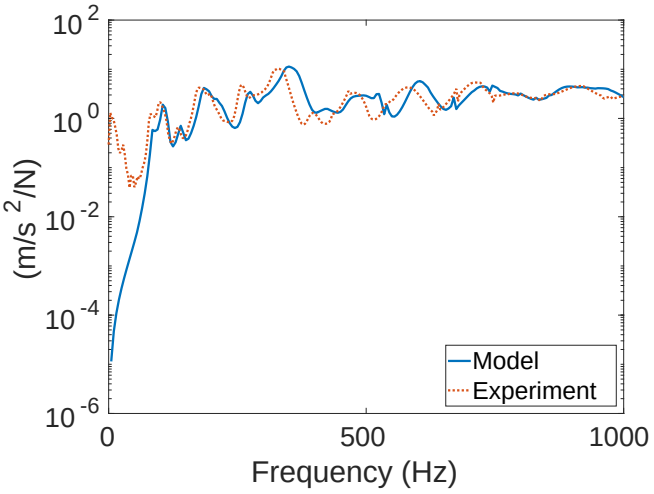

Figure 4.17: Comparison between the experiment and the numerical simulation. ψ_{exp} and ψ_{FEM} curves at the top plate due to the action of the shaker in the position ACC6.

and numerical curves is 7.25%. The agreement is deemed sufficient .

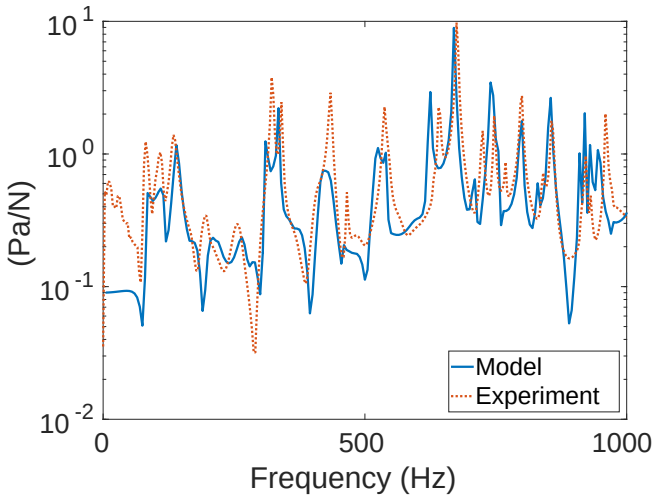

Figure 4.18: Absolute value of the averaged square pressure divided by the point force $|p/F|$ at the micros inside the cavity due to the action of the shaker in the position ACC6. Comparison between the experiment and the numerical simulation.

The global agreement between the numerical results and the experimental measurements is good both in terms of vibration and acoustic pressure. Moreover, the usual outputs of interest and regulation parameters are presented in dB . This means

that the relevance of these differences from the engineering point of view is of less importance . It is also true that the chosen parameters are somehow spatially averaged (few positions are considered). When outputs in a specific position are regarded, the differences are expected to be a bit larger due to the spatial shift of the pressure and vibration waves.

Chapter 5

Eigenvalue and eigenmode synthesis in elastically coupled subsystems[1]

5.1 Introduction

Many products consist of an active device; e.g. engines, compressor units, frequency converters, etc. and a structure which is defined to meet a functionality target. Such structures may be for example trains, cars, refrigerators, etc. and the corresponding active devices which supply energy to the entire system are frequently categorized as auxiliary equipment.

Other type of products which may be partitioned in a similar way are all kind of machines installed on top of a supporting structure, as typically encountered in industrial facilities.

The assembly of the two aforementioned elements, typically through elastic joints (see Figure 5.1), may generate noise and/or vibration complications due to the dynamic coupling between them. For instance, let an engine, whose dynamics are known, having no resonances at its fundamental excitation frequency. The engine is installed by means of elastic supports on a structure also not having resonances at excitation frequency. Then, the question that arises is whether the engine-structure

[1]Chapter based on the paper Magrans and J.Poblet-Puig (2018)

assembly will resonate. A resonance of the assembly at the excitation frequency would be critical since it may cause noise issues as well as ill-functioning of the product.

Now, consider that the modal frequencies and mode shapes of each subsystem are known when the subsystems are subject to an infinite impedance condition through the elastic joints at their interface, c.f. Figure 5.2. Then, the problem to be solved is determining the assembled system modal frequencies.

The problem of devising the behavior of a system from which one knows that of its two composing subsystems has been widely studied. The fields in which this problem has been addressed are widespread. As a matter of example one can cite in the field of electrical networks a method developed in ref. Kron (1963), the method is known as the Kron method. It was immediately applied to dynamics in Simpson and Tabarrok (1968), Simpson (1973) and has been further developed recently in Weng et al. (2009), Cui et al. (2016), Kaveh and Fazli (2011), Lui (2000). One can also cite methods in the field of physics of composite systems such as those applied to sets of phonons Dobrzynski and Puszkarski (1989) or to composite materials Sylla et al. (1989). Eventually, one may refer to methods in the field of dynamics, for which a non-exhaustive review of methods may be found in de Klerk et al. (2008).

The latter reference exposes an historic review of methods from which it summarizes the problem in just three equations and, subsequently, it examines the different approaches for its solution in the physical space, the modal space or the frequency space. The first equation is the dynamic equation for each of the subsystems subjected to external forces as well as coupling reaction forces. The second equation defines a linear dependency between coupling interface coordinates, usually trough a boolean matrix. Finally, the third equation defines the relation between the forces that each subsystem exerts on the other. Notice that the second equation assumes that the coupling interfaces are rigid or, generically, holonomic[2].

From this historical review one can note that the substructuring problem with elastic joints is not of frequent study. Yet, references Liu and Ewins (2000), Cuppens et al. (2001),Allen et al. (2010) have studied the problem with elastic couplings

[2]A coupling interface is holonomic if one or more functions relating the degrees of freedom of the coupling interface exist $f(x_1, x_2.., x_n) = 0$. Consider a structure is split in two parts and the coupling interface coinciding degrees of freedom are labelled x_{1F} y x_{2F}, then the continuity condition is simply $x_{1F} - x_{2F} = 0$. Conversely, if the coupling interface degrees of freedom are non-coincident, e.g. they are linked by an elastic joint as in the example problem, it can only be said that $k(x_{1F} - x_{2F}) = f$ being f a force of unknown magnitude, so that the problem constraints are no longer holonomic.

through modal or FRF based methods. The first of these two references confirms the fact that the vast majority of analysis methods for substructures coupling consider the interface being of rigid coupling kind.

The present work addresses the synthesis of eigenmodes as an algebraic problem. It is based on solving the eigenvalues of a block matrix having one or more anti-diagonal elements in antisymmetric positions, from the knowledge of each matrix block's eigenvalues and eigenvectors and of the antidiagonal elements.

The solution to this algebraic problem is achieved through a *Divide and Conquer* approach. One of the basic articles of such solution method is that of Cuppen (Cuppen, 1980), which studies the synthesis of eigensolutions of a tridiagonal matrix through a first order perturbation approach. Also, an article by Arbenz, ref. (Arbenz et al., 1988), extends the method to modifications of higher order.

The references in the former paragraph solve a very similar problem to that posed in the present work, given that a tridiagonal matrix may be regarded as a block matrix having two antisymmetric elements in its anti-diagonal. However, opposite to the Divide and Conquer method, the method proposed here does not modify the matrix blocks in order to achieve the solution.

This chapter is divided into three parts. The first part demonstrates the equivalence between the dynamic and the algebraic problems and the solution to the eigenvalues' algebraic problem is described for one, two and multiple coupling terms (section 5.2 and section 5.3). In the second part (section 5.4) the algebraic solution is applied to the physical problem (section 5.4.1) and the physical interpretation of the solution is discussed (section 5.4.2). This physical interpretation substantiates the computation of the eigenvectors in subsection 5.4.3.

Thence, the first part gives a formal solution to the algebraic problem which is applicable to any linear system, regardless of its physical interpretation, and the second part provides a physical meaning to the eigenvalue solution and to the computation of the eigenmodes.

The third part (section 5.5) presents two examples, one on a simple system shows the basic mechanics of the method and a second example shows the performance of the method on a system with many degrees of freedom and multiple connections.

5.2 Equivalence of the physical and algebraic problems

In the present work an algorithm which computes the eigenfrequencies and eigenvectors of a system consisting of two parts is developed from the eigenfrequencies and eigenvectors of each of the two parts and the characteristics of the elastic elements which join them.

The proposed problem is equivalent to obtaining the eigenvalues and eigenvectors of a block matrix in which the two composing blocks are connected at m degrees of freedom, hence having non-zero valued anti-diagonal elements.

Let a mechanical system consisting of two subsystems such as shown in Figure 5.1

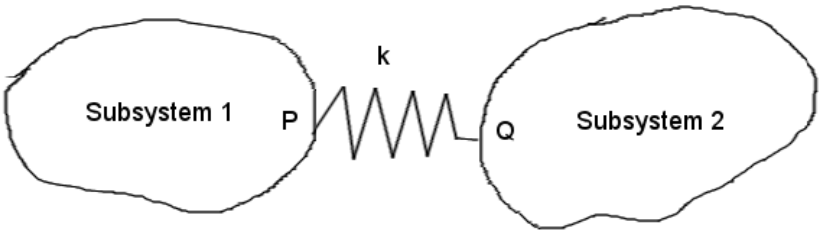

Figure 5.1: Subsystems 1 and 2 with one or more coupling spring

Let $\mathbf{A}_1$ and $\mathbf{A}_2$ be the dynamic matrices of the two subsystems in isolation as depicted in Figure 5.2, i.e. including fixed boundary conditions at the coupling interface.

Then

$$\begin{aligned} \mathbf{A}_1 &= \mathbf{K}_1 - \omega^2 \mathbf{M}_1 \\ \mathbf{A}_2 &= \mathbf{K}_2 - \omega^2 \mathbf{M}_2 \end{aligned} \tag{5.1}$$

Where the mass matrices $\mathbf{M}$ are diagonal matrices and $\mathbf{K}$ are the stiffness matrices.

Let k be the stiffness of the coupling spring.

The assembled system dynamic matrix $\mathbf{A}$ may be described as:

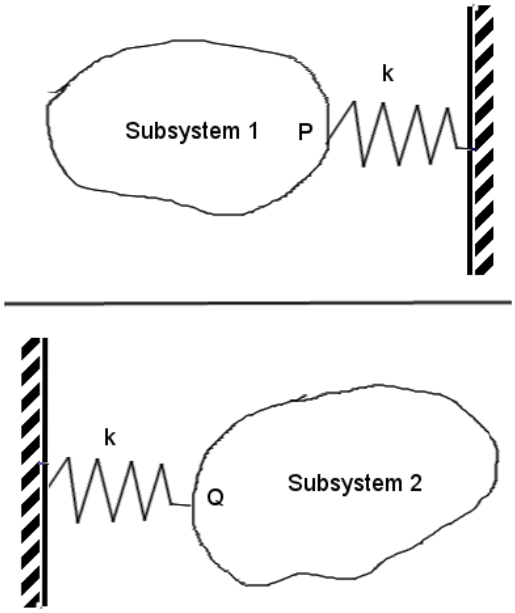

Figure 5.2: The total system is split into subsystems 1 and 2 as shown in the figure. This decomposition allows the blocks that define the subsystems not to vary by forming the total system.

$$\mathbf{A} = \begin{pmatrix} \mathbf{K}_1 & \mathbf{0} \\ \mathbf{0} & \mathbf{K}_2 \end{pmatrix} - \omega^2 \begin{pmatrix} \mathbf{M}_1 & \mathbf{0} \\ \mathbf{0} & \mathbf{M}_2 \end{pmatrix} + \begin{pmatrix} 0 & \dots & 0 & 0 & \dots & 0 \\ \vdots & \ddots & \vdots & \vdots & \ddots & \vdots \\ 0 & \dots & 0 & k & \dots & 0 \\ 0 & \dots & k & 0 & \dots & 0 \\ \vdots & \ddots & \vdots & \vdots & \ddots & \vdots \\ 0 & \dots & 0 & 0 & \dots & 0 \end{pmatrix} \tag{5.2}$$

Be it P and Q labels corresponding to the degrees of freedom linked by the elastic element, P in subsystem 1 and Q in subsystem 2. The system eigenmodes and eigenfrequencies correspond to the eigenvalues and eigenvectors of the matrix

$$\mathbf{H} = \begin{pmatrix} \mathbf{M}_1^{-1}\mathbf{K}_1 & \mathbf{0} \\ \mathbf{0} & \mathbf{M}_2^{-1}\mathbf{K}_2 \end{pmatrix} + \begin{pmatrix} 0 & \dots & 0 & 0 & \dots & 0 \\ \vdots & \ddots & \vdots & \vdots & \ddots & \vdots \\ 0 & \dots & 0 & \frac{k}{m_P} & \dots & 0 \\ 0 & \dots & \frac{k}{m_Q} & 0 & \dots & 0 \\ \vdots & \ddots & \vdots & \vdots & \ddots & \vdots \\ 0 & \dots & 0 & 0 & \dots & 0 \end{pmatrix} \tag{5.3}$$

In this equation m_P is the diagonal coefficient of matrix $\mathbf{M}_1$ corresponding to the degree of freedom labelled as P and, likewise, m_Q is the diagonal coefficient of matrix $\mathbf{M}_2$ corresponding to the degree of freedom labelled as Q.

According to Eq. (5.3), matrix $\mathbf{H}$, from which the eigensolutions are seeked, is of the kind:

$$\mathbf{H} = \mathbf{B} + \mathbf{C} \tag{5.4}$$

Where $\mathbf{B}$ is a block matrix, as it is explicit in Eq. (5.5), and $\mathbf{C}$ is a matrix with non-zero values in, at least, two antisymmetric positions in the two antisymmetric blocks, Eq. (5.6).

$$\mathbf{B} \equiv \begin{pmatrix} \mathbf{B}_1 & \mathbf{0} \\ \mathbf{0} & \mathbf{B}_2 \end{pmatrix} \tag{5.5}$$

$$\mathbf{C} \equiv \begin{pmatrix} 0 & \dots & 0 & 0 & \dots & 0 \\ \vdots & \ddots & \vdots & \vdots & \ddots & \vdots \\ 0 & \dots & 0 & c_{PQ} & \dots & 0 \\ 0 & \dots & c_{QP} & 0 & \dots & 0 \\ \vdots & \ddots & \vdots & \vdots & \ddots & \vdots \\ 0 & \dots & 0 & 0 & \dots & 0 \end{pmatrix} \tag{5.6}$$

The equivalent algebraic problem involves the calculation the eigenvalues and eigenvectors of matrix $\mathbf{H}$ from those of $\mathbf{B}_1$, $\mathbf{B}_2$ and from the coefficients of matrix $\mathbf{C}$.

5.3 Method

Under the framework of the problem raised in the introduction, the solution for the union of two diagonal blocks in $\mathbf{H}$ will be obtained here for the cases: A single

connecting element (section 5.3.1), two connecting elements (section 5.3.2) and m connecting elements (section 5.3.3).

5.3.1 Single connection. Synthesis of eigenvalues

Let

$$\mathbf{H} = \mathbf{B} + \mathbf{C} \tag{5.7}$$

where the matrix $\mathbf{C}$ and the eigensolutions for $\mathbf{B}$ are known, the eigenvalues of $\mathbf{H}$ are sought. $\mathbf{C}$ may be expressed as:

$$\mathbf{C} = \mathbf{e}_P c_{PQ} \mathbf{e}_Q^T + \mathbf{e}_Q c_{QP} \mathbf{e}_P^T \tag{5.8}$$

where $\mathbf{e}_P$ is a basis vector unity valued at the degree of freedom labelled P and zero valued elsewhere. The same holds for $\mathbf{e}_Q$.

If $\mathbf{B}$ is diagonalizable (over the complex field C, any matrix either is diagonalizable or is arbitrarily close to a matrix with distinct eigenvalues that does), it may be formulated as:

$$\mathbf{B} = \mathbf{V}_B \mathbf{D}_B \mathbf{V}_B^{-1} \tag{5.9}$$

with $\mathbf{D}_B$ a diagonal matrix containing the eigenvalues of the isolated subsystems and $\mathbf{V}_B$ the corresponding matrix of eigenvectors. Matrix $\mathbf{V}_B$ has, naturally, the same block structure as $\mathbf{B}$.

Consequently, $\mathbf{H}$ is reformulated as:

$$\mathbf{H} = \mathbf{V}_B(\mathbf{D}_B + \mathbf{V}_B^{-1}\mathbf{C}\mathbf{V}_B)\mathbf{V}_B^{-1} = \mathbf{V}_B \mathbf{H}^{'} \mathbf{V}_B^{-1} \tag{5.10}$$

where

$$\mathbf{H}^{'} = \mathbf{D}_B + \mathbf{V}_B^{-1}\mathbf{C}\mathbf{V}_B \tag{5.11}$$

Equation (5.10) demonstrates that $\mathbf{H}$ and $\mathbf{H}^{'}$ are similar matrices, ergo they certainly have identical eigenvalues and eigenvectors.

Let

$$\mathbf{u}_P = \mathbf{V}_B^{-1}\mathbf{e}_P \qquad\qquad \mathbf{v}_P^T = \mathbf{e}_P^T \mathbf{V}_B \tag{5.12}$$

where $\mathbf{u}_P$ is the column vector corresponding to degree of freedom P in matrix $\mathbf{V}_B^{-1}$ and $\mathbf{v}_P^T$ is the row vector corresponding to degree of freedom P in matrix $\mathbf{V}_B$. Analogous formulation holds for Q.

Substituting $\mathbf{C}$ by Eq. (5.8) in equation Eq. (5.11)

$$\mathbf{H}^{'} = \mathbf{D}_B + c_{_{PQ}}\mathbf{u}_{_P}\mathbf{v}_{_Q}^T + c_{_{QP}}\mathbf{u}_{_Q}\mathbf{v}_{_P}^T \tag{5.13}$$

if $\mathbf{x}$ is an eigenvector of $\mathbf{H}^{'}$ with associated eigenvalue λ_H it holds that:

$$\left(\mathbf{D}_B + c_{_{PQ}}\mathbf{u}_{_P}\mathbf{v}_{_Q}^T + c_{_{QP}}\mathbf{u}_{_Q}\mathbf{v}_{_P}^T\right)\mathbf{x} = \lambda_H\mathbf{x} \tag{5.14}$$

The inverse of $(\lambda_H\mathbf{I} - \mathbf{D}_B)^{-1}$ exists provided that the eigenvalues of the coupled system do not coincide with those of the subsystems. For very weak coupling, the system eigenvalues will be very close to the eigenvalues of the isolated blocks, but they will not be strictly equal unless the blocks were fully decoupled. Therefore, in general, the inverse of $(\lambda_H\mathbf{I} - \mathbf{D}_B)^{-1}$ must exist. Hence, equation (5.14) may be rearranged as follows

$$\mathbf{x} = (\lambda_H\mathbf{I} - \mathbf{D}_B)^{-1}(c_{_{PQ}}\mathbf{u}_{_P}\mathbf{v}_{_Q}^T\mathbf{x} + c_{_{QP}}\mathbf{u}_{_Q}\mathbf{v}_{_P}^T\mathbf{x}) \tag{5.15}$$

Then, taking the scalar product of Eq. (5.15) with $\mathbf{v}_{_Q}^T$ and, separately, with $\mathbf{v}_{_P}^T$, and given that $\mathbf{v}_{_P}^T$ only has non zero valued components in subsystem 1 and $\mathbf{v}_{_Q}^T$ only has non zero valued components in subsystem 2, one obtains:

$$\mathbf{v}_{_Q}^T\mathbf{x} = c_{_{QP}}\mathbf{v}_{_Q}^T(\lambda_A\mathbf{I} - \mathbf{D}_B)^{-1}\mathbf{u}_{_Q}\mathbf{v}_{_P}^T\mathbf{x} \tag{5.16}$$

$$\mathbf{v}_{_P}^T\mathbf{x} = c_{_{PQ}}\mathbf{v}_{_P}^T(\lambda_H\mathbf{I} - \mathbf{D}_B)^{-1}\mathbf{u}_{_P}\mathbf{v}_{_Q}^T\mathbf{x} \tag{5.17}$$

Substituting Eq. (5.17) in Eq. (5.16) results in

$$\mathbf{v}_{_Q}^T\mathbf{x} = c_{_{QP}}c_{_{PQ}}\mathbf{v}_{_Q}^T(\lambda_H\mathbf{I} - \mathbf{D}_B)^{-1}\mathbf{u}_{_Q}\mathbf{v}_{_P}^T(\lambda_H\mathbf{I} - \mathbf{D}_B)^{-1}\mathbf{u}_{_P}\mathbf{v}_{_Q}^T\mathbf{x} \tag{5.18}$$

Assuming that $\mathbf{v}_{_Q}^T\mathbf{x} \neq 0$, equation (5.18) proves that the eigenvalues of $\mathbf{H}$, λ_H, must satisfy:

$$1 = c_{_{PQ}}c_{_{QP}}\sum_{i=1}^{n_1}\frac{v_{_{P,i}}^T u_{_{i,P}}}{\lambda_H - \lambda_{B_1,i}}\sum_{j=1}^{n_2}\frac{v_{_{Q,j}}^T u_{_{j,Q}}}{\lambda_H - \lambda_{B_2,j}} \tag{5.19}$$

Thus, as a conclusion to this section, it can be asserted that there exists a function

$$\boxed{\Gamma(\lambda) = 1 - c_{_{PQ}}c_{_{QP}}\sum_{i=1}^{n_1}\frac{v_{_{P,i}}^T u_{_{i,P}}}{\lambda - \lambda_{B_1,i}}\sum_{j=1}^{n_2}\frac{v_{_{Q,j}}^T u_{_{j,Q}}}{\lambda - \lambda_{B_2,j}}} \tag{5.20}$$

whose zeroes correspond to the eigenvalues of matrix $\mathbf{H}$.

5.3.2 Two connections. Synthesis of eigenvalues

Let $\mathbf{H}$ and $\mathbf{B}$ be the same matrices as in section 5.3.1, but now assuming that $\mathbf{C}$ has two connection elements, one connecting P_1 with Q_1 and another connecting P_2 with Q_2. The degrees of freedom labelled P always correspond to block 1, and those labelled Q belong to block 2.

Under these assumptions, matrix $\mathbf{C}$ may be reformulated as:

$$\mathbf{C} = \mathrm{c}_{Q_1P_1}\mathbf{e}_{Q_1}\mathbf{e}_{P_1}^T + \mathrm{c}_{P_1Q_1}\mathbf{e}_{P_1}\mathbf{e}_{Q_1}^T + \mathrm{c}_{Q_2P_2}\mathbf{e}_{Q_2}\mathbf{e}_{P_2}^T + \mathrm{c}_{Q_2P_2}\mathbf{e}_{P_2}\mathbf{e}_{Q_2}^T$$

Similarly to section 5.3.1 derivations, one may define:

$$\mathbf{u}_{P_s} = \mathbf{V}_B^{-1}\mathbf{e}_{P_s} \qquad\qquad \mathbf{v}_{P_s}^T = \mathbf{e}_{P_s}^T\mathbf{V}_B \tag{5.21}$$

for $s = 1, 2$, and analogous definitions for Q.

If $\mathbf{x}$ is an eigenvector of $\mathbf{H}$ with associated eigenvalue λ_H it holds that

$$\left(\mathbf{D}_B + \mathrm{c}_{Q_1P_1}\mathbf{u}_{Q_1}\mathbf{v}_{P_1}^T + \mathrm{c}_{P_1Q_1}\mathbf{u}_{P_1}\mathbf{v}_{Q_1}^T + \mathrm{c}_{Q_2P_2}\mathbf{u}_{Q_2}\mathbf{v}_{P_2}^T + \mathrm{c}_{P_2Q_2}\mathbf{u}_{P_2}\mathbf{v}_{Q_2}^T\right)\mathbf{x} = \lambda_H\mathbf{x} \tag{5.22}$$

and taking scalar product with $\mathbf{v}_{P_1}^T$ and $\mathbf{v}_{P_2}^T$ yields

$$\begin{pmatrix}\mathbf{v}_{P_1}^T\mathbf{x}\\ \mathbf{v}_{P_2}^T\mathbf{x}\end{pmatrix} = \begin{pmatrix} c_{P_1Q_1}\mathbf{v}_{P_1}^T(\lambda_H\mathbf{I}-\mathbf{D}_B)^{-1}\mathbf{u}_{P_1} & c_{P_2Q_2}\mathbf{v}_{P_1}^T(\lambda_H\mathbf{I}-\mathbf{D}_B)^{-1}\mathbf{u}_{P_2}\\ c_{P_1Q_1}\mathbf{v}_{P_2}^T(\lambda_H\mathbf{I}-\mathbf{D}_B)^{-1}\mathbf{u}_{P_1} & c_{P_2Q_2}\mathbf{v}_{P_2}^T(\lambda_H-\mathbf{D}_B\mathbf{I})^{-1}\mathbf{u}_{P_2}\end{pmatrix}\begin{pmatrix}\mathbf{v}_{Q_1}^T\mathbf{x}\\ \mathbf{v}_{Q_2}^T\mathbf{x}\end{pmatrix} \tag{5.23}$$

Likewise, it is straightforward to prove that

$$\begin{pmatrix}\mathbf{v}_{Q_1}^T\mathbf{x}\\ \mathbf{v}_{Q_2}^T\mathbf{x}\end{pmatrix} = \begin{pmatrix} c_{Q_1P_1}\mathbf{v}_{Q_1}^T(\lambda_H\mathbf{I}-\mathbf{D}_B)^{-1}\mathbf{u}_{Q_1} & c_{Q_2P_2}\mathbf{v}_{Q_1}^T(\lambda_H\mathbf{I}-\mathbf{D}_B)^{-1}\mathbf{u}_{Q_2}\\ c_{Q_1P_1}\mathbf{v}_{Q_2}^T(\lambda_A\mathbf{I}-\mathbf{D}_B)^{-1}\mathbf{u}_{Q_1} & c_{Q_2P_2}\mathbf{v}_{Q_2}^T(\lambda_H\mathbf{I}-\mathbf{D}_B)^{-1}\mathbf{u}_{Q_2}\end{pmatrix}\begin{pmatrix}\mathbf{v}_{P_1}^T\mathbf{x}\\ \mathbf{v}_{P_2}^T\mathbf{x}\end{pmatrix} \tag{5.24}$$

Let the matrices in (5.23) and (5.24) be named $\mathbf{E}$ and $\mathbf{F}$. Substituting the vector to the left of (5.24) in (5.23) one obtains

$$\begin{pmatrix}\mathbf{v}_{P_1}^T\mathbf{x}\\ \mathbf{v}_{P_2}^T\mathbf{x}\end{pmatrix} = \mathbf{EF}\begin{pmatrix}\mathbf{v}_{P_1}^T\mathbf{x}\\ \mathbf{v}_{P_2}^T\mathbf{x}\end{pmatrix} \Rightarrow (\mathbf{I}-\mathbf{EF})\begin{pmatrix}\mathbf{v}_{P_1}^T\mathbf{x}\\ \mathbf{v}_{P_2}^T\mathbf{x}\end{pmatrix} = \mathbf{0} \tag{5.25}$$

So that the non-trivial solution to (5.25), i.e. $\mathbf{x}$ not being a null vector, is:

$$\boxed{\det(\mathbf{I}-\mathbf{EF}) = 0} \tag{5.26}$$

This equation is equivalent to the one obtained for one degree of freedom in Eq. (5.20).

Equation (5.26) is a function of λ, whose zeroes are the eigenvalues λ_H of matrix $\mathbf{H}$.

5.3.3 Arbitrary number of connections. Synthesis of eigenvalues

Following section (5.3.2), the general solution may be readily formulated.

Let

$$\mathbf{E} = \begin{pmatrix} \mathbf{v}_{P_1}^T \mathbf{S}\mathbf{u}_{P_1} & \mathbf{v}_{P_1}^T \mathbf{S}\mathbf{u}_{P_2} & \mathbf{v}_{P_1}^T \mathbf{S}\mathbf{u}_{P_m} \\ \mathbf{v}_{P_2}^T \mathbf{S}\mathbf{u}_{P_1} & \mathbf{v}_{P_2}^T \mathbf{S}\mathbf{u}_{P_2} & \mathbf{v}_{P_1}^T \mathbf{S}\mathbf{u}_{P_m} \\ \vdots & \vdots & \vdots \\ \mathbf{v}_{P_m}^T \mathbf{S}\mathbf{u}_{P_1} & \mathbf{v}_{P_m}^T \mathbf{S}\mathbf{u}_{P_2} & \mathbf{v}_{P_1}^T \mathbf{S}\mathbf{u}_{P_m} \end{pmatrix} \begin{pmatrix} c_{P_1Q_1} & & & \\ & c_{P_2Q_2} & & \\ & & \ddots & \\ & & & c_{P_mQ_m} \end{pmatrix} \tag{5.27}$$

$$\mathbf{F} = \begin{pmatrix} \mathbf{v}_{Q_1}^T \mathbf{S}\mathbf{u}_{Q_1} & \mathbf{v}_{Q_1}^T \mathbf{S}\mathbf{u}_{Q_2} & \mathbf{v}_{Q_1}^T \mathbf{S}\mathbf{u}_{Q_m} \\ \mathbf{v}_{Q_2}^T \mathbf{S}\mathbf{u}_{Q_1} & \mathbf{v}_{Q_2}^T \mathbf{S}\mathbf{u}_{Q_2} & \mathbf{v}_{Q_1}^T \mathbf{S}\mathbf{u}_{Q_m} \\ \vdots & \vdots & \vdots \\ \mathbf{v}_{Q_m}^T \mathbf{S}\mathbf{u}_{Q_1} & \mathbf{v}_{Q_m}^T \mathbf{S}\mathbf{u}_{Q_2} & \mathbf{v}_{Q_1}^T \mathbf{S}\mathbf{u}_{Q_m} \end{pmatrix} \begin{pmatrix} c_{Q_1P_1} & & & \\ & c_{Q_2P_2} & & \\ & & \ddots & \\ & & & c_{Q_mP_m} \end{pmatrix} \tag{5.28}$$

where $\mathbf{S} = (\lambda \mathbf{I} - \mathbf{D}_B)^{-1}$.

The eigenvalues of $\mathbf{H}$, for any given number of connections between the two blocks, are the zeroes of $\mathbf{\Gamma}(\lambda) = \det(\mathbf{I} - \mathbf{EF})$.

That is

$$\boxed{\mathbf{\Gamma}(\lambda_H) = 0} \tag{5.29}$$

Notice that the order of matrix $(\mathbf{I} - \mathbf{EF})$ is m, i.e. the number of connected degrees of freedom per subsystem, which is typically a much lower figure than the total number of degrees of freedom of the coupled system.

5.4 Application of the algebraic solution to the physical problem, physical meaning and eigenmodes

In the following, the formulation obtained in the algebraic problem in Section 5.3 is applied to a mechanical system consisting of two subsystems, the physical meaning of the equations is interpreted and the equations defining the system eigenmodes are derived.

5.4.1 Application to dynamics of mechanical systems

In order to apply the formulation in Eq. (5.29) to a mechanical problem one may interpret the elements in matrices $\mathbf{E}$ and $\mathbf{F}$ in accordance with the eigenvalues and eigenmodes of the mechanical subsystems in isolation.

To this effect, the inverse of the eigenmodes matrix must be known in order to get the $\mathbf{u}_{p_i}$ terms in Eq. (5.21).

Consider a mechanical system represented by the matrix $\mathbf{A}$ and consisting of two undamped subsystems 1 and 2 connected by m elastic elements. Suppose that subsystem 1 has n_1 degrees of freedom and subsystem 2 has n_2 degrees of freedom.

Recall that the connection points are labelled P_i in subsystem 1 and Q_i in subsystem 2, and that the subscripts indicate the elastic elements, i.e. element i joins points P_i and Q_i.

Let $c_{_{P_iQ_i}}$ be the stiffness between P_i and Q_i divided by the mass in P_i.

Let $\mathbf{\Phi}_i$ $i = 1...n_1$ be an eigenmode of subsystem 1 and $\mathbf{\Psi}_j$ $j = 1...n_2$ an eigenmode of subsystem 2, let also $\lambda_{1,i}$ an eigenvalue of subsystem 1, $\lambda_{2,j}$ an eigenvalue of subsystem 2 and $\lambda_{A,s}$ an eigenvalue of the coupled system $\mathbf{A}$.

A discrete (or discretized) mechanical system may be described through analogous equations to those in Eq. (5.1).

If $\mathbf{M}$ is a positive-definite diagonal matrix with coefficients m_i and $\mathbf{K}$ is a symmetric matrix, the corresponding eigenmodes are orthogonal with respect to the scalar product defined by matrix $\mathbf{M}$. If the eigenmodes are normalised to have unity Euclidean norm it follows that

$$\mathbf{\Phi}_i^T \mathbf{M} \mathbf{\Phi}_j = \mu_i \delta_{ij} \tag{5.30}$$

where μ_i are the so called modal masses.

From Eq. (5.30) it can be inferred that the inverse of the eigenmodes matrix is just the transposed eigenmodes matrix right-scaled by the mass matrix and left-scaled by the inverse modal mass matrix. If $\mathbf{\Pi} = \mathrm{diag}(\mu_1, \mu_2 \ldots, \mu_{n1})$, then

$$\mathbf{\Phi}^{-1} = \mathbf{\Pi}^{-1} \mathbf{\Phi}^T \mathbf{M} \tag{5.31}$$

Same formulation holds for $\mathbf{\Psi}$, the eigenmodes matrix of subsystem 2.

The P_i, P_j terms of the elements in matrix $\mathbf{E}$ in subsection (5.3.3) read:

$$\mathbf{v}_{P_s}^T (\mathbf{D}_B - \lambda I)^{-1} \mathbf{u}_{P_l} \tag{5.32}$$

where

$$\mathbf{u}_{P_l} = \mathbf{V}_B^{-1}\mathbf{e}_{P_l} \text{ and } \mathbf{v}_{P_s}^T = \mathbf{e}_{P_s}^T\mathbf{V}_B \tag{5.33}$$

In consequence, for subsystem 1

$$\mathbf{v}_{P_s}^T = \left(\boldsymbol{\phi}_1(P_s), \boldsymbol{\phi}_2(P_s) \dots , \boldsymbol{\phi_{n1}}(P_s) \right) \text{ and } \mathbf{u}_{P_l} = \begin{pmatrix} \boldsymbol{\phi}_1(P_l)\frac{m_l}{\mu_1} \\ \boldsymbol{\phi}_2(P_l)\frac{m_l}{\mu_2} \\ \dots \\ \boldsymbol{\phi}_{n1}(P_l)\frac{m_l}{\mu_{n1}} \end{pmatrix} \tag{5.34}$$

Finally, the P_i, P_j term of matrix $\mathbf{E}$ in Eq. (5.32) is reformulated as

$$m_j \sum_{s=1}^{n1} \frac{\boldsymbol{\phi}_s(P_i)\boldsymbol{\phi}_s(P_j)}{\lambda_s - \lambda}\frac{1}{\mu_s} \tag{5.35}$$

Other than the term m_j, Eq. (5.35) is a system receptance function or, in other words, the Green's function relating the forces applied at P_i and the displacement produced at P_j.

The connection terms in matrix $\mathbf{C}$ are

$$c_{P_j,Q_j} = \frac{k(P_j, Q_j)}{m_j} \tag{5.36}$$

where $k(P_j, Q_j)$ is the stiffness of the element connecting P_j and Q_j, and m_j is mass in subsystem 1 connected to the j^{th} elastic element.

Given that in the final solution the P_i, P_j coefficient in matrix E multiplies with $c(P_j, Q_j)$ (c.f. Eq. (5.27)), the elements of $\mathbf{E}$ will eventually be the P_i, Q_j receptance functions.

At this point, it is worth noting that from an experimental point of view it is easier to measure a receptance function than it is to compute it out of a (experimental) modal analysis which, in turn, would be of limited precision with respect to the measured receptance due to having a finite number of modes.

In order to obtain the coupled system eigenvalues λ, let

$$\mathbf{G}_1 = \begin{pmatrix} \sum_{i=1}^{n1} \frac{\phi_i(P_1)\phi_i(P_1)}{\mu_i(\lambda_i-\lambda)} & \dots & \sum_{i=1}^{n1} \frac{\phi_i(P_1)\phi_i(P_m)}{\mu_i(\lambda_i-\lambda)} \\ \vdots & \vdots & \vdots \\ \sum_{i=1}^{n1} \frac{\phi_i(P_m)\phi_i(P_1)}{\mu_i(\lambda_i-\lambda)} & \dots & \sum_{i=1}^{n1} \frac{\phi_i(P_m)\phi_i(P_m)}{\mu_i(\lambda_i-\lambda)} \end{pmatrix} \tag{5.37}$$

$$\mathbf{K}_c = \begin{pmatrix} k_{P_1Q_1} & \dots & 0 \\ \vdots & \vdots & \vdots \\ 0 & \dots & k_{P_mQ_m} \end{pmatrix} \tag{5.38}$$

and $\mathbf{G}_2$ an equivalent expression to that of $\mathbf{G}_1$.

The system eigenvalues λ are the zeroes of the $\mathbf{I}-\mathbf{EF}$ determinant, with $\mathbf{E} = \mathbf{G}_1\mathbf{K}_c$, $\mathbf{F} = \mathbf{G}_2\mathbf{K}_c$ and being $\mathbf{I}$ an identity matrix of order m.

$$\boxed{\det\left(\mathbf{I} - \mathbf{EF}\right) = 0} \tag{5.39}$$

5.4.2 Physical meaning of the solution

As discussed above, the elements of $\mathbf{G}_1$ and $\mathbf{G}_2$ are frequency response functions relating force to displacement. Element ij in $\mathbf{G}_1$ is the displacement in P_j due to a unit force with frequency $f = \frac{\sqrt{\lambda}}{2\pi}$ applied at P_i.

Now, let $\mathbf{G} = (\mathbf{I} - \mathbf{EF})$, the elements γ of matrix $\mathbf{G}$ are

$$\gamma_{ij} = \sum_l g_1(P_iP_l)k(P_lQ_l)g_2(Q_lQ_j)k(Q_jP_j) \tag{5.40}$$

$$\gamma_{ii} = 1 - \sum_l g_1(P_iP_l)k(P_lQ_l)g_2(Q_lQ_i)k(Q_iP_i) \tag{5.41}$$

Figs. 5.3 and 5.4 show how a force applied at P_1 in subsystem 1 is transmitted into P_1 itself through the springs which couple subsystems 1 and 2.

Figure 5.3 shows the displacements produced at points P_1 to P_4 by the force applied at P_1. These displacements are simply $g(P_1, P_1)$ for P_1, $g(P_1, P_2)$ for P_2, $g(P_1, P_3)$ for P_3 and $g(P_1, P_4)$ for P_4. Each of these displacements produce a force at points Q_1 to Q_4 in subsystem 2, these being $g(P_1, P_i)k_{P_i,Q_i}$ for $i = 1, 2, 3, 4$.

In Figure 5.4 it is shown how the forces on points Q_1 to Q_4 produce a total displacement in Q_1 equal to $\sum_{i=1}^{4} g(P_1, P_i)k_{P_i,Q_i}g'(Q_i, Q_1)$. Finally, the coupled system reaction force on P_1 is $\sum_{i=1}^{4} g(P_1, P_i)k_{P_i,Q_i}g'(Q_i, Q_1)k_{Q_i,P_1}$.

Thus, the matrix element $\gamma_{i,i}$ is the reaction force over P_i as a result of a unit force applied at the same point P_i. Therefore, the resonance condition in Eq. (5.39) means that if a point unit force is applied only at P_i, the reaction force at P_i is unity, and zero elsewhere.

This means that the forces acting on $P1$ are self equilibrated at some of the frequencies without the need of external loading. It is, indeed, the resonance condition.

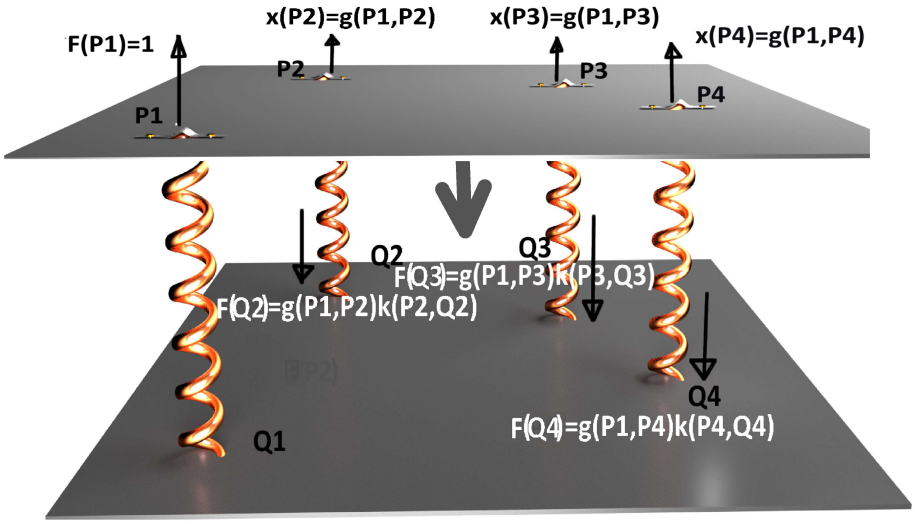

Figure 5.3: A force in P1 produces forces on the Q points

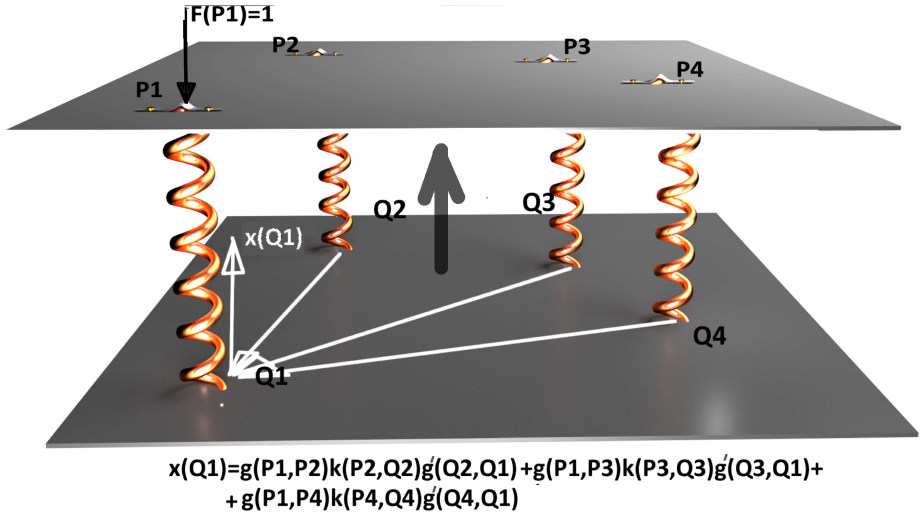

Figure 5.4: The forces in the Q points produces a reaction force on P1

Formally, including forces in Eq. (5.39) it holds that

$$\det(\mathbf{G}) = 0 \Leftrightarrow \exists \mathbf{f} \mid \mathbf{Gf} = \mathbf{0} \Longleftrightarrow \mathbf{Rf} = \mathbf{f} \text{ being } \mathbf{R} \neq \mathbf{I} \text{ and } \mathbf{f} \neq \mathbf{0} \tag{5.42}$$

where $\mathbf{R} = \mathbf{I} - \mathbf{G}$.

For any given λ and $\mathbf{f}$ it holds that $\mathbf{Rf} = \mathbf{f}'$. Under the hypothesis that a force $\mathbf{f}$ is applied to the connection points of one of the subsystems, such force may be

decomposed into two parts: the reaction force of the other subsystem, i.e. $\mathbf{Rf}$, and the external forces. Thereof, $\mathbf{f} = \mathbf{Rf} + \mathbf{f}_{\text{Exterior}}$. Solving $\mathbf{Rf} = \mathbf{f}$ implies finding a set of forces that may exist without the need of any external loading. These forces correspond to the reaction $\mathbf{Rf}$ at the couplings in absence of external forces, thus, at resonance. In consequence, Eq. (5.39) is a resonance condition.

The conclusion is therefore that the function derived here from algebraic considerations is a resonance condition from a physical point of view, which states that the coupling forces at resonance are the result of the action of same forces through the connections.

5.4.3 Eigenmodes calculation

Given that the resonance condition requires $\mathbf{Rf} = \mathbf{f}$, it can be ascertained that matrix $\mathbf{R}(\lambda_A)$, whose eigenvalues λ_A are zeroes of $\det \mathbf{G}$, has at least one eigenvector with eigenvalue equal to 1. Name this eigenvector $\mathbf{f}_A$.

The components of $\mathbf{f}_A$ over subsystem 1 are the coupling forces that apply on subsystem 1 at system resonance with eigenvalue λ_A.

Considering that $\mathbf{G}$ is of order m, i.e. the number of connections, which is a very small dimension as compared to the number of degrees of freedom of the subsystems specifically in the present target problem, the calculation of its eigenvectors will be very simple in terms of computation burden.

Once obtained the eigenvector $\mathbf{f}_A$ with associated eigenvalue 1, one must just apply the force vector $\mathbf{f}_A$ to the matrix of subsystem 1 in order to obtain the corresponding displacement that the applied forces produce. The computed displacements are those of the system eigenmode with eigenvalue λ_A over subsystem 1.

Proceeding in the same way on subsystem 2, displacements for the corresponding eigenmode are found.

5.5 Examples

In this section two examples are considered. The first example is a simple system so to explicitly illustrate the method steps towards the final solution. Also, the resemblance of this example to that in reference Simpson (1973) is exploited so to briefly remark the differences between both methods with regards to the subsystems selection.

The second example is a system with many degrees of freedom, having 5 connections between two composing subsystems, so to illustrate the method performance in a much more complex problem.

5.5.1 Simple discrete system

The first example is a discrete system involving three masses and four springs, whose values are defined without magnitude units for brevity.

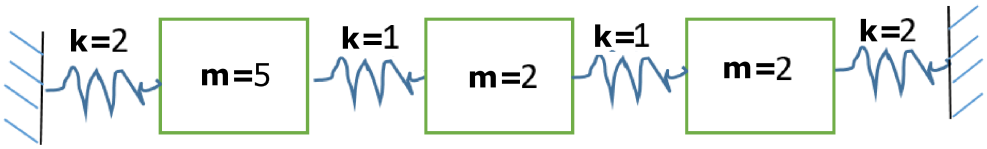

Figure 5.5: Simple discrete system example. k and m are stiffness and masses values.

This is a very similar problem to the one exposed in Simpson (1973) as an application example of Kron's method.

In order to apply Kron's method, or any other method applicable to rigid connexions, the system must be split by dividing the masses elements. See for example Figure 5.6.

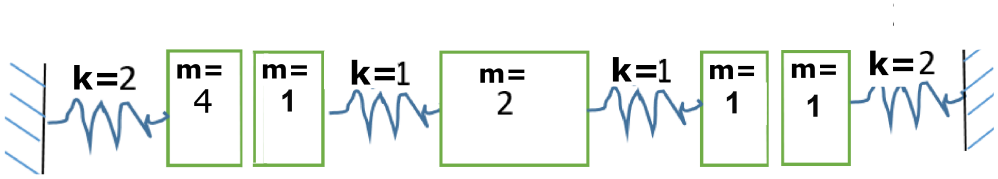

Figure 5.6: Subsystems division in order to apply Kron's method Simpson (1973).

Notice that masses are split in Kron's method in order to make the connections holonomic. This is optimal to subdivide an structure, but it is virtually of no use for an auxiliary equipment.

The method proposed here decomposes the problem into two smaller problems with the coupling interface set at the springs (see Figure 5.7).

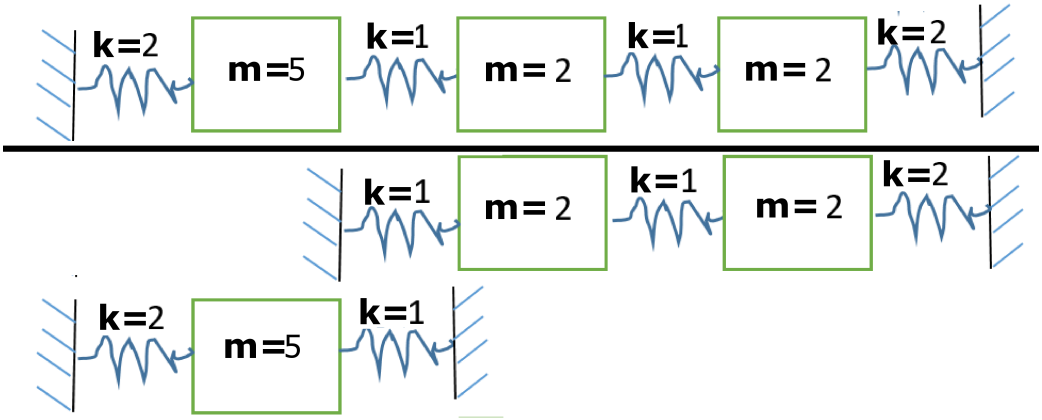

Figure 5.7: Top (above black line): Problem to solve. Middle: Subsystem 1. Bottom: Subsystem 2

The subsystems' mass matrices are:

$$\mathbf{M}_1 = \begin{pmatrix} 2 & 0 \\ 0 & 2 \end{pmatrix} \; ; \; \mathbf{M}_2 = \begin{pmatrix} 5 \end{pmatrix} \tag{5.43}$$

and the subsystems' stiffness matrices:

$$\mathbf{K}_1 = \begin{pmatrix} 3 & -1 \\ -1 & 2 \end{pmatrix} \; ; \; \mathbf{K}_2 = \begin{pmatrix} 3 \end{pmatrix} \tag{5.44}$$

The eigenmodes of subsystems 1 and 2 are

$$\mathbf{\Phi}_1 = \begin{pmatrix} -0.5257 & -0.8507 \\ -0.8507 & 0.5257 \end{pmatrix} \; ; \; \mathbf{\Phi}_2 = \begin{pmatrix} 1 \end{pmatrix} \tag{5.45}$$

and their corresponding eigenvalues

$$\mathbf{\Lambda}_1 = \begin{pmatrix} 0.6910 & 0 \\ 0 & 1.8090 \end{pmatrix} \; ; \; \mathbf{\Lambda}_2 = \begin{pmatrix} 0.6000 \end{pmatrix} \tag{5.46}$$

The coupled system stiffness and mass matrices are:

$$\mathbf{K} = \begin{pmatrix} 3 & -1 & 0 \\ -1 & 2 & -1 \\ 0 & -1 & 3 \end{pmatrix} \; ; \; \mathbf{M} = \begin{pmatrix} 2 & 0 & 0 \\ 0 & 2 & 0 \\ 0 & 0 & 5 \end{pmatrix} \tag{5.47}$$

Since the mass matrix is positive definite and diagonal the generalized eigenvalues problem may be converted to an standard eigenvalues problem.Thence we have to find the eigenvalues and eigenvectors of:

$$\mathbf{M}^{-1}\mathbf{K} = \begin{pmatrix} 1.5 & -0.5 & 0 \\ -0.5 & 1 & 0.5 \\ 0 & 0.2 & 0.6 \end{pmatrix} \tag{5.48}$$

Eq. (5.48) may be decomposed as

$$\mathbf{M}^{-1}\mathbf{K} = \begin{pmatrix} 1.5 & -0.5 & 0 \\ -0.5 & 1 & 0 \\ 0 & 0 & 0.6 \end{pmatrix} + \begin{pmatrix} 0 & 0 & 0 \\ 0 & 0 & 0.5 \\ 0 & 0.2 & 0 \end{pmatrix} \tag{5.49}$$

Now, identifying the decomposition terms as

$$\mathbf{H} = \begin{pmatrix} 1.5 & -0.5 & 0 \\ -0.5 & 1 & 0.5 \\ 0 & 0.2 & 0.6 \end{pmatrix}; \mathbf{B} = \begin{pmatrix} 1.5 & -0.5 & 0 \\ -0.5 & 1 & 0 \\ 0 & 0 & 0.6 \end{pmatrix}; \mathbf{C} = \begin{pmatrix} 0 & 0 & 0 \\ 0 & 0 & 0.5 \\ 0 & 0.2 & 0 \end{pmatrix} \tag{5.50}$$

it is clear that this decomposition corresponds with the proposed problem approach, where the $\mathbf{H}$ matrix eigenvectors and eigenvalues correspond to the eigenmodes and eigenfrequencies of the full system, the $\mathbf{B}$ matrix contains the decoupled subsystem matrices and $\mathbf{C}$ is the coupling matrix.

Notice that the coefficients in matrix $\mathbf{C}$, $c_{PQ} = 0.5$ and $c_{QP} = 0.2$, are normalised by the contiguous masses.

Then, following the notation used in the derivations in Section 5.3.1

$$\mathbf{V}_B = \begin{pmatrix} -0.5257 & -0.8507 & 0 \\ -0.8507 & 0.5257 & 0 \\ 0 & 0 & 1 \end{pmatrix}; \mathbf{D}_B = \begin{pmatrix} 0.6910 & 0 & 0 \\ 0 & 1.8090 & 0 \\ 0 & 0 & 0.6 \end{pmatrix} \tag{5.51}$$

$$\mathbf{u} = \begin{pmatrix} -0.8507 \\ 0.5257 \\ 0 \end{pmatrix}; \mathbf{w} = \begin{pmatrix} 0 \\ 0 \\ 1 \end{pmatrix}; \mathbf{v}^T = \mathbf{w}^T; \mathbf{y}^T = \mathbf{u}^T \tag{5.52}$$

the solution are the zeroes of:

$$\begin{aligned} 1 =& (0.5)(0.2) \begin{pmatrix} 0 & 0 & 1 \end{pmatrix} \begin{pmatrix} \frac{1}{\lambda-0.6910} & 0 & 0 \\ 0 & \frac{1}{\lambda-1.8} & 0 \\ 0 & 0 & \frac{1}{\lambda-0.6} \end{pmatrix} \begin{pmatrix} 0 \\ 0 \\ 1 \end{pmatrix} \\ & \begin{pmatrix} -0.8507 & 0.5257 & 0 \end{pmatrix} \begin{pmatrix} \frac{1}{\lambda-0.6910} & 0 & 0 \\ 0 & \frac{1}{\lambda-1.8} & 0 \\ 0 & 0 & \frac{1}{\lambda-0.6} \end{pmatrix} \begin{pmatrix} -0.8507 \\ 0.5257 \\ 0 \end{pmatrix} \end{aligned} \tag{5.53}$$

that is, the zeroes of:

$$1 = 0.1 \frac{1}{\lambda - 0.6} \left(\frac{0.8507^2}{\lambda - 0.6910} + \frac{0.5257^2}{\lambda - 1.8} \right) \tag{5.54}$$

In Figure 5.8 it can be observed that the zeroes of Eq. (5.54) coincide with the

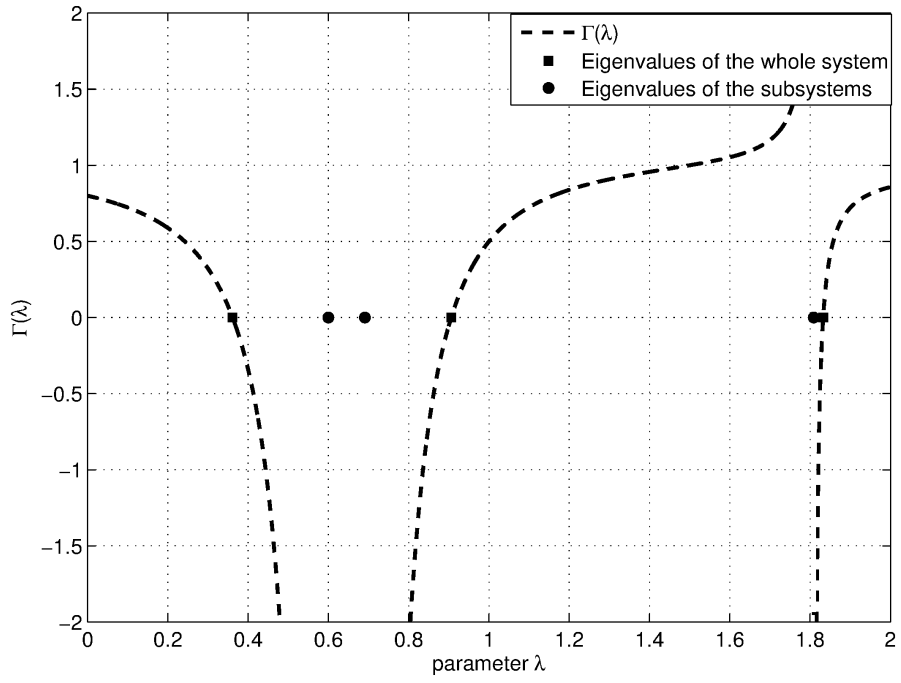

Figure 5.8: The total system eigenvalues calculated using standard methods (black squares) correspond to the zeroes of the $\Gamma(\lambda)$ function. The eigenvalues of the subsystems (black circles) are also represented.

eigenvalues of the system, namely 0.3614, 0.9060 and 1.8327. In this figure black

circles represent subsystem eigenvalues and black squares represent coupled system eigenvalues.

Given the significant frequency shift of the eigenvalues for coupled system vs. that of the decoupled subsystems, the interest in knowing the resonant frequencies of the coupled system is justified, since the excitation frequency may then coincided with a resonant frequency of the coupled system.

5.5.2 Two plates connected by five springs

The following example illustrates the performance of the method on a continuous system which is discretised, giving a mesh of 13x23 degrees of freedom.

The feature of having several degrees of freedom connected trough springs is also introduced in this example having 5 connections.

The model involves two plates with dimensions: 1.3 m length, 2.3 m width and 20 cm thickness and material properties as indicated in Table 5.1.

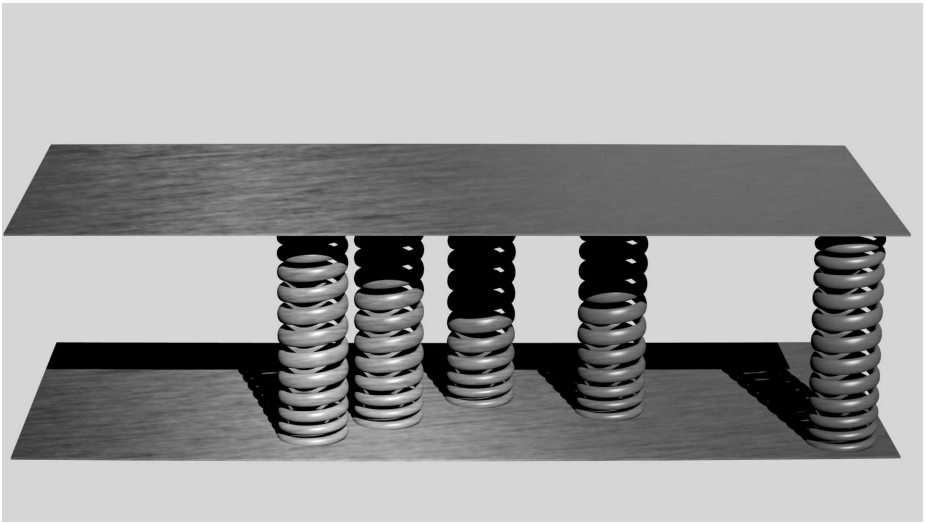

Figure 5.9: Example of continuous system with several non-holonomic coupling connections. Two plates connected through 5 springs.

In Figure 5.10, the continuous line is $\Gamma(\lambda)$ as defined in Eq. (5.39), computed over a λ sweep from 0 to 4 with $1E-3$ incremental step. In a real case the zone to explore will be defined by the nature of the problem, engine RPM, fan characteristics, etc. As it is known already, its zero value crossings correspond to the modal frequencies

Material	ρ_v (kg/m^3)	ν	E (Pa)	L_x (m)	L_y (m)	h (m)
Concrete	2000	0.2	$2 \cdot 10^{10}$	2.3	1.3	0.2
Concrete	2000	0.2	$2 \cdot 10^{10}$	2.3	1.3	0.2

Table 5.1: Geometric and mechanical properties of the two plates (ρ_v is the volumetric density, ν is the Poisson's ratio, E is the Young modulus, L_x, L_y the plate dimensions and h the plate thickness).

Spring	K ($\frac{\text{N}}{\text{m}}$)	x (m)	y (m)
1	$2 \cdot 10^5$	0.3	0.4
2	$2 \cdot 10^5$	0.6	0.1
3	$2 \cdot 10^5$	0.2	0.4
4	$2 \cdot 10^5$	0.5	0.5
5	$2 \cdot 10^5$	0.1	0.1

Table 5.2: Stiffness K and position of each spring that connects the plates.

of the system, $*$ symbols indicate these zero crossings, which are the eigenvalues of the system.

The accuracy of the obtained result is analysed in Figure 5.11, which shows on top the eigenvalues computed through $\Gamma(\lambda)$ (abscissa axis) versus the eigenvalues of the system directly compute with standard eigenvalue solver (ordinate axis). The scatter of resulting points is then least squares approximated by a straight line with equation $\text{y} = 0.99999\text{x} + 0.00066$, meaning that the correlation of the method results to those of a standard eigensolver is 0.99998, which is regarded as an optimal result.

Figure 5.12 shows the relative error in the eigenmodes. Such relative error is computed in vector form as the difference between the eigenvectors computed through the gamma function and the eigenvectors obtained with standard solver, each of them normalised by the norm of the (standardly computed) eigenvector. In all cases the error is below $1E-9$.

5.6 Conclusions

For two coupled subsystems, a function $\Gamma(\lambda)$ whose zeroes correspond to the eigenfrequencies of the coupled system has been derived, in which $\Gamma(\lambda)$ is the determinant of a matrix of order equal to the number of subsystem connections, typically a smaller

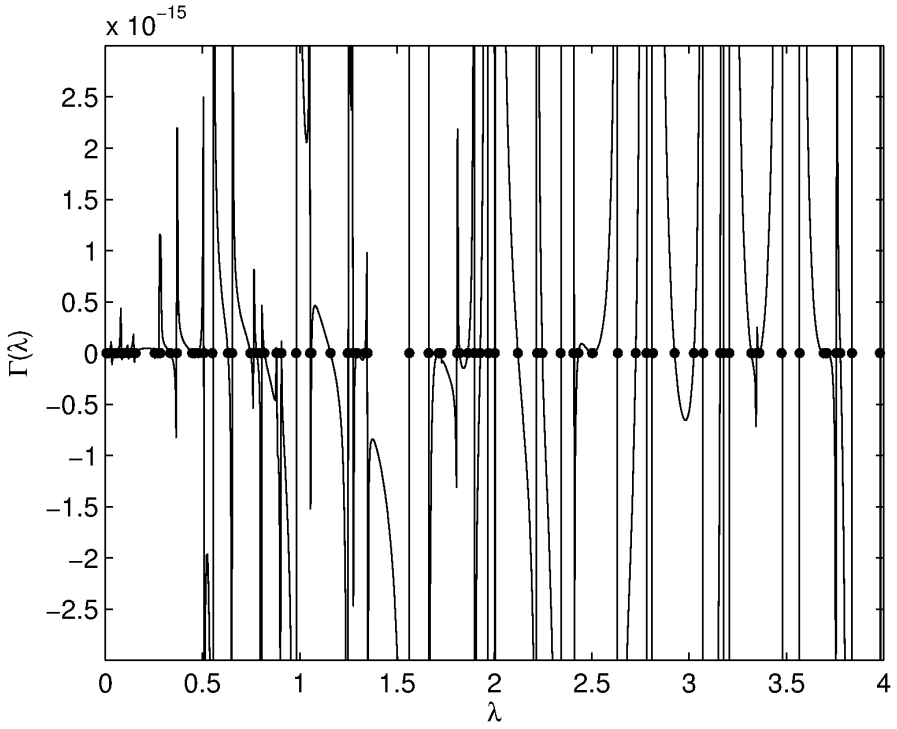

Figure 5.10: —Γ (λ) function whose zeros are the system eigenvalues, ∗ Eigenvalues of the system calculated using standard numerical methods

number than the subsystems' number of degrees of freedom.

Function $\Gamma(\lambda)$ depends on the eigenvalues and eigenvectors of each of the two subsystems as well as on the elastic constants of the springs which connect them. Yet, in the solution procedure of the proposed method, the subsystem eigenvalues and eigenvectors get combined into receptance functions. Therefore, for an experimental application of the method, it is not needed to know the subsystems' eigenmodes and eigenfrequencies. Knowing the receptances between the coupling degrees of freedom suffices.

Furthermore, it has been demonstrated the procedure for obtaining the corresponding eigenvectors based on the matrix whose determinant generates $\Gamma(\lambda)$.

Finally, the method has been applied to two examples, a discrete system with one single connection and a continuous system with 5 connections. In both examples the proposed method shows fully satisfactory performance.

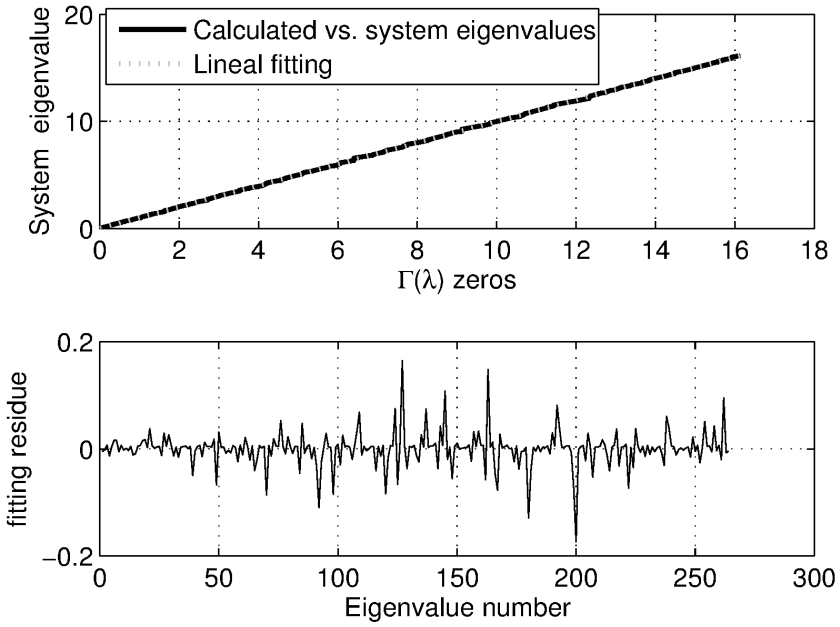

Figure 5.11: Linear correlation between the system eigenvalues and the $\Gamma(\lambda)$ zeros. Top curve: Linear approximation. Bottom curve: Differences between the linear approximation and the value calculated with this paper method (fitting residue).

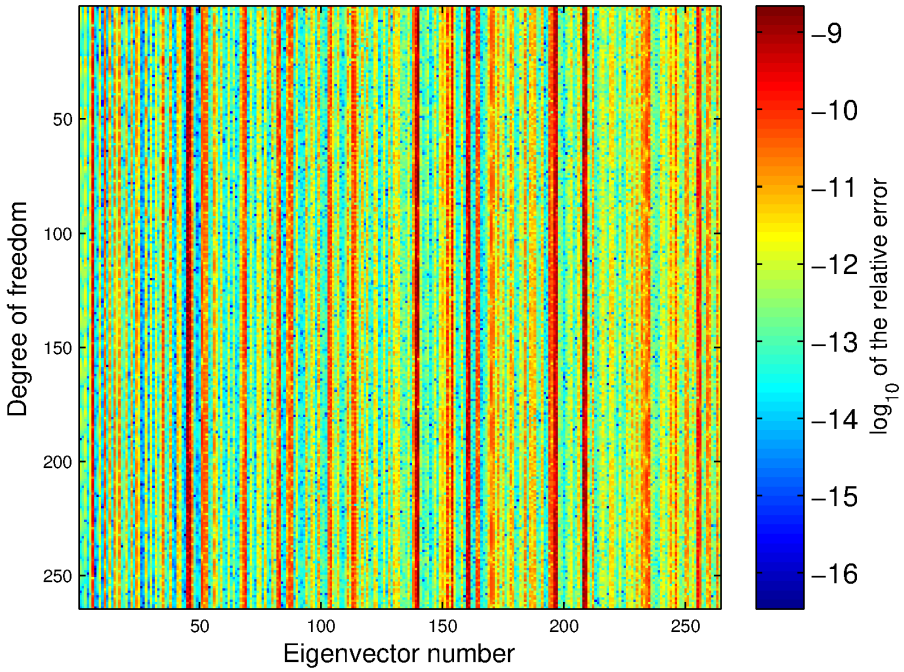

Figure 5.12: Relative error on the obtained eigenvectors vs. system ones

Chapter 6

Conclusions

6.1 Contributions

The contributions of this thesis are as follows:

- The formal definition of Path (Chapter 2).
- Proof of the completeness of the description of the system behaviour by means of paths (Chapter 2).
- A methodology for the automatic identification of subsystems . It is based on the cluster analysis applied to powers of the transfer matrix. It is shown, through numerical examples, how the method works and is able to identify subsystems on its own without additional information or guidelines (Chapter 3).
- An important parameter in order to explain the good behaviour of the proposed technique is the contrast of the matrix. It is also used as an estimator of the coupling strength between subsystems (Chapter 3).
- A consistent comparison between the laboratory measurement of a box with air cavity inside and a numerical model of the same box is shown. This validates somehow both the numerical simulations and the reliability of the experimental measurement. To neglect the radiation losses (effect of the air outside) is a reasonable hypothesis if the interest is focused on the box and air cavity inside.

The combination of a multiphysics FEM software (Code Aster EDF (2017) with Gmsh Geuzaine and Remacle (2009)) with an automatic pre and post-processing set of scripts is a valid option to reproduce the ATPA procedures (Chapter 4).

- ATPA method properly characterises all the transmission paths, not only the dominant ones (Chapter 4).

- The mechanical connectivity of the system can be defined by means of direct transfer functions. This is frequency-dependent and can be influenced by a proper definition of the measured degrees of freedom and points at the beginning of the process. By taking into account the frequencies that are below the first eigenfrequency, the physical structure of the system is identified.(Chapter 4)

- To the best of my knowledge it is the first eigenvalue and eigenvectors synthesis approach for elastic(rather than rigid) coupled subsystems based on eigenvalues and eigenvectors of the subsystems (Chapter 5).

6.2 Publications derived from the thesis

Here a list of the publications, including papers and conferences
Articles in indexed journals

1. Magrans, F., J. Poblet-Puig, and A. Rodríguez-Ferran (2017). The solution of linear mechanical systems in terms of path superposition. *Mech. Syst. Signal Proc. 85*, 111–125.

2. Magrans, F. X., J. Poblet-Puig, and A. Rodríguez-Ferran (2018). A subsystem identification method based on the path concept with coupling strength estimation. *Mech. Syst. Signal. Proc. 100*, 588–604.

3. Aragonès, À., J. Poblet-Puig, K. Arcas, P. V. Rodríguez, F. X. Magrans, and A. Rodríguez-Ferran (2019). Experimental and numerical study of advanced transfer path analysis applied to a box prototype. *Mech. Syst. Signal. Proc. 114*, 448–466.

4. Magrans, F. X. and J. Poblet-Puig (2018). Eigenvalue and eigenmode synthesis in elastically coupled subsystems. *J. Sound Vib. 432*, 405 – 419.

Conferences

1. Magrans, F., J. Poblet-Puig, and A. Rodríguez-Ferran (2016, Aug). Substructuring of mechanical systems based on the path concept. In *International Congress and Exposition on Noise Control Engineering*, pp. 2485–2494. Deutsche Gesellschaft fr Akustik e.V. (DEGA).

2. Magrans, F. X., K. Arcas, P. Vicens Rodríguez, J. Poblet-Puig, and A. Rodríguez Ferran (2017). Experimental numerical correlation of subsystem contributions in the advanced transfer path analysis framework. In *24th International Congress on Sound and Vibration*, pp. 1–8.

6.3 Future work

The following are some topics that might, perhaps, be of interest as fields of study of vibroacoustic problems from the point of view of path theory.

- Forwarded problems. In many problems the propagation is important in one direction only. In a building, for example, the noise is considered to go from the emitter to a wall, from the wall to the ceiling, from the wall to a wall in the upper room, always propagating in the same direction as it approaches the receiver so that,in that situations, if T_{ij}^D is not zero, T_{ij}^D is zero or can be neglected. When this happens, the T matrix can be arranged so that the upper triangle is zero or negligible. In this case the maximum power of the matrix that can be other than zero is its dimension, i.e. $\mathbf{T}^{n+1} = \mathbf{0}$, being n the dimension of the matrix. This can be understood because loops cannot be formed. Not forming loops should be equivalent to not having resonances and in effect, as the finite Neumann series will be convergent and the complementary series will be unnecessary according to the idea that there will be no resonances. Studying what happens when feedback is minimal can be interesting.

- Physical interpretation: The complementary term of the Neumman series is consistent with the interpretation of the system's response to the excitation it

receives. It contains the system's eigenvalues that depend on the characteristics of the system and are applied to the terms that have the highest power of the matrix $\mathbf{T}^D$ that indicate that they are the paths in stationary state. Further physical interpretation of the complementary term of the Neumann series can provide useful information for the applications of the method.

- Energy consequences: We have seen the relationship of the direct transfer matrix with the interaction potentials. It is also clear that the lower powers of the series represent the direct field and the first reflections. An interesting step is to study the energetic interpretation of this form of expressing the solution, including the SEA by adding the usual hypotheses, uncorrelated excitation, weak coupling or not, etc.

- Numerical methods: Application of TD to numerical methods. If global transfers are known for an open enclosure over n+2 points, degrees of freedom or subsystems, in which there is a sender and a receiver, say n+1 and n+2, the Direct Transfer from n+1 to n+2 is in turn the Global Transfer from n+1 to n+2 when the other points are blocked. If the blocked points form a closed or semi-closed contour (with one or more openings remaining), this is the solution for the closed enclosure found using the solution for the free field. Developing this concept and applying it to real cases can be interesting.

- Paths/Waves relationships:According to the Huygens principle Huygens (1962) in its wave interpretation of light a wave propagates because each point of the wave front radiates a new spherical wave. Fresnel and Fraunhofer developed this idea by adding the necessary hypotheses to justify it quantitatively. The interpretation of the solution of any linear system by means of paths coincides exactly with the hypothesis of Huygens.

In reference to the Figure 6.1 the central bronze-coloured sphere would be the source whose direct transfer is other than zero only for the stencil represented as a bronze-coloured 3D cross. The paths of order 1 contained in the $\mathbf{T}$ matrix connect the source to the small red spheres that will be the first wavefront. The $\mathbf{T}^2$ matrix contains all the second order paths, including the ones that reach the little green balls. This defines the second wavefront represented in the Figure 6.1 as a green surface. The $\mathbf{T}^3$ matrix contains all the third order paths, including those that are

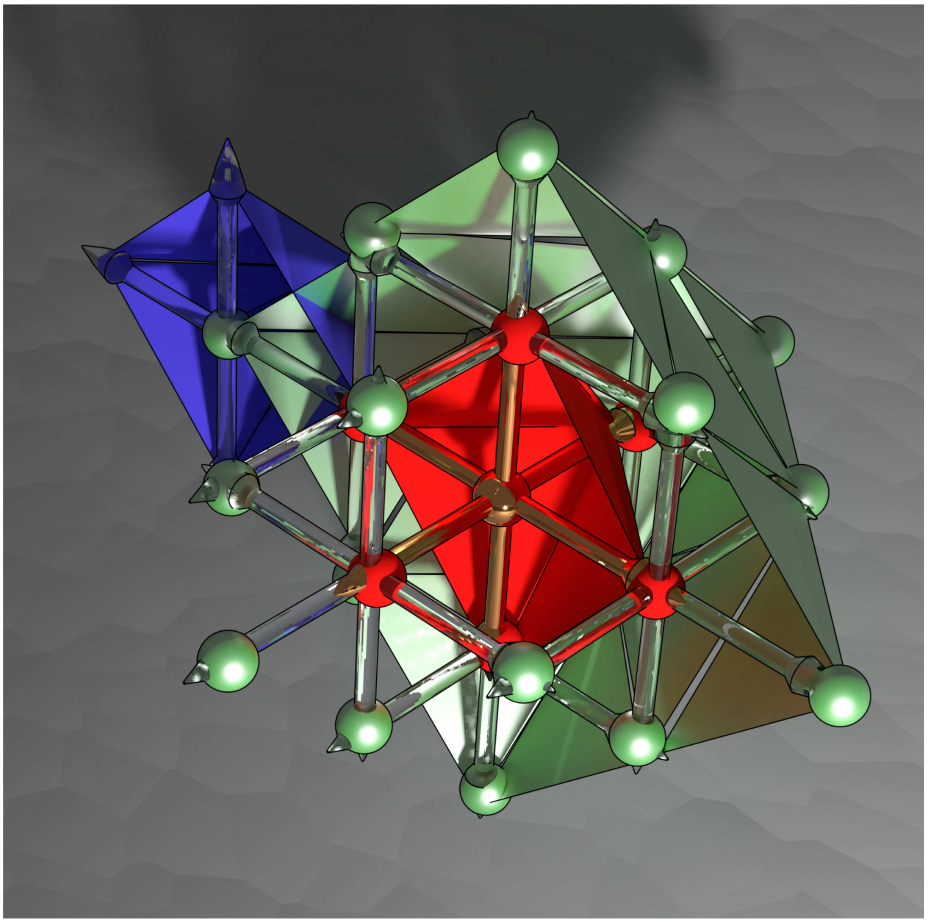

Figure 6.1: For a source placed in the center. Red -Half of an "spherical" wavefront for the first order paths. Green-Half of an "spherical" wavefront for the farthest second order paths. Blue- Third order paths "spherical" wavefront growing from a point in the second order paths wavefront. This will happen in all wavefront

born on the points of the order wave front 2 and are directed to the outside. These will form the spherical radiation from each point of the green wavefront according to the Huygens hypothesis.

Appendix A

Taking a walk through the paths

A.1 History, background and some comments

A.1.1 The problem in its origins

In vibroacoustic a transmission path is a very intuitive idea that for a long time has remained a non cognitive understanding.

In the late 70's of the past century there was a need to understand precisely what a "path" actually means. This was caused by the fast development of the vibroacoustic modelling and design, especially in the automotive industry were the silence was becoming a label of quality and determinant aspect to increase the sales.

Solving noise and vibration problems in a car, was of major importance in order to know which were the noise and vibration transmission "paths".

Most of the automotive vibroacoustical laboratories in the 60's had two main problems to be solved. The first problem was the quantification of the contribution to the total noise of each vibrating part of the passengers cabin. Lets call this problem, problem A.

In those years, the method used to solve problem A was the called "Strip method". In this method the noisy object was totally covered with insulating blankets in order to attain a very reduced noise. Then the surfaces were uncovered one by one and their contributions obtained from direct measurement.

With this method two problems appear. The first one is that when wrapping the noise radiating object with insulating blankets a heavy mass is being loaded on the

structure and it is possible that his dynamical properties changed.

The second problem is the long time needed to cover all surfaces with the necessary complex blankets.

A representation of this method can be observed in the Figure A.1. On the lower car the floor blanket on the backward seats has been removed and the contribution of that part of the floor can be measured.

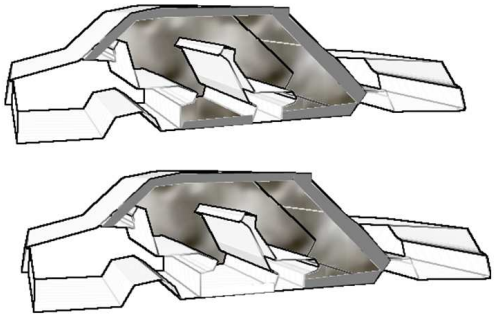

Figure A.1: Problem A, Strip method used in a car interior

In the Figure A.2 a real application of the strip method (problem A) on an engine can be seen.

Figure A.2: Problem A, Strip method used in an engine Lebresne (1975)

The contributions obtained may be seen in the Figure A.3. At the upper part of these figure appear the contributions of each part of the engine to the total noise in a microphone placed in the engine test room.

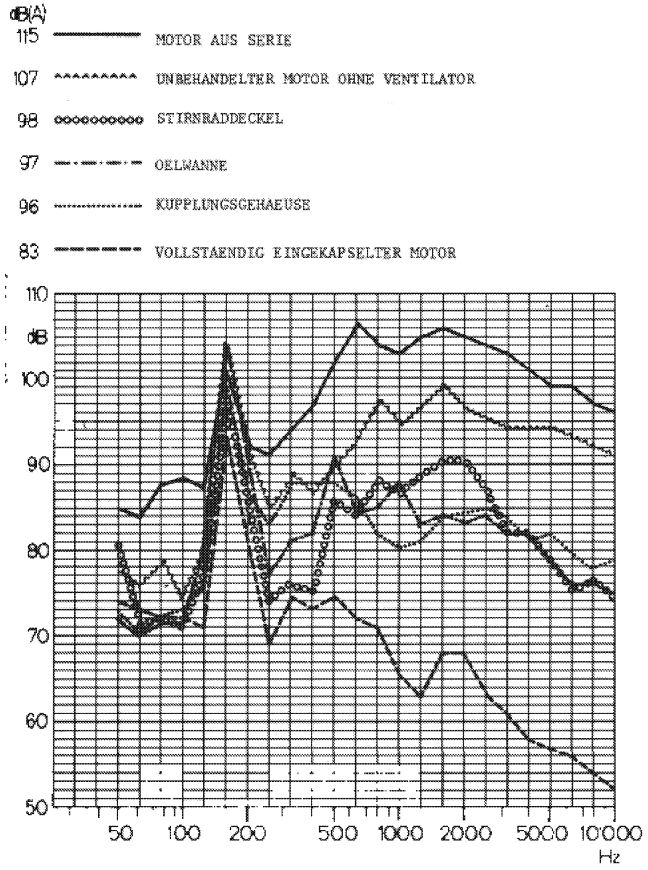

Figure A.3: Problem A, Contributions from the top to down. Normal engine, untreated motor without fan, gear cover, oil pan, clutch housing and the last one engine totally encapsulated, Lebresne (1975)

The "strip" method has been applied to engines, cars or even to trains , and it is still being applied nowadays.

The second problem, problem B, consisted on determining the noise produced by each force that was acting on a mechanical system. It was important to identify which was the contribution to the noise in the passenger cabin coming from each support of the engine, the exhaust pipe or other mechanical elements.

In order to solve this problem, the method used was to uncouple the engine from the car body and then to attach the supports one by one.

Even if both problems A, B look similar they have deep differences.

In problem B it is desired to know how much noise makes each one of the forces applied by the motor on the car structure, but it is not attempted to know through

which elements the noise/vibration passes through. It is simply accepted that the noise may have passed through any possible component. It may be that when the excitation arrives to the gear-shift lever a certain frequency becomes amplified by a resonance but, as the aim is not to modify the structure this is not important.

Problem A, even looking similar, is very different. It pretends to know the contribution to the total noise of the vibration of one panel, but this noise needs to be able to be added to the noises coming from the other panels. In this case the path it is important.

The noise of the door vibration can be tested by exciting it through a hammer impact or any other method, but this vibration produces the vibration of the rest of the panels, the measured noise will not be already additive because it does not correspond to the door noise only. Exciting all panels and adding the previously measured noises we will take into account each panel several times.

It is necessary then to know the path through which the perturbation goes across. The pictures in Figure A.4 show this idea.

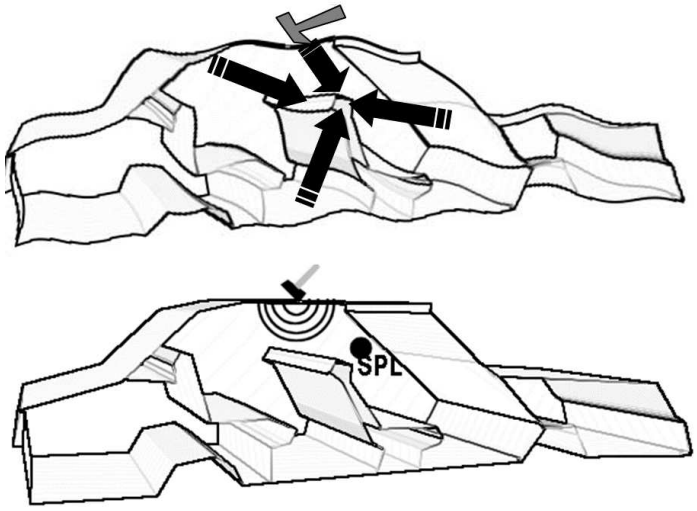

Figure A.4: If the whole surface is divided in a set of sub-surfaces, to have an additive noise the noise made only by the excited surface needs to be measured. Uper: Non additive noise. Bottom: Additive noise

In the 70's several papers were published Koss and Alfredson (1974b),Potter (1977),Bendat (1976b),Bendat (1976a), describing a method to obtain the contri-

butions of the displacements or accelerations of each part of a mechanical system, on the pressure in a microphone. A set of nodes were active emitters and one of them was a passive receiver. The objective was not to find the paths but to separate the contributions of different parts.

The method used in the above-mentioned articles is the same that now is called OTPA (Operational Transfer Path Analysis) but had the addendum of implementing the partial coherence approach to identify the different sources.

It was applied in several problems, for example in Koss and Alfredson (1974a),Alfredson (1977).

Later, in Magrans (1981), the concept of path and its quantification were defined. This does not preclude a more formal definition in the article Magrans et al. (2017) published as a result of this thesis.

The transfer function normally understood as a relationship between the acceleration at one point and the force applied on another point was regularly used to characterize structures.

In some way this transfer functions represent the sensitivity in one point due to the excitation in another. The excitation that arrives to the second point has travelled through all paths and can only identify the contributions but not the paths, for this reason it was named Global Transfer.

In the paper Magrans (1981) a new type of transfer function (using the force or not) was defined. This so called Direct Transfer function characterizes the paths. The Direct Transfer is very difficult to obtain experimentally but it can be obtained from the Global transfer, which is easily measurable, through the equations obtained in the paper.

As a conclusion, a method to find the paths, from a theoretical and experimental point of view, based on the equations that relate Global Transfers (the measurable ones) and Direct Transfers (the paths) with no use of the forces, was obtained.

The same paper explained how to find the so-called external signal, directly related to the force, using the Global Transfer or through the Direct Transfer. In any case, the characterization of the paths, as clearly stated in the paper, were the Direct Transfers.

As this appendix is about the paths history the next step has to be to explain why the paper Magrans (1981) was the source of the two methods more used in the industry nowadays, the TPA and the ATPA methods.

One main-actor of the vibroacoustic research in the automotive industry in the 80s in the last century was the Keller company based in Zurich. For this reason, the methods exposed in the Magrans (1981) paper were discussed in that company. The technical document with the conclusions was Gillard (1980). Note that the title of the document "Method of measurement for determining the **transmission paths** and the **contributions** of the different excitation forces simultaneously applied to a linear mechanical system" highlights two aspects of it, identification of transmission paths and identification of force contributions. This study, Gillard (1980), as a conclusion gave preference to the forces transmission method nowadays called TPA (Classical Transfer Path Analysis).

This TPA method in reality is not related with the paths but with the contributions of different forces applied on the structure and it is nothing but an inversion of the dynamical model and it was the one adopted by the car industry in preference.

A path method should be independent of the Forces as it describes the topology of the mechanical system.

The path method based on Direct Transfer function, has been developed all along 30 years by the private company ICR S.L. based in Barcelona and demonstrated his ability to identify and to quantify the paths.

In the academic world this method is called GTDT and in the industrial one is called ATPA (Advanced Transfer Path Analysis)

The method has been applied in railways to find the parts of the noise coming from the vibration of each panel and from the leaks to several microphones. Also, it is being used to know the vibration that arrives through the structural links to the final noise in the microphone and to know which part of the noise gets to the microphone after passing through a link and then through some selected panels.

After this exposition of the history of the transmission paths, let's look at some basic concepts.

A.1.2 Some basic ideas, paths, connectivity, higher order paths

Now some general concepts about paths will be explained in a simple way.

Specially the ideas of connectivity and flow will be given and related to the physical parameters.

Even if a path is a very intuitive idea, some times it is easy to confuse paths with contributions. A contribution may be thought as a certain signal that goes from one node to other but through all possible paths.

Special importance vis a vis of this thesis will be given to the examples in order to explain the higher order paths.

To make it a bit more amusing than just about a black box imagine that in Figure A.5 the paths connecting the villages need to be identified and that the only possible access points are the villages (input/output).

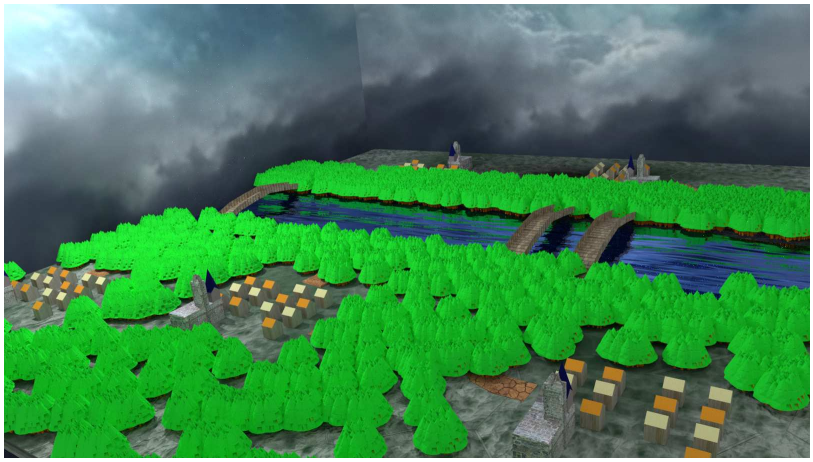

Figure A.5: Hidden paths problem

The dense woods and even the clouds do not allow to see the paths even flying above the land.

A method to know if two villages are connected without having to pass by another village (directly connected)would be to prevent from any input/output of people in all villages but two of them. Introduce, then, people (signal) in a non-blocked one. If this village is connected to the other not blocked village a certain part of the introduced people will appear in the connected village, if the path does not exist no new people will appear in the other non-blocked village.

Unfortunately, it is not allowed to block input/output in villages and it is only possible to see how all villages change the population when people are introduced into a village. The problem is that from village A people can reach village B through a road that passes through village C or through village C and D or any other combination. So this type of test does not show the villages connected via a direct path. With

this test we can only know the contribution from the village A to all other villages regardless of the used paths.

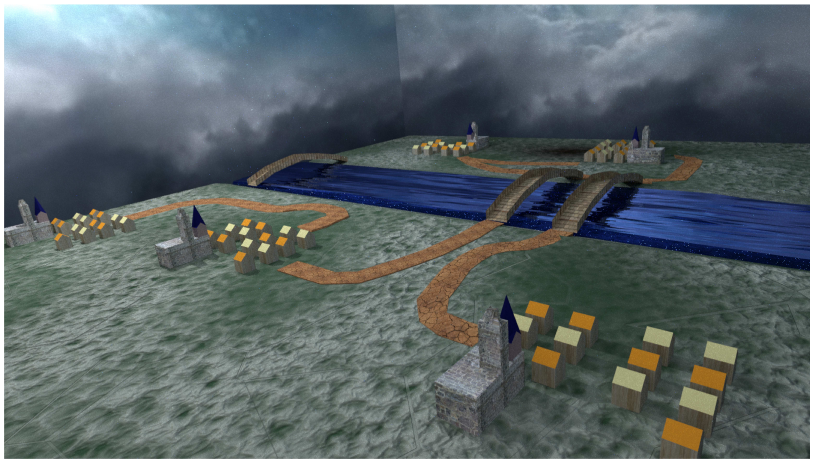

Figure A.6: Hidden paths problem

In Figure A.6 we can see the actual paths that are aimed to be found.

A closer example to the problems of the type encountered in the car industry can be seen in Figure A.7.

In Figure A.7 there is a force applied to the wheel, for example the dynamical forces produced by the irregular surface of the road.

This force has a certain frequency spectrum but let's imagine that the interior noise has a peak at 80 Hz that was not-existent in the input force. The question is who produces this peak. We can make an exploration of the responses of the elements in the chain of paths, the semi-axe, the damper, the spring, the gear lever, etc., trying to discover the responsible the 80 Hz amplification. Some times that can be a successful strategy but when an element in the chain is excited we can "ear" also the response of other elements in the chain on the excited element preventing to conclude who is the real responsible.

The path analysis will allow to know the response of the subsystems and of any set of subsystems isolated from the rest.

If the 80 Hz are a consequence of a local resonance of the semi-axe it will be seen in the paths as if it is a resonance of the damper.

The analysis of the paths will describe the response of any subset of subsystems and then allow to know where the problem is.

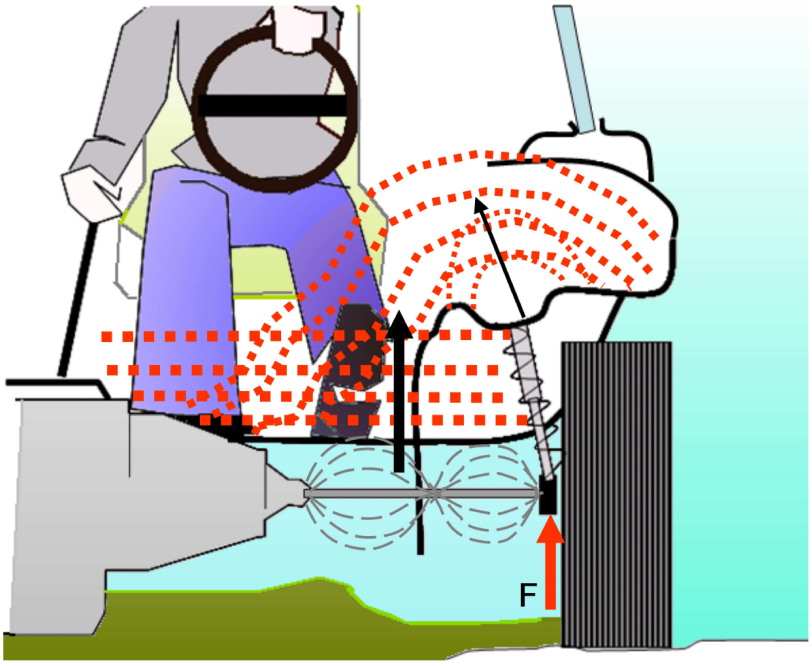

Figure A.7: Sketch of the vibroacoustic transmission in a car. Dynamical force on the wheel generates sound in the passengers cabin. Who is amplifying the 80 Hz?

Let us begin to introduce numbers into these path concepts. Consider, as an example of mechanical system, a chair .

In the upper left of Figure A.8 the mechanical system can be seen. On the right the chair representation is transformed in a flat figure in order to show that the 3D is not an important characteristic. On the left of the middle row the nodes, arbitrarily choosen, are numbered. On the right figure of this intermediate row this figure is transformed into a graph.

In the lower row of the same Figure A.8 the graph is described through the adjoin matrix $\mathbf{\Lambda}$. Rows and columns are the nodes, the coefficients are 1 if the row and column of this coefficient are connected and 0 if they are not connected. Therefore is a connectivity matrix with only zeros and ones.

Connectivity in this example is purely geometric, says only if two nodes are joined from a geometrical point of view.

In this example the nodes 1 and 2 are not connected if only the vibrations are taken in consideration, if the acoustic phenomena are included in the problem both nodes are joined through the air.

As a conclusion, the physical phenomena being studied can change the connectiv-

ity of the graph.

In addition to the connectivity there is another objective when defining a path. A number has to be associated to the path to inform about how the signals in one node influences the signal in the other through this path. That means that a path has to inform about the connectivity of the couples of nodes through the physical signals present in the problem and, furthermore through an associated number that explains which part of the signal in $P2$ comes from $P1$, being $P2$ and $P1$ two nodes of the problem.

If the adjoin matrix is called $\boldsymbol{\Xi}$ and a coefficient is called ξ_{ij}, the coefficients ik of the product of the adjoin matrix by herself will be $\xi_{ij} * \xi_{jk}$ with the repeated coefficient convention.

If the coefficients of $\boldsymbol{\Xi}$ represent the connectivity of the couples of nodes, the coefficients of $\boldsymbol{\Xi}^2$ will represent the connectivity of all the couples of nodes through the paths of second order.

For the same reason the power k of the matrix $\boldsymbol{\Xi}$ will represent the connectivity of all couples of nodes through the paths of order k.

If the adjoin matrix $\boldsymbol{\Xi}$ represents the connectivity of the nodes of a maze, where the nodes are the intersections of the straights parts, it will be possible to know if it is possible to arrive to the node j from the node i making powers of the adjoin matrix. If it is possible to arrive to j coming from i, there should be some power k where the coefficient ij will become different from zero. Let say this happens at $k = n$, this will mean that there exists n paths of order k that link i with j.

In Figure A.9 it can be seen the adjoin matrix raised to the powers 1 to 4 . Each element counts the number of n^{th} order paths that links each couple of nodes. For example, element ξ_{67} in the upper row of the right hand matrix (power 2) has a value of 2 showing that there are two paths of second order joining the nodes 6 and 7.

This paths are represented in the Figure A.10 and they are the paths going from 6 to 7 through 3 and through 4.

A.1.3 Paths in linear systems

Some definitions and the concepts called Global Transfer and Direct Transfer in agreement with Magrans (1981) will now be given .

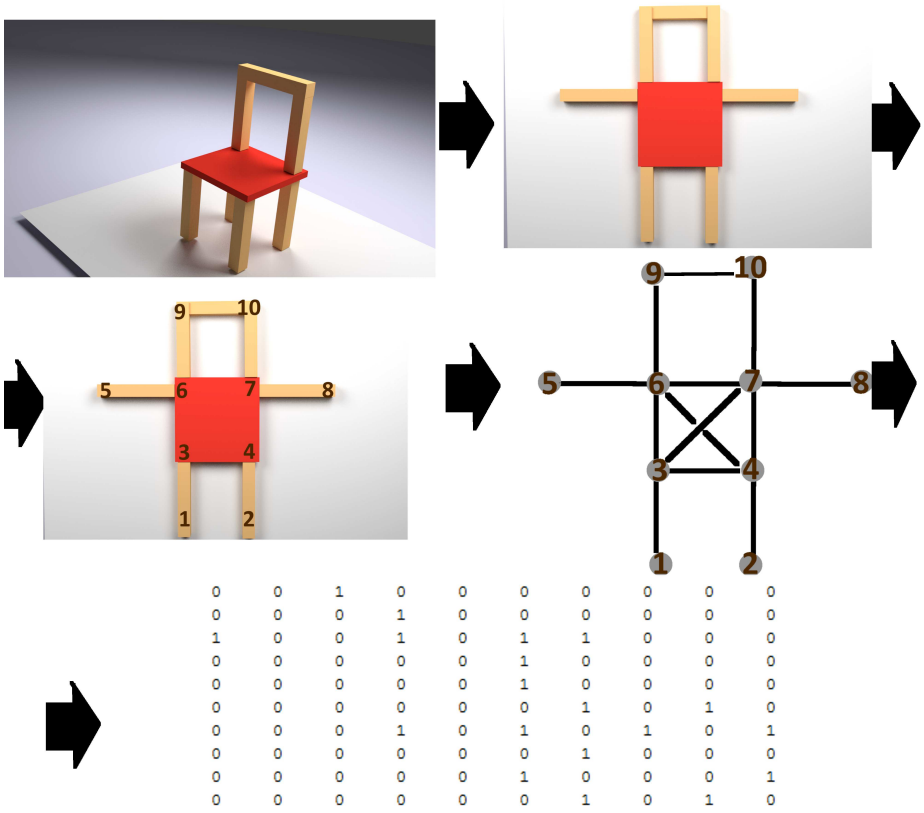

Figure A.8: A mechanical system example and his final geometrical adjoin matrix

We will call Global transfer between the subsystem i and the subsystem j to the ratio of the signal in j and the signal in i when an external excitation is applied to i and no external excitations are applied to the rest of the points.

$$T_{ij}^{G} \equiv \frac{s_j}{s_i} \quad f_i \neq 0 \quad f_j = 0 \forall j \neq i \tag{A.1}$$

If, as an example, the subsystems are degrees of freedom in a mechanical system and the signals are displacements, each row i of the global transfer matrix corresponds to the deformed shape of the system normalized to the displacement in i, when a force is applied to i.

From the point of view of paths it is "global" in the sense that the excitation in i has arrived to j through all possible paths between i and j.

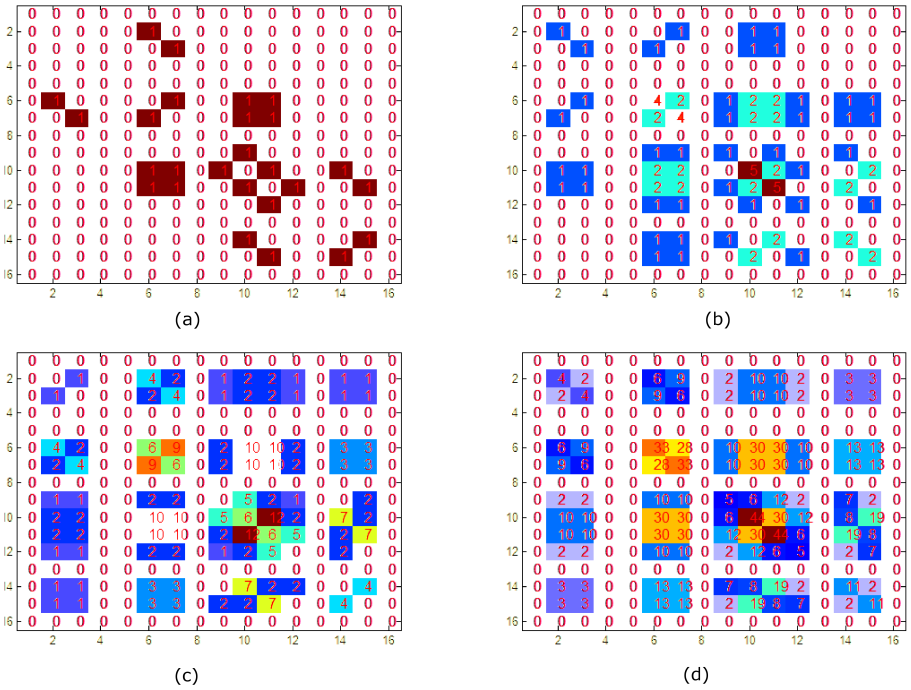

Figure A.9: Chair adjoin matrix raised to powers 1 to 4. a) power 1, b) power 2, c) power 3, d) power 4

We can think of exciting with a hammer in a point i on the body of a car, for example. The noise in a microphone placed at j has arrived through all paths that links the point i with the point j, in other words the noise in j is a consequence of the vibration of all points of the body of the car that had as origin the impact in i.

We will call Direct Transfer from i to j, being $j \neq i$ to the ratio between the signal in j and the signal in i, $\frac{s_j}{s_i}$, when i has been excited with an external force and the other points,except the point j, are blocked.

$$T_{ij}^D \equiv \frac{s_j}{s_i} \quad f_i \neq 0 \quad f_j = 0 \quad s_k = 0 \quad \forall k \neq i, j \tag{A.2}$$

From a paths point of view, that is the signal that arrives from i to j when all other paths are blocked, then it is by definition the path that links i with j.

Take into account that , assuming the system to be linear, the image of zero is zero and then the contribution of all blocked points to the signal in j is zero.

Some additional definitions are still necessary. First one is direct transfer from i to i.

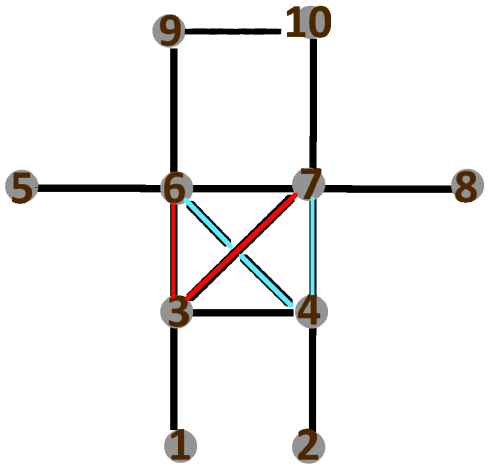

Figure A.10: Graph representation of the paths on the chair. Colour lines shows the second order paths from 6 to 7

The Direct Transfer from i to i will be the part of the signal in i that does not come from the movement in the other points.

$$T_{ii}^{D} \equiv \frac{s_i}{s_i^e} \tag{A.3}$$

$$\text{being } s_i \text{ the signal in i when } \; f_i \neq 0 \; s_j = 0 \; \forall j \neq i$$
$$\text{and } \; s_i^e \text{ the signal in i when } \; f_i \neq 0 \text{ and } f_j = 0 \, \forall j \neq i$$

The signal at point labelled i coming from an external excitation applied to i will be called "external signal" and noted as s_i^e

In the paths sense T_{ij}^{D} is the part of the total signal in i that is produced by the response in the rest of the points to the force applied to i. That is, the feedback on i of the signal transmitted through all paths of the system.

Lets say, if the rest of the points in the chosen set were blocked the signal in i coming from an external excitation applied to i, that normally should be s_i^e, would then be $T_{ij}^{D} s_i^e$.

The quantity defined as Global Transfer function is the only that can be measured easily in a structure.

In a mechanical system, for example, we can excite the degree of freedom corresponding to the normal displacement with a hammer or with an electromechanical

shaker applied to i and measure the relationship between the response of the vibration amplitude of the degree of freedom i and all other degrees of freedom j. These relationships are the Global transfer functions.

The presence of background noise causes the measurement to be in the sense of the optimal statistic approximation, cross spectra, coherence etc.

On the other side the Direct transfer function quantifies the transmission path by blocking the paths that are not direct between i and j. However, this measure is complicated, as it has been shown in the strip method.

The relationship between the measurable Global Transfer T^G and the searched Direct Transfer is done by Eq. (A.4) and by Eq. (A.5)

$$T_{ij}^G = \sum_{k=1 k\neq i}^{n} T_{ik}^G T_{kj}^D \tag{A.4}$$

and

$$1 = \sum_{k=1}^{n} T_{ik}^G T_{ki}^D \tag{A.5}$$

In the context of the above definitions, if in a system we choose a set (p_k), the external signal in the subsystems may be defined into two different ways that match with the explained a priori concepts.

First way to recover the external signals, or its equivalent forces, is to know the signal on the system and to use the A.7.

$$s_i = T_{ki}^G s_k^e \tag{A.6}$$

or in his matrix form

$$\boxed{\mathbf{s} = T^G \mathbf{s^e} \Leftrightarrow \mathbf{s} = T^G B \mathbf{f}} \tag{A.7}$$

Where B is a diagonal matrix relating force with signal at every point.

Eq. (A.7) is the solution of the problem B and it is simply an inversion method.

Measuring T^G between all points using or not forces, the signals in the chosen points can be used to recover the forces or their effects s^e, through matrix inversion,

when the system is excited by its own excitation sources,engine , fan or any other source of force.

This method is the so called TPA, it does not provide information on the transmission paths but only about contributions.

The second way to obtain the external signals is to split s_i using the T^D

$$s_i = T^D_{ii} s^e_i + \sum_{\substack{j=1 \\ j \neq i}}^{n} s_j T^D_{ji} \tag{A.8}$$

or also in matrix form

$$\boxed{\begin{bmatrix} s_1 \\ s_2 \\ ... \\ s_n \end{bmatrix} = \begin{bmatrix} T^D_{11} & ... & 0 & 0 \\ 0 & T^D_{22} & ... & 0 \\ ... & ... & ... & ... \\ 0 & 0 & ... & T^D_{nn} \end{bmatrix} \begin{bmatrix} s^e_1 \\ s^e_2 \\ ... \\ s^e_n \end{bmatrix} + \begin{bmatrix} 0 & T^D_{21} & ... & T^D_{n1} \\ T^D_{12} & 0 & ... & T^D_{n2} \\ ... & ... & ... & ... \\ T^D_{1n} & T^D_{2n} & ... & 0 \end{bmatrix} \begin{bmatrix} s_1 \\ s_2 \\ ... \\ s_n \end{bmatrix}} \tag{A.9}$$

Eq. (A.9) will let us know the contributions of the subsystems, the paths linking them and the exterior signal. To do it we need to measure T^G and to calculate T^D. This is the method called ATPA.

A.1.4 Example

To better understand the differences between T^G and T^D we will apply the concepts to a 2D acoustic room with rigid walls.

In any acoustical space the Helmholtz equation should be fulfilled at any frequency.

$$\Delta p_\omega + \frac{\omega^2}{c^2} p_\omega = \delta_\omega (\mathbf{r} - \mathbf{r_0}) \tag{A.10}$$

$$\forall \text{P on the walls} \quad \left(\frac{\partial p_\omega}{\partial \bar{n}} \right)_{\text{P}} = 0 \tag{A.11}$$

Let a rectangular 2D box of 1mx1m. In this example we will make a 8x8 grid, being the central point of each cell an element of our set of points to study the Direct Transfer.

Using the modal expansion, in a rectangular 2D room with rigid walls the pressure that a delta source placed in (x_C, y_C) produces in (x_D, y_D) is:

$$p_\omega(x_D, y_D) = \sum_{m=0}^{M} \sum_{n=0}^{N} \frac{\Psi_{mn}(x_C, y_C)\Psi_{mn}(x_D, y_D)}{\Lambda_{mn}\left(\omega_{mn}^2 - \omega^2\right)} \tag{A.12}$$

where Λ_{mn} is a normalization constant and

$$\Psi_{mn}(x, y) = \cos(m\pi\frac{x}{L_x})\cos(n\pi\frac{y}{L_y}) \quad \text{m=0, 1, ..., 8 and n=0, 1, ..., 8} \tag{A.13}$$

$$\omega_{m,n} = \pi c\sqrt{\left(\frac{m}{L_x}\right)^2 + \left(\frac{n}{L_y}\right)^2} \tag{A.14}$$

being $\Psi_{mn}(x, y)$ the eigenmode m, n and $\omega_{m,n}$ the eigenvalue angular velocity .

The modal expansion truncated at N, M means that the source has dimensions L_x/M and L_y/N. The truncation matches in our case to the grid size and then $M = 8$, $N = 8$.

In agreement with the definition of T^G the global transfer from point C to point D has to be:

$$T^G_{CD} = \frac{\sum_{m=0}^{M} \sum_{n=0}^{N} \frac{\Psi_{mn}(x_C, y_C)\Psi_{mn}(x_D, y_D)}{\Lambda_{mn}\left(\omega_{mn}^2 - \omega^2\right)}}{\sum_{m=0}^{M} \sum_{n=0}^{N} \frac{\Psi_{mn}^2(x_C, y_C)}{\Lambda_{mn}\left(\omega_{mn}^2 - \omega^2\right)}} \tag{A.15}$$

and the T^G, which may be observed in in Figure A.11, is a full matrix and his rows are the pressures when the force is applied on the element of this row.

The T^D matrix calculated by means of Eq. (A.4) can be seen in Figure A.12

The T^D matrix is a sparse matrix that gives the connectivity of the degrees of freedom.

in Figure A.13 and Figure A.14 the meaning of the T^G matrix rows can be seen.

As told before, T^G rows are the pressures in all grid's points when a delta source acts on an element of the row.

The T^D matrix expresses the connectivity of the elements of the analysed grid and that connectivity can be seen in first order as a typical first order stencil in Finite differences or in Finite elements. It can be seen in Figure A.15 and Figure A.16

As told before the Global transfers are the deformed shapes of the system under an excitation unity and the Direct Transfers are the connectivities between the grid

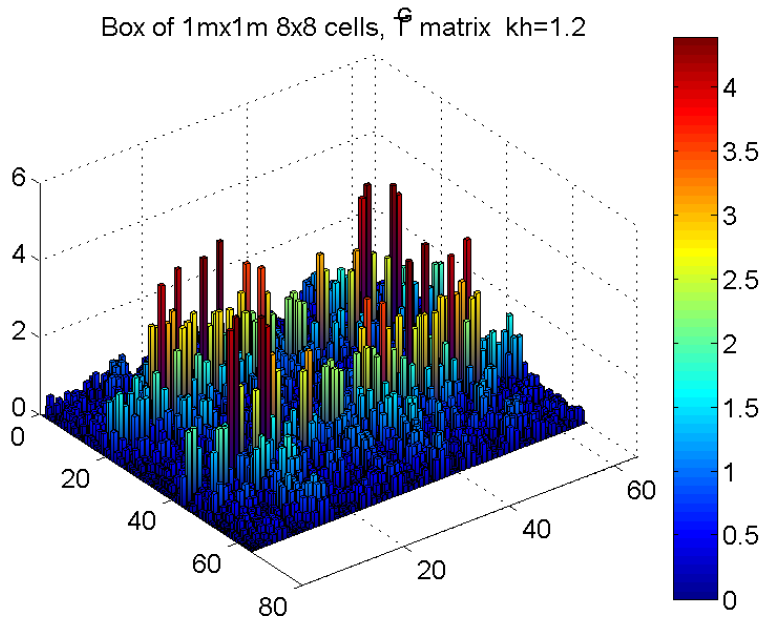

Figure A.11: $k = \frac{2\pi}{\lambda}, h = \frac{1}{8}$, logaritmic representation of the modulus of the coeficients of the Global transfer matrix when $kh = 1.2$

points but, also by definition that Direct transfers multiplied by the pressures on each point and added is the pressure in the destination point, this case the pressure in 1 or in 28.

Multiplying each value in Figure A.14 cell by cell with the same cells in Figure A.15 we find the value of the pressure in cell 28 when an unitary strength monopole source is acting on cell 1. That is the meaning of the expression Eq. (A.9) which is is equivalent to the numeric methods but taking a full stencil filling all calculus space.

It can be seen that the more important values are the ones normally used in the stencils but some other values exist that can give significant contributions.

A.2 A glimpse of the path travelled

Apart from the most recent articles already described in chapter 2, a list, sorted by concepts and holding only some selected references, is given hereunder.

- Introductory papers

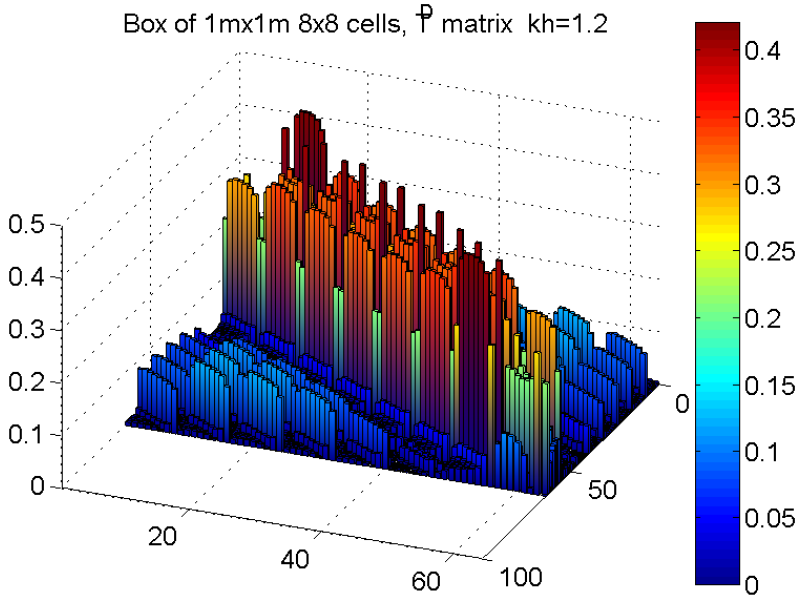

Figure A.12: $k = \frac{2\pi}{\lambda}, h = \frac{1}{8}$,logaritmic representation of the modulus of the coeficients of the Direct transfer matrix when $kh = 1.2$

1. Low and Mid-High frequency Advanced Transmission Path Analysis , ICSV 2005, Magrans et al. (2005). It is a first simple and intuitive introduction to the paths method.
2. Path Analysis. Magrans (2009). NAG DAGA 2009 conference in Rotterdam; Explains the history and the reasons to develop TPA and ATPA , this last one also called in Academic environment GTDT (Global Transfer, Direct Transfer), basic explanations on the meaning of both techniques are given.
3. General framework for transfer path analysis:History, theory and classification of techniques,ref.Van der Seijs et al. (2016); It is a resume of the methods using the word paths in vibroacoustic. Has to be evaluated with care as mixes true Path methods as the OTPA and the GTDT with the called classical TPA that is any more that a model inversion method.

- Theory and historical remarks

1. Method of Measuring Transmission Paths; The original paper published

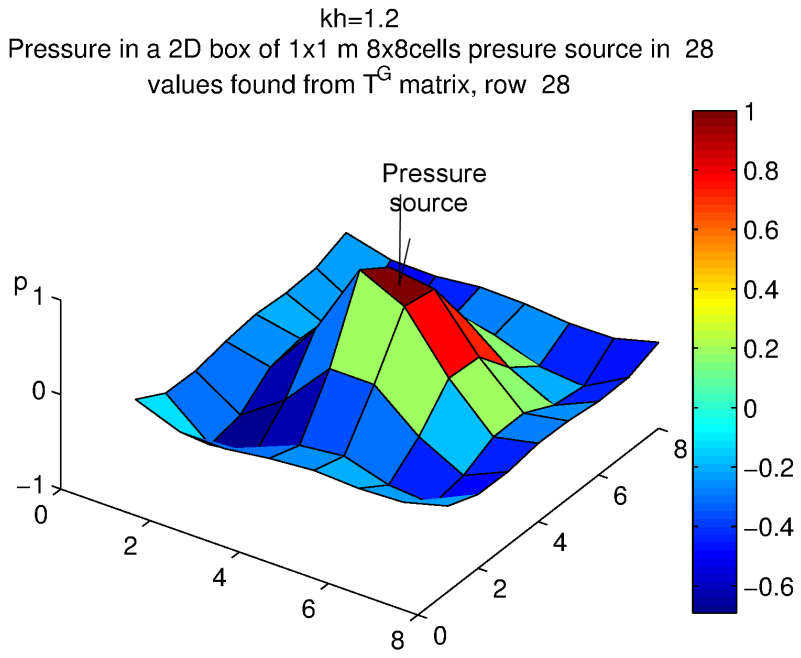

Figure A.13: Global transfer matrix when $kh = 1.2$, source of pressure in 29

in the JSV Magrans (1981) ; States the basic theory, mathematics and physical interpretation.

2. Rapporto Technico N. 80.21 Settembre 1980 metodo,; Discussion of the previous paper in the Keller Company in Italian translated from the French original report.

3. The solution of linear mechanical systems in terms of path superposition Magrans et al. (2017); Even if published a lot later it is a basic element in the coherence of the path interpretation. Show how the solution of all linear system may be expressed as a sum of paths of all order with independence of the norm of the matrix of the problem. Is the first article of this thesis

- Problems solved in path framework

1. Direct Transference applied to the study of room acoustics Magrans (1984); Application to a synthesis problem going from the local behaviour between two walls to the total behaviour of the room.

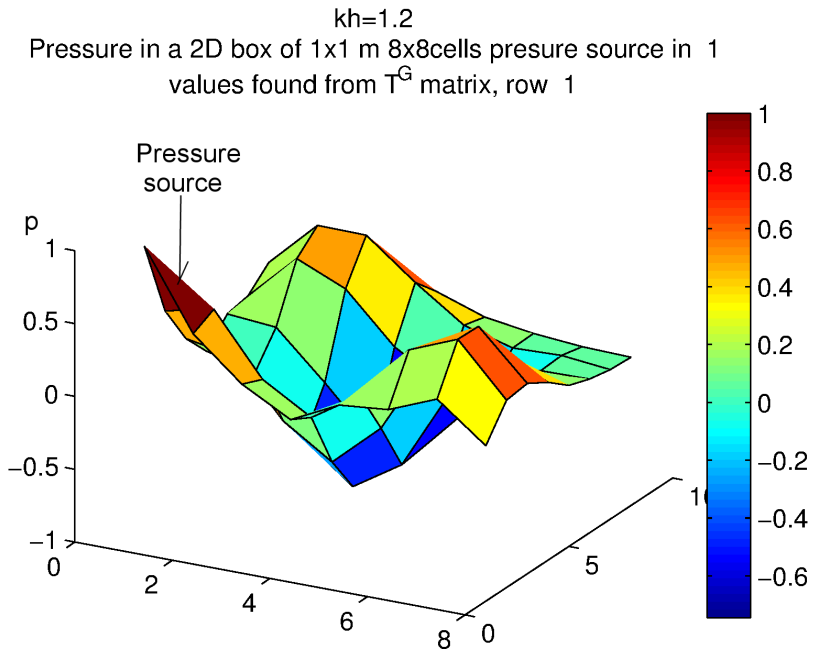

Figure A.14: Global transfer matrix when $kh = 1.2$,source of pressure in 1

2. Definition and calculation of Transmission Paths within a S.E.A. framework Magrans (1993); Extension of the Paths definition to the Statistical Energy Analysis.Explicit graph of the problem.
3. The Global Transfer Direct Transfer Method applied to a finite simply supported elastic beam Guasch and Magrans (2004a); A study of the connectivity of a beam using the Direct Transfer Function.
4. The role of the Direct Transfer Matrix as a connectivity matrix and application to the Helmholtz equation in 2D. Relation to numerical methods and free field radiation example; Direct Transfer matrix used to evaluate the connectivity in acoustics and use of the DTF to calculate the radiation of a circle Magrans and Guasch (2005)
5. A compact formulation for conditioned spectral density function analysis by mean of the LDLH matrix factorization Guasch and Magrans (2004b);

- Research on useful concepts in path framework.

1. A comparison of two in-situ transfer path analysis methods Zafeiropoulos et al. (2013); Experimental comparison between ATPA and iTPA to see

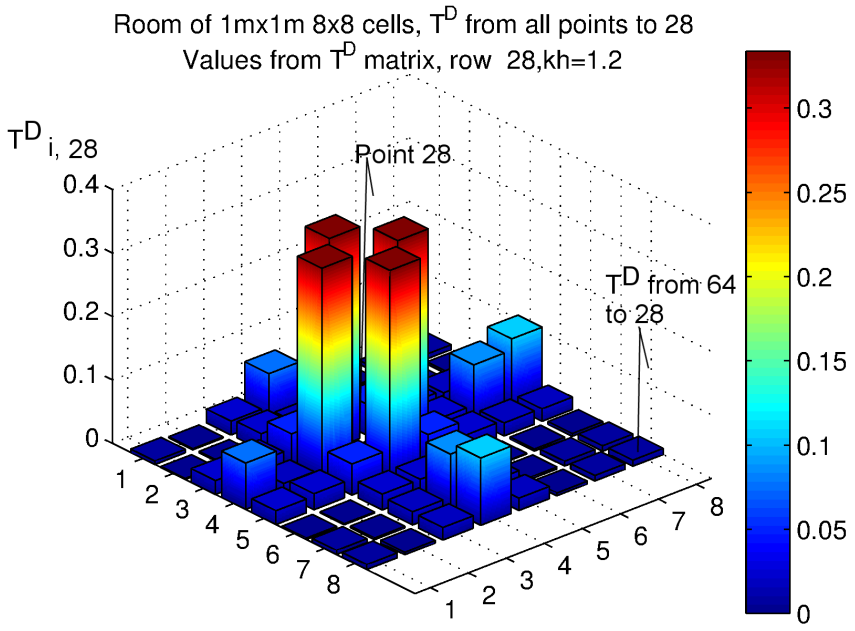

Figure A.15: Direct transfer matrix row 28, Direct transfer from all other points to 28 $kh = 1.2$

their applicability to car industry in collaboration with Bentley Motors Ltd.

2. Graph theory applied to noise and vibration control in statistical energy analysis models Guasch and Cortés (2009); The Path ideas were always based in the graphs concepts as can be seen in Fig. 4 of the Magrans (1993). This paper makes it formal applying the previous knowledge on paths to this specific case and studying the possibility of found an approximate solution based on to obtain the paths with more important contributions. In this way to solve a linear system is equivalent to make a few multiplications and additions. Several papers and even a Thesis has been published on the same way.

3. A subsystem identification method based on the path concept with coupling strength estimation Magrans et al. (2018); In the theory as in the experimentation to know what a subsystem is and his coupling force is basic. This paper helps in the concepts and in the methods based in the DTF matrix powers. This is the second paper developed and published in

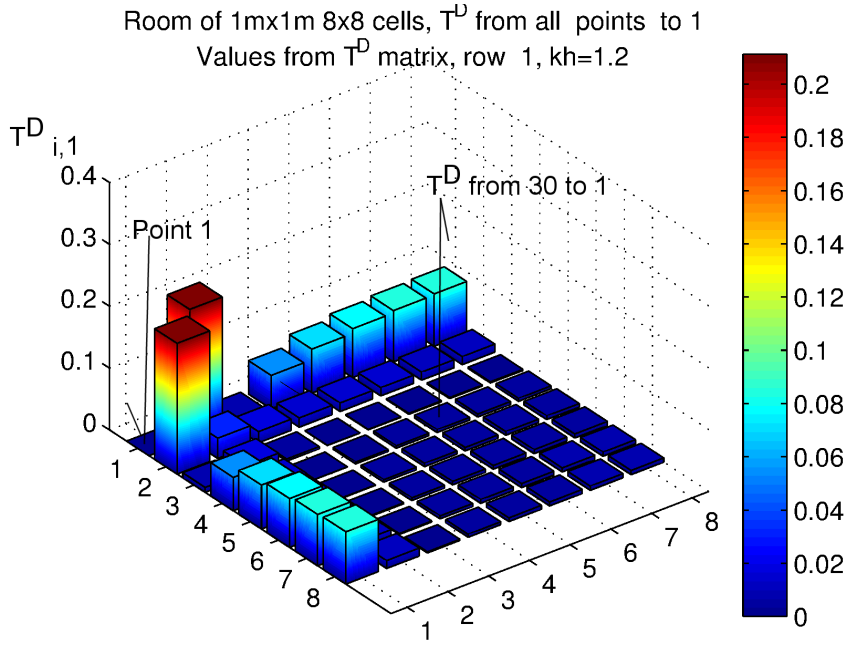

Figure A.16: Direct transfer matrix row 1, Direct transfer from all others points to the point 1 ,$kh = 1.2$

the frame of this Thesis.

4. Analytical transmissibility based transfer path analysis for multi-energy-domain systems using bond graphs Jalali Mashayekhi and Behdinan (2017); This work enlarges the field of application of the GTDT to unexpected fields as the hydraulic and electrical machines. The used tool are the Bond Graphs

5. Response prediction techniques and case studies of a path blocking system based on Global transmissibility Direct transmissibility method Wang et al. (2017); Evaluation of the effect in the Global Transfers of some Direct Transfers for a selected set of cases. Very important to have a systematic method to modify the topology of an structure.

6. Response Prediction of a mechanical system with virtual boundary conditions based on the blocked transfer function methodTan, Xu, and Sui (Tan et al.); Extension of the DTF concept to sets of nodes to define a called BTF, Blocked Transfer Function.

7. Direct responses and Force transmissibility in the characterization of cou-

pled structures Jové and Guasch (2017); In the same line that the previous paper but adding the Forces coupling and transmission.

8. Vehicle and rail noise separation method proposal based on transfer path analysis techniques; A dynamic GTDT method to identify the noise radiated by the rail and the noise radiated by the wheels Malkoun, Sapena, Arcas, and Magrans (Malkoun et al.)

9. Vehicle and rail noise separation method proposal based on Transfer path analysis techniques Thompson et al. (2018). Experimental application of the GTDT method on railways problem where several sources acts simultaneously and changes their transfer values along the time with the aim of to split the noise coming from the rail or from the wheels. Practical comparison with several other methods.

Bibliography

Alfredson, R. (1977). The partial coherence technique for source identification on a diesel engine. *Journal of Sound and Vibration 55*(4), 487–494.

Allen, M. S., R. L. Mayes, and E. J. Bergman (2010). Experimental modal substructuring to couple and uncouple substructures with flexible fixtures and multi-point connections. *Journal of Sound and Vibration 329*(23), 4891–4906.

Aragonès, A., L. Maxit, and O. Guasch (2015). A graph theory approach to identify resonant and non-resonant transmission paths in statistical modal energy distribution analysis. *Journal of Sound and Vibration 350*, 91–110.

Aragonès, A., J. Poblet-Puig, K. Arcas, P. Rodríguez, F. X. Magrans, and A. Rodríguez-Ferran (2019). Experimental and numerical study of advanced transfer path analysis applied to a box prototype. *Mechanical Systems and Signal Processing 114*, 448–466.

Arbenz, P., W. Gander, and G. H. Golub (1988). Restricted rank modification of the symmetric eigenvalue problem: Theoretical considerations. *Linear Algebra and its Applications 104*, 75–95.

Batoz, J.-. L., K.-. J. Bathe, and L.-. W. Ho (1980). A study of three-node triangular plate bending elements. *International Journal for Numerical Methods in Engineering 15*(12), 1771–1812.

Bendat, J. (1976a). Solutions for the multiple input/output poblem. *Journal of Sound and Vibration 44*(3), 311 – 325.

Bendat, J. (1976b). System identification from multiple input/output data. *Journal of Sound and Vibration 49*(3), 293–308.

Bessac, F. (1996, May). *Investigating the vibroacoustic behaviour of coupled systems through the coupling eigenvalues and eigenvectors*. Theses, INSA de Lyon.

Bhushan, B. and Z. Burton (2005). Adhesion and friction properties of polymers in microfluidic devices. *Nanotechnology 16*(4), 467.

Biggs, N. (1993). *Algebraic graph theory*. Cambridge University Press.

Ciarlet, P. G., B. Miara, and J.-M. Thomas (1989). *Introduction to numerical linear algebra and optimisation*. Cambridge University Press.

Craik, R. (1990). Sound transmission paths through a statistical energy analysis model. *Applied Acoustics 30*, 45–55.

Cui, J., X. Guan, and G. Zheng (2016). A simultaneous iterative procedure for the Kron's component modal synthesis approach. *International Journal for Numerical Methods in Engineering 105*(13), 990–1013.

Culla, A. and A. Sestieri (2006). Is it possible to treat confidentially SEA the wolf in sheep's clothing? *Mechanical Systems and Signal Processing 20*(6), 1372–1399.

Cuppen, J. (1980). A divide and conquer method for the symmetric tridiagonal eigenproblem. *Numerische Mathematik 36*(2), 177–195.

Cuppens, K., P. Sas, and L. Hermans (2001). Evaluation of the FRF based substructuring and modal synthesis technique applied to vehicle FE data. In *Proceed.ings of the International seminar on modal analysis*, Volume 3, pp. 1143–1150. KU Leuven; 1998.

de Klerk, D. and A. Ossipov (2010). Operational transfer path analysis: Theory, guidelines and tire noise application. *Mechanical Systems and Signal Processing 24*(7), 1950–1962.

de Klerk, D., D. J. Rixen, and S. Voormeeren (2008). General framework for dynamic substructuring: history, review and classification of techniques. *AIAA journal 46*(5), 1169–1181.

de Sitter, G., C. Devriendt, P. Guillaume, and E. Pruyt (2010). Operational transfer path analysis. *Mechanical Systems and Signal Processing 24*(2), 416–431.

Demmel, J. (1997). *Applied Numerical Linear Algebra*. EngineeringPro collection. Society for Industrial and Applied Mathematics (SIAM, 3600 Market Street, Floor 6, Philadelphia, PA 19104).

Díaz-Cereceda, C., J. Poblet-Puig, and A. Rodríguez-Ferran (2015). Automatic subsystem identification in statistical energy analysis. *Mechanical Systems and Signal Processing 5455*(0), 182–194.

Dobrzynski, L. and H. Puszkarski (1989). Eigenvectors of composite systems. general theory. *Journal of Physics: Condensed Matter 1*(7), 1239.

EDF (2017). Code-Aster home page. http://www.code-aster.org.

Fahy, F. and P. Gardonio (2007). 7 - acoustic coupling between structures and enclosed volumes of fluid. In P. G. F. Fahy (Ed.), *Sound and Structural Vibration (Second Edition)* (Second Edition ed.)., pp. 403 – 448. Oxford: Academic Press.

Finnveden, S. (2011). A quantitative criterion validating coupling power proportionality in statistical energy analysis. *Journal of Sound and Vibration 330*(1), 87–109.

Gagliardini, L. and J. Guyader (2000). The coupling eigenvalues method: a new basis for the study of vibro-acoustics coupled systems. In *NOVEM*, Lyon, France.

Gagliardini, L., L. Houillon, G. Borello, and L. Petrinelli (2005). Virtual sea-fea-based modeling of mid-frequency structure-borne noise. *Sound and Vibration 39*(1), 22.

Gajdatsy, P., K. Janssens, W. Desmet, and H. Van Der Auweraer (2010). Application of the transmissibility concept in transfer path analysis. *Mechanical Systems and Signal Processing 24*(7), 1963–1976.

Geuzaine, C. and J.-F. Remacle (2009). Gmsh: a three-dimensional finite element mesh generator with built-in pre- and post-processing facilities. *Int. J. Numer. Meth. Engng. 11*(79), 1309–1331.

Gillard, Stahel, V. L. (1980, September). *Metodo di misura per la determinazione delle vie de transmissione e dei contributi delle diverse force di eccitazione reali applicate simultaneamente ad un sistema mecanico lineare*. Keller, Santhia, Italy.

Guasch, O. (2009). Direct transfer functions and path blocking in a discrete mechanical system. *Journal of Sound and Vibration 321*(3), 854–874.

Guasch, O. and A. Aragonès (2011). Finding the dominant energy transmission paths in statistical energy analysis. *Journal of Sound and Vibration 330*(10), 2325–2338.

Guasch, O. and L. Cortés (2009). Graph theory applied to noise and vibration control in statistical energy analysis models. *The Journal of the Acoustical Society of America 125*(6), 3657–3672.

Guasch, O., C. García, J. Jové, and P. Artís (2013). Experimental validation of the direct transmissibility approach to classical transfer path analysis on a mechanical setup. *Mechanical Systems and Signal Processing 37*(1), 353–369.

Guasch, O. and F. Magrans (2004a). The global transfer direct transfer method applied to a finite simply supported elastic beam. *Journal of Sound and Vibration 276*(12), 335 – 359.

Guasch, O. and F. X. Magrans (2004b). A compact formulation for conditioned spectral density function analysis by means of the ldlh matrix factorization. *Journal of Sound and Vibration 277*(45), 1082–1092.

Hambric, S. A., S. H. Sung, and D. J. Nefske (2016). *Engineering Vibroacoustic Analysis: Methods and Applications*. John Wiley & Sons.

Hopkins, C. (2012). *Sound insulation*. Routledge.

Huygens, C. (1962). Treatise on light, 1690. *Translated by SP Thompson, Project Gutenberg eBook*.

Ihlenburg, F. (1998). *Finite element analysis of acoustic scattering*. Springer.

Jalali Mashayekhi, M. and K. Behdinan (2017). Analytical transmissibility based transfer path analysis for multi-energy-domain systems using bond graphs. *Journal of Vibration and Control*, 1077546317696362.

Jove, J. and O. Guasch (2012). Mathematical link between direct transmissibility functions and the discrete characterization of mechanical systems. In *INTER-NOISE and NOISE-CON Congress and Conference Proceedings*, Volume 244, pp. 725–736. Institute of Noise Control Engineering.

Jové, J. and O. Guasch (2017). Direct response and force transmissibilities in the characterization of coupled structures. *Journal of Sound and Vibration 407*, 1–15.

Kassem, M., C. Soize, and L. Gagliardini (2011). Structural partitioning of complex structures in the medium-frequency range. An application to an automotive vehicle. *Journal of Sound and Vibration 330*(5), 937 – 946.

Kaveh, A. and H. Fazli (2011). Approximate eigensolution of locally modified regular structures using a substructuring technique. *Computers & Structures 89*(5), 529–537.

Koss, L. and R. Alfredson (1974a). Identification of transient sound sources on a punch press. *Journal of Sound and Vibration 34*(1), 11 – IN4.

Koss, L. and R. Alfredson (1974b). Multiple input correlation theory and the least squares method for the analysis of transient sound. *Journal of Sound and Vibration 32*(3), 423 – 427.

Kovalevsky, L. and R. Langley (2012). Automatic recognition of the components of a hybrid FE-SEA model. In *Proceedings of the Acoustics 2012 Nantes Conference*, Nantes, France, 23 - 27 April 2012.

Kron, G. (1963). *Diakoptics: the piecewise solution of large-scale systems*, Volume 2. MacDonald.

Lafont, T., N. Totaro, and A. Le Bot (2014). Review of statistical energy analysis hypotheses in vibroacoustics. *Proceedings of the Royal Society of London. Series A 470*(2162), 20130515.

Lafont, T., N. Totaro, and A. Le Bot (2017). Coupling strength assumption in statistical energy analysis. *Proceedings of the Royal Society of London. Series A 473*(2200), 20160927.

Le Bot, A. (2015). *Foundation of statistical energy analysis in vibroacoustics*. OUP Oxford.

Lebresne (1975). Interventions pratiques contre les bruits exterieurs des vehicles routiers. *Interkeller Gap Conferences,Switzerland*.

Liu, W. and D. Ewins (2000). Substructure synthesis via elastic media part i: Joint identification. In *Proceedings of the International Modal Analysis Conference, San Antonio, TX*.

Lohrmann, M. (2008). Operational transfer path analysis: Comparison with conventional methods. *The Journal of the Acoustical Society of America 123*(5), 3534–3534.

Lui, S. (2000). Domain decomposition methods for eigenvalue problems. *Journal of Computational and Applied Mathematics 117*(1), 17–34.

Luzzato, E. and E. Ortola (1988). The characterization of energy flow paths in the study of dynamic systems using S.E.A. theory. *Journal of Sound and Vibration 123*(1), 189–197.

Lyon, R. (1975). *Statistical Energy Analysis of Dynamical Systems*. M.I.T. Press.

Magrans, F. X. (1981). Method of measuring transmission paths. *Journal of Sound and Vibration 74*(3), 321 – 330.

Magrans, F. X. (1984). Direct transference applied to the study of room acoustics. *Journal of Sound and Vibration 96*(1), 13–21.

Magrans, F. X. (1993). Definition and calculation of transmission paths within an sea framework. *Journal of Sound and Vibration 165*(2), 277–283.

Magrans, F. X. (2009). Path analysis. In *NAG/DAGA 2009 International Conference on Acoustics*.

Magrans, F. X. and O. Guasch (2005). The role of the direct transfer matrix as a connectivity matrix and application to the helmholtz equation in 2d: relation to numerical methods and free field radiation example. *Journal of Computational Acoustics 13*(02), 341–363.

Magrans, F. X. and J.Poblet-Puig (2018). Eigenvalue and eigenmode synthesis in elastically coupled subsystems. *Journal of Sound and Vibration 432*, 405 – 419.

Magrans, F. X., J. Poblet-Puig, and A. Rodríguez-Ferran (2016, Aug). Substructuring of mechanical systems based on the path concept. In *International Congress and Exposition on Noise Control Engineering*, pp. 2485–2494. Deutsche Gesellschaft fr Akustik e.V. (DEGA).

Magrans, F. X., J. Poblet-Puig, and A. Rodríguez-Ferran (2017). The solution of linear mechanical systems in terms of path superposition. *Mechanical Systems and Signal Processing 85*, 111–125.

Magrans, F. X., J. Poblet-Puig, and A. Rodríguez-Ferran (2018). A subsystem identification method based on the path concept with coupling strength estimation. *Mechanical Systems and Signal Processing 100*, 588–604.

Magrans, F. X., P. V. Rodríguez, and G. C. Cousin (2005). Low and mid-high frequency advanced transmission path analysis. In *Proceedings of the Twelfth International Congress on Sound and Vibration ICSV12*.

Maidanik, G. (1976). Response of coupled dynamic systems. *Journal of Sound and Vibration 46*(4), 561–583.

Malkoun, A., J. Sapena, K. Arcas, and F. X. Magrans. Vehicle and rail noise separation method proposal based on transfer path analysis techniques. In *ICSV 21 proceedings*.

Oktav, A., Ç. Yılmaz, and G. Anlaş (2017). Transfer path analysis: Current practice, trade-offs and consideration of damping. *Mechanical systems and signal processing 85*, 760–772.

Potter, R. (1977). Matrix formulation of multiple and partial coherence. *The Journal of the Acoustical Society of America 61*(3), 776–781.

Reynders, E. (2012). System identification methods for (operational) modal analysis: review and comparison. *Archives of Computational Methods in Engineering 19*(1), 51–124.

Reynders, E. and G. De Roeck (2008). Reference-based combined deterministic–stochastic subspace identification for experimental and operational modal analysis. *Mechanical Systems and Signal Processing 22*(3), 617–637.

Roozen, N. B. and Q. Leclere (2013). On the use of artificial excitation in operational transfer path analysis. *Applied Acoustics 74*(10), 1167–1174.

Sapena, J., A. Tabbal, J. Jovié, and F. Guerville (2012). Interior noise prediction in high-speed rolling stock drivers cab: Focus on structure-borne paths (mechanical and aero sources). In T. Maeda, P.-E. Gautier, C. Hanson, B. Hemsworth, J. Nelson, B. Schulte-Werning, D. Thompson, and P. de Vos (Eds.), *Noise and Vibration*

Mitigation for Rail Transportation Systems, Volume 118 of *Notes on Numerical Fluid Mechanics and Multidisciplinary Design*, pp. 445–452. Springer Japan.

Simpson, A. (1973). *Kron's method: An algorithm for the eigenvalue analysis of large-scale structural systems*. HM Stationery Office.

Simpson, A. and B. Tabarrok (1968). On Kron's eigenvalue procedure and related methods of frequency analysis. *The Quarterly Journal of Mechanics and Applied Mathematics 21*(1), 1–39.

Sylla, B., L. Dobrzynski, and H. Puszkarski (1989). Eigenvectors of composite systems. ii. phonon eigenvectors in some layered materials. *Journal of Physics: Condensed Matter 1*(7), 1247.

Tan, S., H. Xu, and F. Sui. Response prediction of a mechanical system with virtual boundary conditions based on the blocked transfer function method. In *ICSV 24 proceedings*.

Thompson, D., G. Squicciarini, J. Zhang, I. L. Arteaga, E. Zea, M. Dittrich, E. Jansen, K. Arcas, E. Cierco, F. X. Magrans, A. Malkoun, E. Iturritxa, A. Guiral, M. Stangl, G. Schleinzer, B. M. Lopez, C. Chaufour, and J. Wndell (2018). Assessment of measurement-based methods for separating wheel and track contributions to railway rolling noise. *Applied Acoustics 140*, 48 – 62.

Totaro, N. and J. Guyader (2006). SEA substructuring using cluster analysis: The MIR index. *Journal of Sound and Vibration 290*(1-2), 264–289.

Trefethen, L. and D. Bau (1997). *Numerical Linear Algebra*. Society for Industrial and Applied Mathematics.

Ungar, E. (1966). Fundamentals of statistical energy analysis of vibrating systems. Technical report, DTIC Document.

Van der Seijs, M., D. de Klerk, and D. Rixen (2016). General framework for transfer path analysis: History, theory and classification of techniques. *Mechanical Systems and Signal Processing 68*, 217–244.

Wang, Z., P. Zhu, and J. Zhao (2017). Response prediction techniques and case studies of a path blocking system based on global transmissibility direct transmissibility method. *Journal of Sound and Vibration 388*, 363–388.

Wei, G., B. Bhushan, N. Ferrell, and D. Hansford (2005). Microfabrication and nanomechanical characterization of polymer microelectromechanical system for biological applications. *Journal of Vacuum Science & Technology A: Vacuum, Surfaces, and Films 23*(4), 811–819.

Weng, S., Y. Xia, Y.-L. Xu, X.-Q. Zhou, and H.-P. Zhu (2009). Improved substructuring method for eigensolutions of large-scale structures. *Journal of Sound and Vibration 323*(3), 718–736.

Wilson, D. (2014). *Prediction of bending wave transmission across coupled plates affected by spatial filtering and non-diffuse vibration fields*. Ph. D. thesis, University of Liverpool.

Zafeiropoulos, N., A. T. Moorhouse, A. Mackay, and U. Senapati (2013). Advanced transfer path analysis of a vehicle. In *Proceedings of the 11 RASD conference, Pisa*.